CONDENSATION OF STEAM
ON
MULTIPLE HORIZONTAL TUBES

A THESIS SUBMITTED TO
THE GRADUATE SCHOOL OF NATURAL AND APPLIED SCIENCES
OF
THE MIDDLE EAST TECHNICAL UNIVERSITY

BY

AYTAÇ MAKAS

IN PARTIAL FULFILLMENT OF THE REQUIREMENTS FOR THE DEGREE OF
MASTER OF SCIENCE
IN
THE DEPARTMENT OF MECHANICAL ENGINEERING

APRIL 2004

Approval of the Graduate School of Natural and Applied Sciences

_____
Prof. Dr. Canan ÖZGEN
Director

I certify that this thesis satisfies all the requirements as a thesis for the degree of Master of Science.

_____
Prof. Dr. S. Kemal İDER
Head of Department

This is to certify that we have read this thesis and that in our opinion it is fully adequate, in scope and quality, as a thesis for the degree of Master of Science.

_____
Assoc. Prof. Dr. Cemil YAMALI
Supervisor

Examining Committee Members

Prof. Dr. Canan ÖZGEN _____

Prof. Dr. Kahraman ALBAYRAK _____

Assoc. Prof. Dr. Cemil YAMALI _____

Asst. Prof. Dr. İlker TARI _____

Asst. Prof. Dr. Abdullah ULAŞ _____

ABSTRACT

CONDENSATION OF STEAM

ON MULTIPLE HORIZONTAL TUBES

Makas, Aytaç

M.S., Department of Mechanical Engineering

Supervisor: Assoc. Prof. Dr. Cemil Yamalı

April 2004, 107 pages

The problem of condensation of steam on a vertical tier of horizontal tubes is investigated by both analytical and experimental methods in this study. A computer program is written to perform the analysis of laminar film condensation on the horizontal tubes. The program is capable to calculate condensate film thickness and velocity distribution, as well as the heat transfer coefficient within the condensate. An experimental setup was also manufactured to observe the condensation phenomenon.

Effects of tube diameter and temperature difference between steam and the tube wall on condensation heat transfer have been analytically investigated with the computer program. Experiments were carried out at different inclinations of the tier

of horizontal tubes. Effects of the steam velocity and the distance between the horizontal tubes are also experimentally investigated. Results of the experiments are compared to those of the studies of Abdullah et al., Kumar et al. and Nusselt as well as to the analytical results of the present study.

Keywords: Condensation, laminar flow, horizontal tube, inclination, film thickness

ÖZ

ÇOK SIRALI YATAY BORULARDA

SU BUHARININ YOĞUŞMASI

Makas, Aytaç

Yüksek Lisans, Makina Mühendisliği Bölümü

Tez Yöneticisi: Doç. Dr. Cemil Yamalı

Nisan 2004, 107 sayfa

Bu çalışmada, dikey eksende sıralanmış yatay boruların üzerinde su buharının yoğuşması problemi analitik ve deneysel yöntemlerle incelenmiştir. Yatay boruların üzerindeki laminer film yoğuşmasını analiz eden bir bilgisayar programı yazılmıştır. Program, yoğuşan su tabakası içindeki ısı transferi katsayısı ile film kalınlığı ve hız dağılımını hesaplayabilmektedir. Yoğuşma problemini gözlemleyebilmek için bir deney düzeneği de hazırlanmıştır.

Boru çapının ve buhar ile boru yüzeyi arasındaki sıcaklık farkının ısı transferine etkileri bilgisayar programı yardımıyla incelenmiştir. Deneyler yoğuşma borularının eğimi değiştirilerek farklı açılarda gerçekleştirilmiştir. Buharın hızının ve yoğuşma boruları arasındaki mesafenin etkileri deneysel olarak incelenmiştir.

Deneylerden elde edilen sonuçlar, Abdullah et al., Kumar et al. ve Nusselt'in çalışmalarıyla ve analitik araştırmadan elde edilen sonuçlarla karşılaştırılmıştır.

Anahtar Kelimeler: Yoğuşma, laminer akış, yatay boru, eğim, film kalınlığı

To my parents,

who always support me in all aspects of my life

ACKNOWLEDGEMENTS

I express my sincere appreciation to Assoc. Prof. Dr. Cemil Yamalı for his guidance, support and valuable contributions throughout the study. I gratefully acknowledge Mustafa Yalçın, Fahrettin Makas and İlhan Erkinöz for their technical assistance in manufacturing and operating the setup. I am grateful to the jury members for their valuable contributions.

I express my deepest gratitude to my mother Şükran Makas and my father Fahrettin Makas for their encouragements throughout my education life.

TABLE OF CONTENTS

ABSTRACT iii

ÖZ v

ACKNOWLEDGEMENTS viii

TABLE OF CONTENTS ix

LIST OF TABLES xi

LIST OF FIGURES xii

LIST OF SYMBOLS xvi

CHAPTER

1. INTRODUCTION 1

    1.1 Condensation 1

    1.2 Flow Regimes 3

2. LITERATURE SURVEY 5

3. ANALYTICAL MODEL 15

    3.1 Governing Equations 15

    3.2 Method of Solution 20

4. EXPERIMENTAL STUDY 25

    4.1 Cooling Water Tank 27

    4.2 Boiler 28

    4.3 Test Section 29

4.4 Temperature Measurement System 32

4.5 Experimental Procedure 35

5. RESULTS AND DISCUSSIONS 38

5.1 Analytical Results 38

5.1.1 Effect of Tube Diameter on Condensation Heat Transfer 44

5.1.2 Effect of Steam to Wall Temperature Difference on Condensation Heat Transfer 49

5.2 Experimental Results 54

5.2.1 Results of the Experiments Made at Different Angular Orientation of Tube Columns 54

5.2.2 Effect of Steam Velocity over the Tubes 61

5.2.3 Effect of Distance Between Condensation Tubes 64

5.3 Comparison of Results 66

5.3.1 Comparison of Experimental Results with Literature 66

5.3.2 Comparison of Experimental Results with Analytical Results 70

6. CONCLUSIONS 72

6.1 Recommendations for Future Work 73

REFERENCES 74

APPENDICES

A. CONDENSATE BEHAVIOUR AT DIFFERENT ANGLES 78

B. RESULTS OF THE EXPERIMENTS 83

C. UNCERTAINTY ANALYSIS 86

D. MATHCAD PROGRAM SOURCE 89

LIST OF TABLES

TABLE

B.1 Experimental Data and Results for 0° of Inclination 83

B.2 Experimental Data and Results for 3° of Inclination 84

B.3 Experimental Data and Results for 6° of Inclination 84

B.4 Experimental Data and Results for 10° of Inclination 85

B.5 Experimental Data and Results for 15° of Inclination 85

C.1 Uncertainties of the Independent Variables Used in Equation 5.3 and 5.4.... 87

C.2 Uncertainties in the Experimental Results 88

LIST OF FIGURES

FIGURE

3.1 Physical Model and Coordinate System 16

3.2 Physical Model for the Lower Tubes 24

4.1 Schematic Representation of the Apparatus 26

4.2 Water Division Apparatus 28

4.3 Drawing of the Gauge and the Metal Rings 30

4.4 Drawing of the Test Section 31

4.5 Thermocouple Layout 33

4.6 General View of the Test Section 34

4.7 Top View of the Test Section with Flow Delimiters 36

4.8 Demonstration of the Stage 3 37

5.1 Variation of Film Thickness with Angular Position at D=19mm and ΔT=9K 42

5.2 Variation of Velocity of the Condensate with Angular Position at D=19mm and ΔT=9K 42

5.3 Variation of Heat Flux with Angular Position at D=19mm and ΔT=9K 43

5.4 Variation of Heat Transfer Coefficient with Angular Position at D=19mm and ΔT=9K 43

5.5 Variation of Film Thickness of the Upper Tube with Angular Position for Different Tube Diameters 45

5.6 Variation of Film Thickness of the Middle Tube with Angular Position for Different Tube Diameters 45
5.7 Variation of Film Thickness of the Bottom Tube with Angular Position for Different Tube Diameters 46
5.8 Variation of Velocity of the Condensate of the Upper Tube with Angular Position for Different Tube Diameters 46
5.9 Variation of Velocity of the Condensate of the Middle Tube with Angular Position for Different Tube Diameters 47
5.10 Variation of Velocity of the Condensate of the Bottom Tube with Angular Position for Different Tube Diameters 47
5.11 Variation of Mean Heat Flux with the Tube Diameter 48
5.12 Variation of Mean Heat Transfer Coefficient with the Tube Diameter 48
5.13 Variation of Film Thickness of the Upper Tube with Angular Position for Various Steam to Wall Temperature Differences 50
5.14 Variation of Film Thickness of the Middle Tube with Angular Position for Various Steam to Wall Temperature Differences 50
5.15 Variation of Film Thickness of the Bottom Tube with Angular Position for Various Steam to Wall Temperature Differences 51
5.16 Variation of Velocity of the Condensate with Angular Position for Various Steam to Wall Temperature Differences 51
5.17 Variation of Velocity of the Condensate with Angular Position for Various Steam to Wall Temperature Differences 52
5.18 Variation of Velocity of the Condensate with Angular Position for Various Steam to Wall Temperature Differences 52

5.19 Variation of Mean Heat Flux With Respect To the Steam to Wall Temperature Difference 53
5.20 Variation of Mean Heat Transfer Coefficient With Respect To the Steam to Wall Temperature Difference 53
5.21 Heat Transfer Rates for 0° of Inclination 56
5.22 Heat Transfer Coefficients for 0° of Inclination 56
5.23 Heat Transfer Rates for 3° of Inclination 57
5.24 Heat Transfer Coefficients for 3° of Inclination 57
5.25 Heat Transfer Rates for 6° of Inclination 58
5.26 Heat Transfer Coefficients for 6° of Inclination 58
5.27 Heat Transfer Rates for 10° of Inclination 59
5.28 Heat Transfer Coefficients for 10° of Inclination 59
5.29 Heat Transfer Rates for 15° of Inclination 60
5.30 Heat Transfer Coefficients for 15° of Inclination 60
5.31 Heat Transfer Rates for Half Power of the Steam 62
5.32 Heat Transfer Coefficients for Half Power of the Steam 62
5.33 Heat Transfer Rates for Full Power of the Steam 63
5.34 Heat Transfer Coefficients for Full Power of the Steam 63
5.35 Heat Transfer Rates of the Experiments Without Middle Tube 65
5.36 Heat Transfer Coefficients of the Experiments Without Middle Tube 65
5.37 Comparison of Heat Transfer Coefficients Between the Present Study and Abdullah et al. 67
5.38 Comparison of Heat Transfer Coefficients Between the Present Study and Kumar et al. 68

5.39 Comparison of Heat Transfer Coefficients Between the Present Study and the Nusselt Analysis 69

5.40 Comparison of Heat Transfer Coefficients Between Analytical and Experimental Analyses for the Upper Tube 70

5.41 Comparison of Heat Transfer Coefficients Between Analytical and Experimental Analyses for the Middle Tube 71

5.42 Comparison of Heat Transfer Coefficients Between Analytical and Experimental Analyses for the Bottom Tube 71

A.1 Condensate Behaviour in the Setup at 0 Degree of Inclination 78

A.2 Condensate Behaviour in the Setup at 3 Degree of Inclination 79

A.3 Condensate Behaviour in the Setup at 6 Degree of Inclination 80

A.4 Condensate Behaviour in the Setup at 10 Degree of Inclination 81

A.5 Condensate Behaviour in the Setup at 15 Degree of Inclination 82

LIST OF SYMBOLS

C_p	Specific heat at constant pressure	[J/(kg.K)]
g	Gravity	[m/s^2)
h	Heat transfer coefficient	[W/(m^2.K)]
h_{fg}	Latent heat of evaporation	[J/kg]
k	Thermal conductivity	[W/(m.K)]
L	Length	[m]
Nu	Nusselt number	
q	Heat flux	[W/m^2]
Q	Heat transfer rate	[W]
r	Radius of the cylinder	[m]
Re	Reynolds number	
T	Temperature	[°C]
T1,..,T10	Thermocouples	
u	Velocity	[m/s]
U	x component of condensate velocity	[m/s]
x	Coordinate parallel to surface	
y	Coordinate normal to surface	

Greek Letters

δ	Film thickness of the condensate	[m]
Δ	Condensate thickness	[m]
φ	Angular position measured from the top of the tube	[degree]
μ	Dynamic viscosity	[Pa.s]
ν	Kinematic viscosity	[m^2/s]
ρ	Density	[kg/m^3]
τ	Shear stress	[Pa]
Ψ	Derivative matrix	

Subscripts

cond	Condensation
f	Fluid
g	Water vapor
i	Loop variable
in	Inlet
inc	Increment
out	Outlet
sat	Saturation
v	Vapor
w	Wall
∞	Free stream

CHAPTER 1

INTRODUCTION

1.1 Condensation

Condensation is defined as the phase change from vapor state to liquid state. When the temperature of a vapor goes below its saturation temperature, condensation occurs. A certain amount of subcooling is required for condensation. Hence, energy in the latent heat form must be removed from the condensation area during the phase change process. A pressure decrease happens in the region of condensation resulting a mass diffusion toward this region.

Condensation can be classified as bulk condensation and surface condensation.

Vapor condenses as droplets suspended in a gas phase in the bulk condensation. When condensation takes place randomly within the bulk of the vapor, it is called homogeneous condensation. If condensation occurs on foreign particles exist in the vapor, this type of bulk condensation is defined as heterogeneous condensation. Fog is a typical example of this type of condensation.

Surface condensation occurs when the vapor contacts with a surface whose temperature is below the saturation temperature of the vapor. Surface condensation has a wide application area in the industry. It is classified as filmwise and dropwise condensation.

Film condensation occurs when the liquid wets the surface and the condenser surface is blanketed by a condensate film. This film represents a thermal resistance to heat transfer and a temperature gradient exists in the film. The analytical investigation of film condensation was first performed by Nusselt in 1916. He neglected the effects of vapor drag and fluid accelerations. He assumed that flow is laminar throughout the film. It is further assumed that a linear temperature distribution and a parabolic velocity profile exist between wall and vapor conditions. Despite the complexities associated with film condensation, Nusselt achieved to get reasonable and realistic results by making his assumptions.

Dropwise condensation occurs on a surface which is coated with a substance that inhibits wetting. Heat transfer rates in dropwise condensation may be ten times higher than in film condensation. Since very high heat transfer rates can be obtained in dropwise condensation, it is always desired in applications. It is possible to reduce the heat transfer area half or less in a condenser system by using dropwise condensation.

Various surface coatings, such as gold, silicones and teflon, have been used in the industry to maintain dropwise condensation but none of these methods has reached any considerable success. Because the effectiveness of such coatings

gradually decreases due to oxidation and fouling, film condensation occurs after a period of time. Another reason of losing the effectiveness of dropwise condensation is the accumulation of droplets on the condenser surface. Heat transfer rate sharply decreases because of the accumulated droplets. Therefore, most condensers are designed on the assumption of being film condensation.

1.2 Flow Regimes

Consider a fluid motion on a flat plate. Fluid particles making contact with the surface designate zero velocity. These particles cause to retard the motion of other particles in the adjoining layer. This retardation is described in terms of a shear stress τ between the fluid layers. The shear stress can be assumed to be proportional to the normal velocity gradient and it is formulated as;

$$\tau = \mu \frac{du}{dy} \tag{1.1}$$

The proportionality constant μ is a fluid property known as the dynamic viscosity. The region of flow where the influence of viscosity is observed is called the *boundary layer*. The boundary layer thickness is typically defined as the distance from the plate for which the velocity is equal to 99 percent of the free-stream velocity value.

An essential step of dealing with any flow problem is to determine whether the flow is *laminar* or *turbulent*. Flow characteristics are strongly depending on which

flow regime exists in the fluid. In laminar region, flow is highly ordered and it is possible to find out the characteristics at every adjoining fluid layer. Despite the moderate behaviour of fluid motion in the laminar region, it is very difficult to predict the behaviour of fluid motion in the turbulent region. One way of observing the flow in turbulent region is to assume that the fluid particles move in groups. The group motion of fluid particles increases the energy and momentum transportations. A larger viscous shear force is observed in the fluid as expected and this larger viscous action causes the flat velocity profile in turbulent flow. Reynolds number is used to determine of which flow regime exists in the fluid and it is defined as;

$$\mathrm{Re} = \frac{\rho u_{\infty} x}{\mu} \tag{1.2}$$

The flow on a flat plate initially starts in laminar region, but at some distance from the leading edge, small disturbances amplify and transition to turbulent flow begins to occur. Fluid fluctuations begin to develop in the transition region, and the boundary layer eventually becomes completely turbulent. In the fully turbulent region, fluid motion is highly irregular and is characterized by velocity fluctuations.

Three different regions may be observed in the turbulent flow regime. There is a *laminar sublayer* where transport is dominated by diffusion and the velocity profile is almost linear. In the *buffer layer*, diffusion and turbulent mixing are comparable and eventually, transport is dominated by turbulent mixing in the *turbulent zone*.

CHAPTER 2

LITERATURE SURVEY

Review of the previous studies about condensation will be presented in this section. The research is mainly based on two subjects; laminar film condensation and the condensation of vapor on a horizontal cylinder.

The analysis of laminar film condensation was first performed by Nusselt [1]. He proposed a simple model of the physical phenomenon which is capable to calculate film thickness and heat transfer coefficient for different geometrical configurations. He neglected the effects of both energy convection and fluid accelerations within the condensate layer and the shear stress at the liquid-vapor interface. Nusselt assumed that flow throughout the film is laminar and only gravity forces are acting on the condensate layer. A simple balance between the gravity and the shear forces was created in the analysis. The gas is assumed to be a pure vapor at a uniform temperature equal to T_{sat}. Heat transfer from vapor to liquid is only carried out by condensation and constant fluid properties are assumed for the liquid film. It is further assumed that a linear temperature distribution exists across the condensate layer.

Dukler [2] developed new equations for velocity and temperature distribution in thin vertical films. Since these equations are too complex for analytical solution, he used numerical solution. The equations he derived utilize the expression proposed by Deissler for the eddy viscosity and eddy thermal conductivity. He calculated average condensing heat transfer coefficients and liquid film thickness from the velocity and temperature distributions. He showed that results are in good agreement with the classical Nusselt's theory at low Reynolds numbers and in the turbulent region, he obtained agreement with the empirical relationships of Colburn for fully developed turbulent flow in the absence of interfacial shear.

Chen [3] investigated laminar film condensation around a single horizontal tube and a vertical bank of horizontal tubes. He considered the inertia effects and assumed the vapor is stationary for the single tube case. Chen found that the inertia forces have a larger effect on the heat transfer of round tubes than flat plates. For the multiple tube case, he neglected the inertia effects and the unpredictable effects of splashing and ripples. He also stated that boundary condition at the top of the lower tubes is largely influenced by the momentum gain and the condensation between tubes. Comparison of heat transfer coefficients with experimental data had been accomplished and the theoretical results were expressed as approximate formulas for both cases.

Sarma et al. [4] studied condensation of vapors flowing with high velocity around a horizontal tube. They considered wall resistance, body force and the shear force due to the external flow of pure vapors as the external forces in the motion of the condensate film. Flow was assumed as turbulent regime in the region away from

the upper stagnation point. Influence of separation point of vapor was neglected. Estimation of the interfacial shear at the interface by applying Colburn's analogy was found to be successful for high velocities of vapor condensing on the condenser tube. The theory developed was also in good agreement with the experimental data of condensation of steam flowing under high velocities and for freon-112.

Karabulut and Ataer [5] presented a numerical method in order to analyze the case where laminar film-wise condensation takes place on a horizontal tube. The pressure gradient, inertia and convective terms in addition to gravity and viscous terms were taken into account in their governing equations. The effect of vapor shear on condensation is mainly investigated and they concluded that separation point is very important since film thickness becomes much thicker due to the disappearing effect of vapor shear at the interface.

Abdullah et al. [6] performed an experimental setup so as to investigate condensation of steam and R113 on a bank of horizontal tubes and the influence of a noncondensing gas. Data were in good agreement with single-tube theory at the top of the bank but were found very lower in the vapor side heat transfer coefficient. Air, which is a noncondensing gas, causes a sharp decrease in the heat transfer coefficient when exists in the vapor.

Sparrow and Gregg [7] dealt with the problem of laminar filmwise condensation on a vertical plate which was studied by Nusselt and Rohsenow before. Nusselt neglected the effects of both energy convection and fluid acceleration in his research. On the other hand, Rohsenow extended Nusselt's research by considering

the effect of energy convection. Sparrow and Gregg started their analysis by including fluid acceleration as well as energy convection which yields to reduce partial differential equations to ordinary differential equations by means of a similarity transformation. The researchers found that inclusion of acceleration terms have a little effect on the heat transfer for Prandtl numbers greater than 1.0 whereas acceleration terms play a more important role for lower Prandtl numbers.

Sparrow and Gregg [8] performed a boundary-layer analysis for laminar film condensation on a single horizontal cylinder. Their study extended Nusselt's simple theory by including the inertia forces and energy convection terms. The starting point of their study is the boundary layer equations appropriate to the horizontal cylinder. They transformed partial differential equations of the boundary layer equations to ordinary differential equations which are valid over a major portion of the cylinder. The transformation they made coincide resulting ordinary differential equations with those for condensation on a vertical flat plate. Utilizing numerical solutions of the transformed equations, heat transfer results were presented for the horizontal cylinder over the Prandtl number range from 0.003 to 100.

Denny and Mills [9] obtained an analytical solution based on the Nusselt assumptions for laminar film condensation of a flowing vapor on a horizontal cylinder. They had shown that the proposed analytical solution and the Nusselt assumptions are in good agreement for ϕ, the angle measured from the vertical axis, less than 140 deg. In a typical situation 85 percent of the total condensation occurs when ϕ is less than 140 deg.

Fujii and Uehara [10] developed two-phase boundary layer equations of laminar filmwise condensation with an approximate method. It was found that the effects of forced and body force convection are dominant near the leading edge and far from it respectively, the limit values of the solutions for the case of body force convection only and forced convection only coincide with respective similarity solutions within the accuracy of a few percent.

The condensation of vapor on a laminar falling film of the liquid coolant was investigated by Rao and Sarma [11] and it was reported that the dynamics of the falling film has an important effect on the condensation heat transfer rates and that direct contact condensers with shorter coolant film lengths would be more effective in terms of condensation heat transfer rates than those calculated by Nusselt analysis.

Hsu and Yang [12] analyzed the effects of pressure gradient and variable wall temperature for film condensation occurring on a horizontal tube with downward flowing vapors. Authors stated that the mean heat transfer coefficient is slightly increasing with the wall temperature variation amplitude, A, when the pressure gradient effect is not accounted whereas the mean heat transfer coefficient considerably decreases with A when the pressure gradient effect is included and increases. Furthermore, the mean heat transfer coefficient is almost unaffected from the pressure gradient for the lower vapor velocity and for the higher vapor velocity, the mean heat transfer coefficient decreases considerably with increasing the pressure gradient effect.

Mosaad [13] studied combined free and forced convection laminar film condensation on an inclined circular tube. Some approximations have been obtained for the evaluation of the interfacial shear stress. The effects of vapor velocity and gravity forces on local and mean Nusselt numbers were investigated by the mean of a numerically obtained solution. He also formulated an explicit simple expression to calculate the mean Nusselt number for an inclined tube with infinite length.

Kumar et al. [14] performed an experimental investigation to find out the behaviour of the condensing side heat transfer coefficient h_o, over a plain tube; a circular integral-fin tube (CIFT) and a spine integral-fin tube (SIFT). It was concluded that CIFT and SIFT have an enhancement on the condensing side heat transfer coefficient by a factor of 2.5 and 3.2, respectively. Besides, SIFT offers about 30 percent more enhancements in h_o with respect to CIFT.

Memory et al. [15] investigated laminar film condensation on a horizontal elliptical tube for free and forced convection. Even though a simple Nusselt type analysis was used for free convection, interfacial shear stress for forced convection was estimated in two ways: 1-Under infinite condensation rate conditions, asymptotic value of the shear stress was used. 2-Two phase boundary-layer and condensate equations were solved simultaneously. The study included the effects of surface tension and pressure gradient. About 11% improvement in the mean heat transfer coefficient was obtained for an elliptical tube with respect to a circular tube for free convection whereas 2 % decrease in the mean heat transfer coefficient had been seen for forced convection.

Browne and Bansal [16] presented a review paper about condensation heat transfer on horizontal tube bundles particularly for shell-and-tube type condensers. They reviewed over 70 papers published on the subject of condensation and concluded followings:

1. Surface geometry is a very important issue on the condensing side heat transfer coefficients.

2. Condensate inundation substantially affects tubes with three dimensional fins first, smooth tubes second and finally integral-fin tubes.

3. Enhancement due to vapor shear on smooth tubes is greater than that on integral-finned tubes.

4. By means of overall heat transfer coefficient, coolant velocity has a large effect for enhanced tube surfaces whereas minimal effect for smooth tubes.

Lee [17] recomputed the heat transfer coefficients for turbulent Nusselt's model. However his formulation includes turbulent transports in the form of eddy diffusivity as different from Nusselt. Although he found that the increased heat transfer coefficients for ordinary fluids are in conformity with the experimental data, the physical model was to be improved for the liquid metals. For the small Prandtl numbers, Lee stated that Dukler's results are unacceptable.

Koh [18] studied laminar film condensation on a flat plate under forced flow. He formulated the problem as an exact boundary-layer solution. It was concluded that the energy transfer by convection is negligibly small for liquids with low Prandtl number (liquid metals) and thus heat transfer decreases monotonically as liquid film

thickness increases. For liquids with high Prandtl number energy transfer by convection is not to be neglected.

A condensation on horizontal tube study was carried out by Lee and Rose [19] under forced convection with and without non-condensing gases. An experimental setup was constructed to investigate the condensation phenomena of pure vapors and vapor-gas mixtures. Results collected from the experiments were demonstrated on the graphics and compared with those from different researchers.

Rose [20] investigated how pressure gradient in film condensation onto a horizontal tube plays a role over condensing heat transfer coefficient. The pressure gradient term becomes important when $\theta = \frac{\rho g d}{8 \rho_g U_\infty^{\ 2}}$ is significantly less than unity. According to author, inclusion of the pressure gradient term has two effects: i) it increases the heat transfer coefficient over the forward part of the tube, especially for the refrigerants. ii) when $\theta < 1$, it makes the condensate film unstable at some location down to the tube.

Kutateladze and Gogonin [21] prepared test sections to investigate the condensation of flowing vapor onto horizontal tube banks. R12 and R21 were used in the experiments and the results were compared with the previous works. The results indicated that the heat transfer in condensation on tube banks depends only on the condensate flow rate when the vapor velocity is low.

Kutateladze and Gogonin [22] also investigated the influence of condensate flow rate on heat transfer in film condensation. Condensation of quiescent vapor on the banks of horizontal smooth tubes of different diameters was analyzed. It was pointed out that vapor condensation on supercooled drops and discrete liquid streamlets contributes to heat transfer at Re > 50 and both Reynolds number and the diameter of the cylinder have a considerable effect on the starting length of the thermal boundary layer.

Churchill [23] extended the classical solution of Nusselt for laminar film condensation by considering the effects of the sensible heat and inertia of the condensate, drag of the vapor and the curvature of the surface. The solutions were given in closed form, hence algebraic equations were also provided that can be solved by iteration. These solutions give very accurate results for large Pr but they are poor for small Pr numbers. It was reported that the effect of curvature increases the rate of heat transfer significantly.

Chen and Hu [24] presented a study which investigated turbulent film condensation on a half oval body employing the model of Sarma et al. [3]. Vapor boundary layer separation of vapor around the condensation film and surface tension effect were neglected. A discussion of heat transfer characteristics, influence of Froude number and system pressure on mean Nusselt number was carried out in the study.

Rose [25] developed approximate equations for condensation from a vapor-gas mixture flowing parallel to a horizontal surface and normal to a horizontal tube. The

equations are conceived to be correct for the limiting cases of zero and infinite condensation rate. Results are in good agreement with the previous studies covering a wide range of condensation rates and for various of Schmidt number for the flat plate case. The results concerning horizontal cylinder case also agree with experimental data for steam-air mixtures covering wide ranges of velocity, composition, condensation rate and pressure.

An experimental study about condensation of flowing vapor on a horizontal cylinder was carried out by Kutateladze and Gogonin [26]. It was found that the friction on the vapor-film interface, which determines the film thickness and thereby the condensation heat transfer of flowing vapor depends appreciably on the magnitude of the cross flow of substance.

Fujii et al. [27] performed an experiment based on low pressure steam condensation through tube banks. They proposed pressure drops through tube banks and simple relationships for steam side heat transfer coefficients. Resistance coefficients were represented graphically. In-line and staggered arrangement tube banks were compared to each other, temperature distribution of tube surface and accumulation of leaked air were also reported in this study.

CHAPTER 3

ANALYTICAL MODEL

The condensation of steam over a vertical tier of horizontal tubes is investigated by both analytical and experimental methods during this study. An analytical model has been developed with the help of the lecture notes of Arpacı [32]. Two equations, which are obtained by applying the principles of conservation of mass and conservation of momentum on the condensate layer, are transformed into the finite difference forms. Thus, the problem is turned to a state that can be solved by the computer. A computer program, which uses the Newton-Raphson method, has been implemented in order to analyze the problem. The program gives the film thickness and the velocity distribution of the condensate for each condensation tubes.

3.1 Governing Equations

The theoretical approach to laminar film condensation is developed from conservation of mass and conservation of momentum principles which are applied to the condensate. Some assumptions should be made before starting the analysis [1]:

- Laminar flow and constant properties are assumed for the film.
- The vapor is at uniform temperature.
- Heat transfer from vapor to liquid is only carried out by condensation.
- The shear stress at the liquid-vapor interface is assumed to be negligible in which case $\left.\frac{\partial u}{\partial y}\right|_{y=\delta} = 0$
- Heat transfer through the condensate film occurs only by conduction. Therefore, temperature distribution in the film is linear.
- Only gravity forces are acting on the condensate.

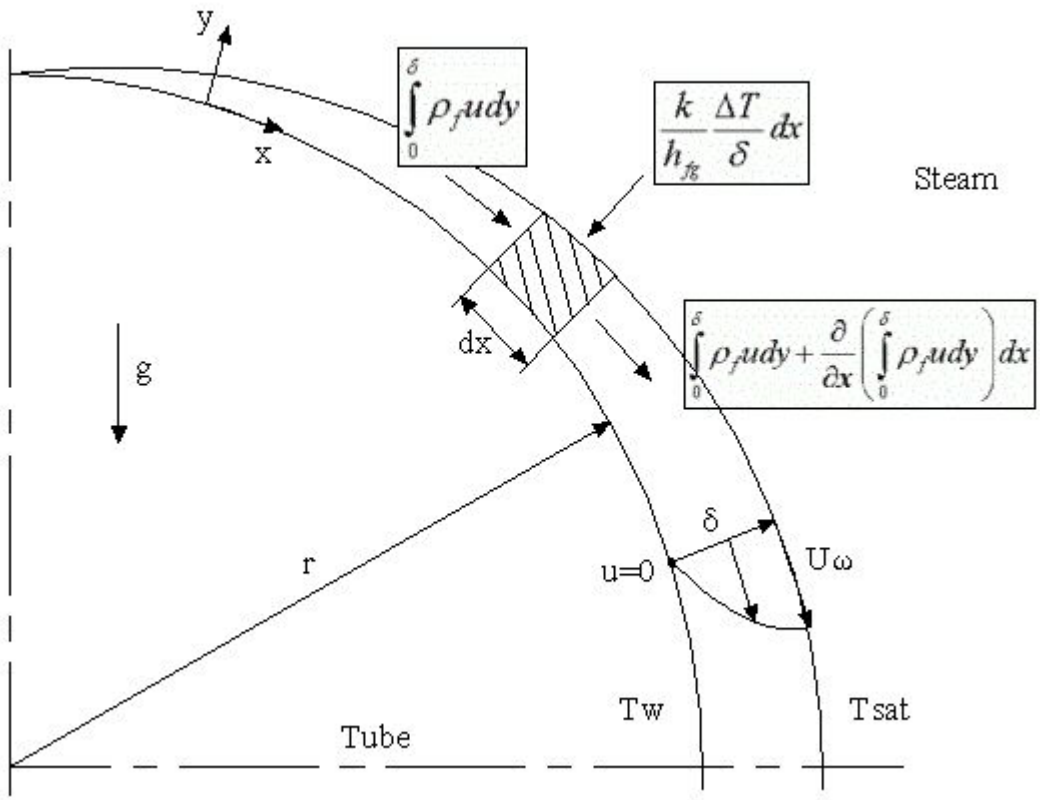

Figure 3.1 Physical Model and Coordinate System

The definition of the problem on the sketch is given in Figure 3.1. The condensate film begins to form at the top of the condensation tube. Film thickness increases while the condensate flows down on the tube as the steam condenses over them.

The velocity profile is expressed in terms of free stream velocity, condensate film thickness and the distance from the wall [32]:

$$u = U_{\infty}\left[\frac{3}{2}\left(\frac{y}{\delta}\right) - \frac{1}{2}\left(\frac{y}{\delta}\right)^{3}\right] \tag{3.1}$$

Boundary conditions satisfying this equation are:

$$At \quad y = 0, \quad x \geq 0: \qquad u = 0\,, \qquad \frac{\partial^2 u}{\partial y^2} = 0$$

$$At \quad y = \delta, \quad x \geq 0: \qquad u = U_{\infty}\,, \qquad \frac{\partial u}{\partial y} = 0$$

The analysis is started by taking an integral control volume within the condensate film. If the conservation of mass principle is applied on the control volume as depicted in Figure 3.1:

$$\int_0^{\delta} \rho_f u dy + \frac{k}{h_{fg}}\frac{\Delta T}{\delta} dx = \int_0^{\delta} \rho_f u dy + \frac{\partial}{\partial x}\left(\int_0^{\delta} \rho_f u dy\right) dx \tag{3.2}$$

$$\frac{d}{dx}\left(\int_0^{\delta} \rho_f u dy\right) = \frac{k}{h_{fg}}\frac{\Delta T}{\delta} \tag{3.3}$$

Since only conduction type heat transfer mechanism and unit depth are assumed at the beginning of the analysis, heat transfer at the wall in the area dx is

$$q = -kdx \left.\frac{\partial T}{\partial y}\right|_{y=0} = kdx \frac{T_{sat} - T_w}{\delta} \tag{3.4}$$

Heat transfer rate can be expressed in terms of the mass flow of the condensate through any x position of the film and the latent heat of condensation of steam. Thus

$$q = \dot{m} h_{fg} \tag{3.5}$$

The second term in the Equation 3.2 can be readily obtained by equalizing Equation 3.4 and Equation 3.5:

$$\dot{m} = \frac{k}{h_{fg}} \frac{\Delta T}{\delta} dx \tag{3.6}$$

Recalling Equation 3.1 and substituting it into Equation 3.3:

$$u = U_\infty \left[\frac{3}{2}\left(\frac{y}{\delta}\right) - \frac{1}{2}\left(\frac{y}{\delta}\right)^3 \right]$$

$$\frac{d}{dx}\left(\int_0^\delta U_\infty \left[\frac{3}{2}\left(\frac{y}{\delta}\right) - \frac{1}{2}\left(\frac{y}{\delta}\right)^3 \right] dy \right) = \frac{k}{\rho_f h_{fg}} \frac{\Delta T}{\delta} \tag{3.7}$$

Solving the integral for y:

$$\frac{5}{8}\frac{d}{dx}\left(\delta U_{\infty}\right)-\frac{k}{\rho_f h_{fg}}\frac{\Delta T}{\delta}=0 \tag{3.8}$$

There are two unknowns in this equation and one more equation is needed to solve the problem. The required equation can be obtained from the conservation of momentum principle. Therefore:

$$\frac{d}{dx}\left(\int_0^{\delta}\rho_f u^2 dy\right)-\rho_f \delta f_x+\tau_s\Big|_{y=0}=0 \tag{3.9}$$

f_x is body force and it is defined in terms of gravity force in this problem. For the condensate around a cylinder:

$$f_x = g\sin\theta \tag{3.10}$$

As gravity force drags the condensate downward, shear force of the condensate layer resists to retard the motion of the condensate. The shear stress in Equation (3.9) may be expressed with Newton's law of viscosity:

$$\tau_s = \mu\frac{du}{dy}\Big|_{y=0} \tag{3.11}$$

Substituting u from Equation 3.1 and taking the derivative, one can obtain:

$$\tau_s = \frac{3}{2}\mu\frac{U_\infty}{\delta} \tag{3.12}$$

As it is done in the conservation of mass principle, similarly recalling Equation 3.1 and integrating Equation 3.9:

$$\frac{17}{35}\rho_f\frac{d}{dx}\left(\delta U_\infty{}^2\right) - \delta\rho_f g\sin\theta + \frac{3}{2}\mu\frac{U_\infty}{\delta} = 0 \tag{3.13}$$

3.2 Method of Solution

Initial values are needed for condensate film thickness and velocity distribution to start the iteration. These initial values can be derived from Nusselt's original theory. Film thickness for a vertical flat plate is given by Nusselt's theory as [1]:

$$\delta(x) = \left[\frac{4k_f\mu_f\left(T_{sat} - T_w\right)x}{g\rho_f\left(\rho_f - \rho_v\right)h_{fg}}\right]^{1/4} \tag{3.14}$$

Neglecting the density of vapor since it is very small compared to the density of the fluid and taking the curvature of the cylinder into consideration, the following expression is obtained for the film thickness [1]:

$$\delta(x) = \left[\frac{3\nu k_f (T_{sat} - T_w) x}{g \rho_f h_{fg} \sin\left(\frac{x}{r}\right)} \right]^{1/4} \tag{3.15}$$

The velocity profile in the film is [1]:

$$u(y) = \frac{g(\rho_f - \rho_v)\delta^2}{\mu_f} \left[\frac{y}{\delta} - \frac{1}{2}\left(\frac{y}{\delta}\right)^2 \right] \tag{3.16}$$

Initial velocity distribution along the liquid-vapor interface can be obtained substituting δ into Equation 3.16:

$$U_\infty = \frac{g \rho_f \delta^2}{2\mu_f} \tag{3.17}$$

It is necessary to transform ordinary differential equations into the finite differences to solve Equation 3.8 and Equation 3.13 simultaneously. Hence, Equation 3.8 yields:

$$\frac{5}{8} \frac{(\delta_i U_{\infty i} - \delta_{i-1} U_{\infty i-1})}{\Delta x} - \frac{k}{\rho_f h_{fg}} \frac{\Delta T}{\delta_i} = 0 \tag{3.18}$$

and Equation 3.13 yields:

$$\frac{17}{35}\rho_f\left(\frac{\delta_i\left(U_{\infty i}\right)^2-\delta_{i-1}\left(U_{\infty i-1}\right)^2}{\Delta x}\right)-\delta_i\rho_f g\sin\theta+\frac{3}{2}\mu\frac{U_{\infty i}}{\delta_i}=0 \tag{3.19}$$

Newton-Raphson method will be used to solve the equations given above.

$$x_{i+1}=x_i-\frac{f\left(x_i\right)}{f'\left(x_i\right)} \tag{3.20}$$

As matrix C corresponds to $f(x_i)$, matrix Ψ corresponds to derivative of the function at x_i. Numerical derivation is used instead of analytical derivative in Equation 3.20. δ and U_∞ variables are increased with δ_{inc} and U_{inc} increments, subtracted from their original states and divided by corresponding increment. Ψ matrix is two by two square matrix and it is constituted as:

$$\psi_{(0,0)}=\frac{\left[\frac{5}{8}\frac{\left(\delta_i+\delta_{inc}\right)U_{\infty i}-\delta_{i-1}U_{\infty i-1}}{\Delta x}-\frac{k_f\Delta T}{\rho_f h_{fg}\left(\delta_i+\delta_{inc}\right)}\right]\cdots-\left[\frac{5}{8}\frac{\delta_i U_{\infty i}-\delta_{i-1}U_{\infty i-1}}{\Delta x}-\frac{k_f\Delta T}{\rho_f h_{fg}\delta_i}\right]}{\delta_{inc}} \tag{3.21}$$

$$\psi_{(0,1)}=\frac{\left[\frac{5}{8}\frac{\delta_i\left(U_{\infty i}+U_{inc}\right)-\delta_{i-1}U_{\infty i-1}}{\Delta x}\right]-\left[\frac{5}{8}\frac{\delta_i U_{\infty i}-\delta_{i-1}U_{\infty i-1}}{\Delta x}\right]}{U_{inc}} \tag{3.22}$$

$$\psi_{(1,0)} = \frac{\left[\frac{17}{35}\rho_f \frac{(\delta_i+\delta_{inc})(U_{\infty i})^2 - \delta_{i-1}(U_{\infty i-1})^2}{\Delta x} - (\delta_i+\delta_{inc})\rho_f g\sin\theta + \frac{3}{2}\mu\frac{U_{\infty i}}{(\delta_i+\delta_{inc})}\right]\cdots - \left[\frac{17}{35}\rho_f \frac{\delta_i(U_{\infty i})^2 - \delta_{i-1}(U_{\infty i-1})^2}{\Delta x} - \delta_i\rho_f g\sin\theta + \frac{3}{2}\mu\frac{U_{\infty i}}{\delta_i}\right]}{\delta_{inc}} \tag{3.23}$$

$$\psi_{(1,1)} = \frac{\left[\frac{17}{35}\rho_f \frac{\delta_i(U_{\infty i}+U_{inc})^2 - \delta_{i-1}(U_{\infty i-1})^2}{\Delta x} - \delta_i\rho_f g\sin\theta + \frac{3}{2}\mu\frac{U_{\infty i}+U_{inc}}{\delta_i}\right]\cdots - \left[\frac{17}{35}\rho_f \frac{\delta_i(U_{\infty i})^2 - \delta_{i-1}(U_{\infty i-1})^2}{\Delta x} - \delta_i\rho_f g\sin\theta + \frac{3}{2}\mu\frac{U_{\infty i}}{\delta_i}\right]}{U_{inc}} \tag{3.24}$$

The method has been iterated 20 times to approach as possible as to the exact values. After obtaining the value of change in the variables by multiplying the inverse of matrix Ψ with matrix C, variables are updated by adding the value of change to the previous iteration.

Once iterations are completed for the first tube, film thickness and velocity values falling from the tube are taken and updated for the second tube by using Bernoulli equation.

The condensate falling down to the second tube can be thought as a second layer above the film thickness, δ. The velocity profile of this layer is uniform. As condensate flows downward around the cylinder, the thickness of the second layer (Δ) goes to zero as seen in Figure 3.2. The analysis is normally carried out after this merge point of two condensate layers.

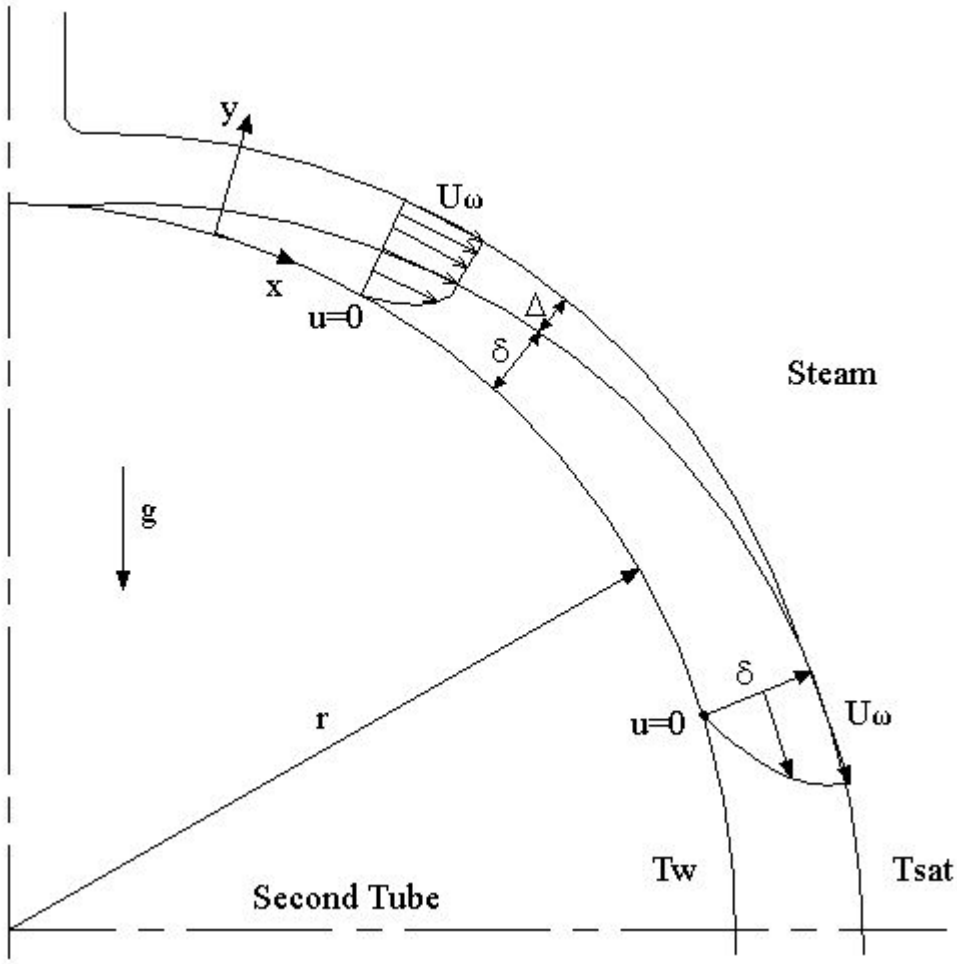

Figure 3.2 Physical Model for the Lower Tubes

CHAPTER 4

EXPERIMENTAL STUDY

Experimental investigation of this study was carried out in the heat transfer laboratory at the Mechanical Engineering Department of METU. Some parts of the apparatus were constructed by earlier researchers. A test section which has been newly designed to investigate film condensation on a vertical tier of horizontal tubes was manufactured in Bursa and mounted on the existing apparatus.

Even though there is no need for some parts of the setup in this study, such as a shaft driven by a pulley connected to an electric motor by a belt and a cylindrical electrical connections unit, no parts of the apparatus is disassembled since we would like to protect the integrity of the setup for future researches about condensation under high centrifugal forces. Therefore, basic components of the setup are as follows excluding unnecessary parts:

- Cooling water tank with electric heater to supply water at any temperature.
- Boiler in order to generate steam.
- Test section which is connected to the frame.
- Temperature measurement system.

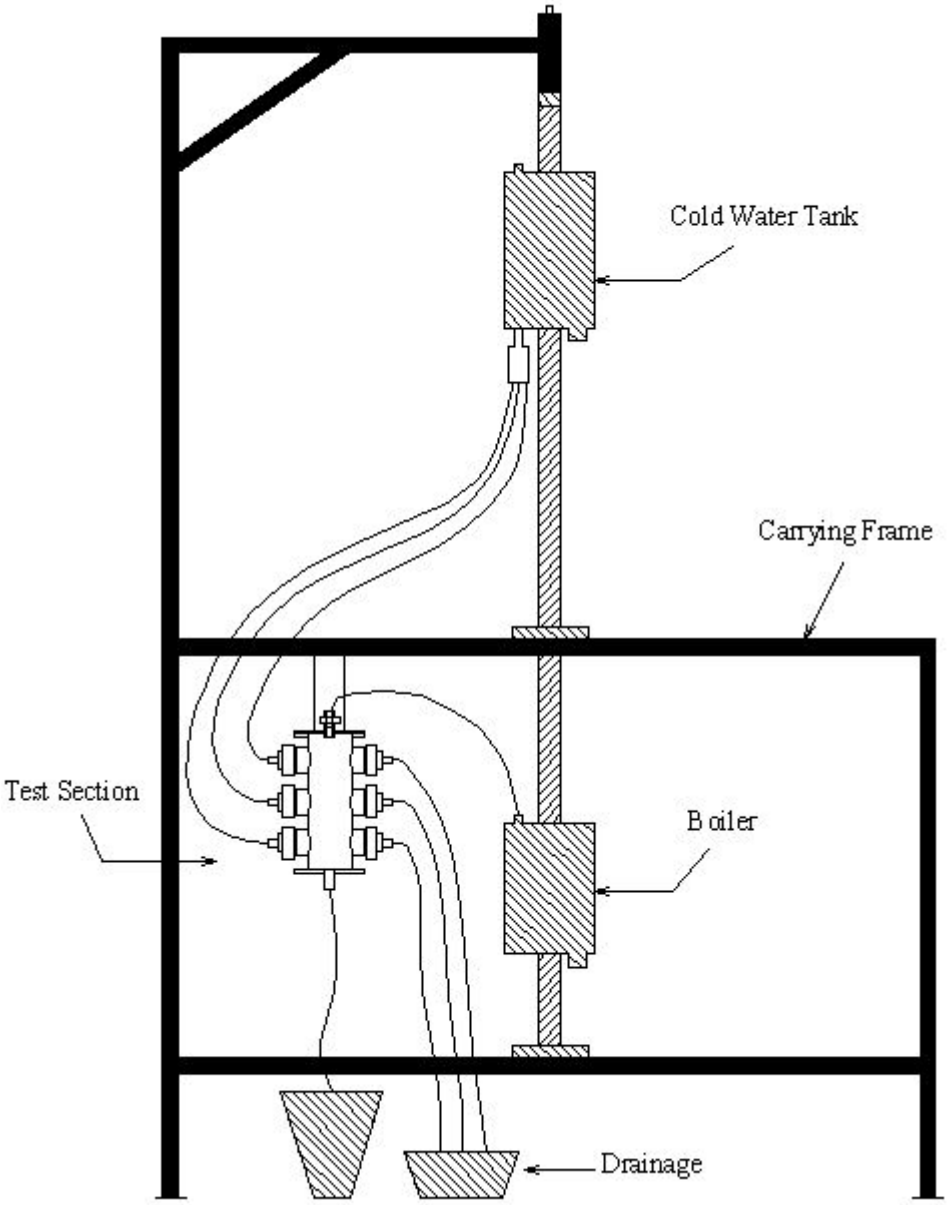

Figure 4.1 Schematic Representation of the Apparatus

4.1 Cooling Water Tank

As the steam flows down to the horizontal tubes and condenses over them, a big amount of heat is transferred from the steam to the tubes which causes temperature increase. In order to keep temperature of the horizontal tubes constant, it is necessary to continuously supply cold water at constant temperature. For this reason, a cold water tank is placed around the shaft and above the test section to provide water flows downward to condensation tubes by the gravity. The dimensions of the tank are 50 cm of height, 30 cm of outer diameter and 9 cm of inner diameter. The tank is filled from the inlet at the top and the water that has been heated up to desired temperature is taken from the bottom exit via a valve connected between the tank and the test section.

A small apparatus has been prepared in order to supply cooling water at equal flow rates and it is shown schematically in Figure 4.2. Water is split into three ways after it comes into the apparatus. Three small valves have been also provided for the hoses to adjust the flow rates since the altitudes of horizontal tubes are different.

An electric heater with 2 kW of heating capacity is located at the bottom of the tank and it is connected to city electric network by well insulated and grounded cables. Another cable is connected to the metal frame of the apparatus to prevent electric shocks just in case an electric short exists.

The tank is well insulated to prevent heat losses as much as possible and it is connected to the shaft strictly by welding.

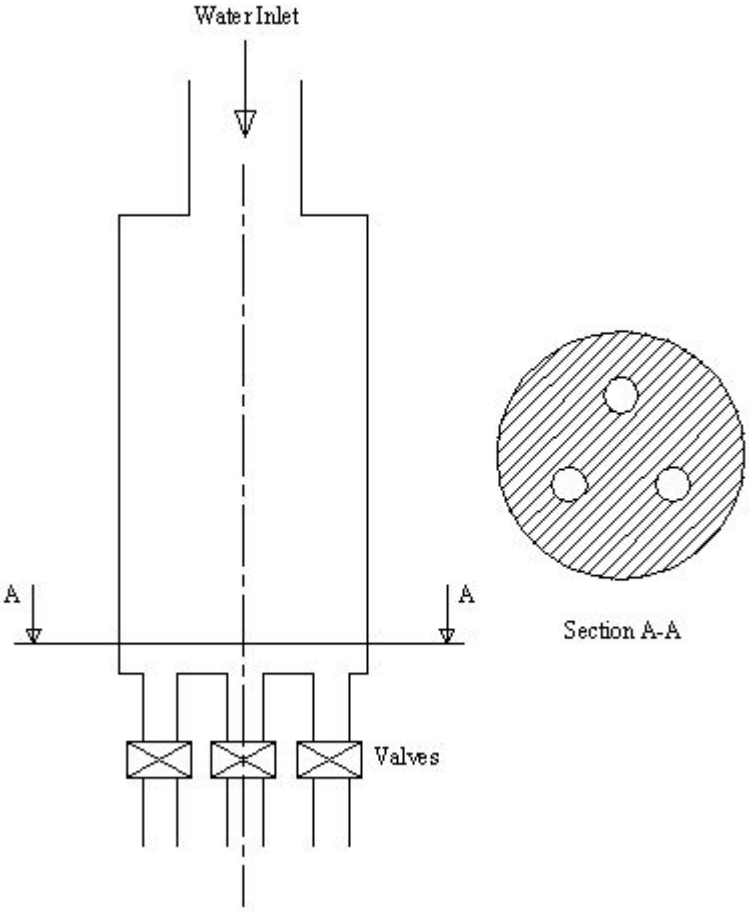

Figure 4.2 Water Division Apparatus

4.2 Boiler

Steam is generated in a boiler and sent to the test section via a high temperature resistant hose from the steam exit at the topside. The boiler is made of stainless steel. It is insulated with climaflex in order to minimize heat losses. Dimensions of the boiler are 40 cm of height, 30 cm of outer diameter and 9 cm of inner diameter.

Distilled water is used to generate steam in the experiments and it is evaporated by a heater which is connected to boiler from bottom side. The electric heater has a

power of 2 kW. Mass flow rate of steam can be arranged by a variac (variable transformer) which is located between the heater and city electric network.

4.3 Test Section

Test section was manufactured in a workshop in Bursa by using an electro-erosion machine and a lathe. The main body of the test section is stainless steel pipe which is 70 mm in diameter. Three horizontal condensation tubes should be placed in a vertical tier across the main pipe with 5 cm of intervals as shown in Figure 4.4. Stainless steel is chosen in the production of the test section in order to prevent corrosion effects of water. Stainless steel is a harder material than ordinary steel. Hence, its manufacture processes require special equipments and attention. To insert the horizontal tubes inside the main pipe, it is required to prepare two coaxial holes across the main pipe. Since the wall thickness of the main pipe is small, it is almost impossible to drill it by using traditional drill techniques, by providing that the holes have the same horizontal axis and without damaging the main pipe. Hence, it is decided to use electro-erosion machine to drill the main pipe in order to keep drill axis in its position and not to damage the pipe. Electro-erosion machines use the principle of eroding the material by removing the electrons from the surface with a high conductive electrode, such as copper. A copper electrode of 38 mm in diameter is prepared to accomplish this task. The electrode is then mounted on the EDM (Electric Discharge Machine which is synonymous with electro-erosion machine) and running the machine, the coaxial holes are obtained on the main pipe. After obtaining three horizontal coaxial hole couples on the main pipe, six pieces of inner threaded stainless steel metal rings are welded on the holes.

During the welding process, since it is reached to very high temperatures, undesired deformations on the material may occur. A gauge which fits inside the metal rings is prepared and screwed into the metal rings to prevent deformations on the material. A section view of the gauge and the metal rings is shown in Figure 4.3. After the welding process is completed and the material gets cold, the gauge is unscrewed from the metal rings. This process is repeated for each of the three horizontal hole couples.

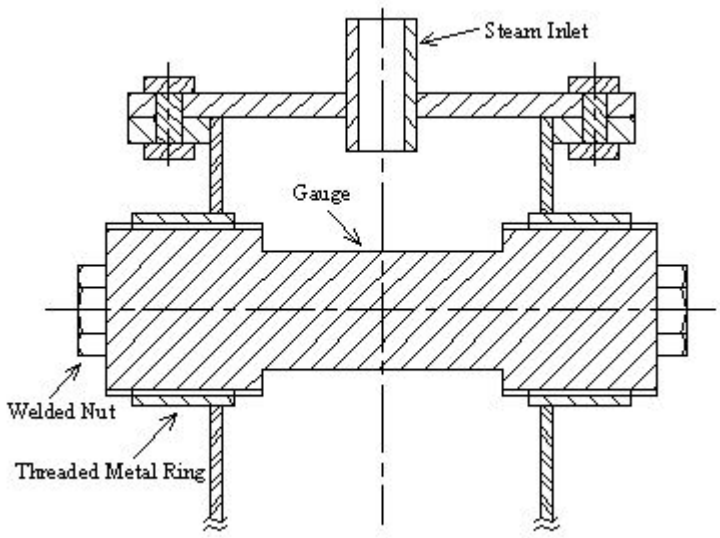

Figure 4.3 Drawing of the Gauge and the Metal Rings

The condensation tubes have 17 mm inner diameter and 19 mm outer diameter. They should be compressed from the both ends by Delrin to make sure they stay in their positions. Delrin is a highly versatile engineering plastic with metal-like properties made by Dupont [31]. It further provides thermal insulation benefits. Delrin connection apparatus is prepared by using a lathe to provide that the outer surface of the cylindrical apparatus can be tightly screwed into the metal rings which were welded on the main pipe before. While one end of Delrin apparatus is

connected to a horizontal condensation tube, the other end will connect to cooling water hose. Therefore, different sizes of holes are needed for both ends. Using the appropriate drills, required holes are bored inside the Delrin apparatus. The condensation tube is placed between the two Delrin apparatus by using seals and liquid gasket in order to prevent steam leakage to the cooling water.

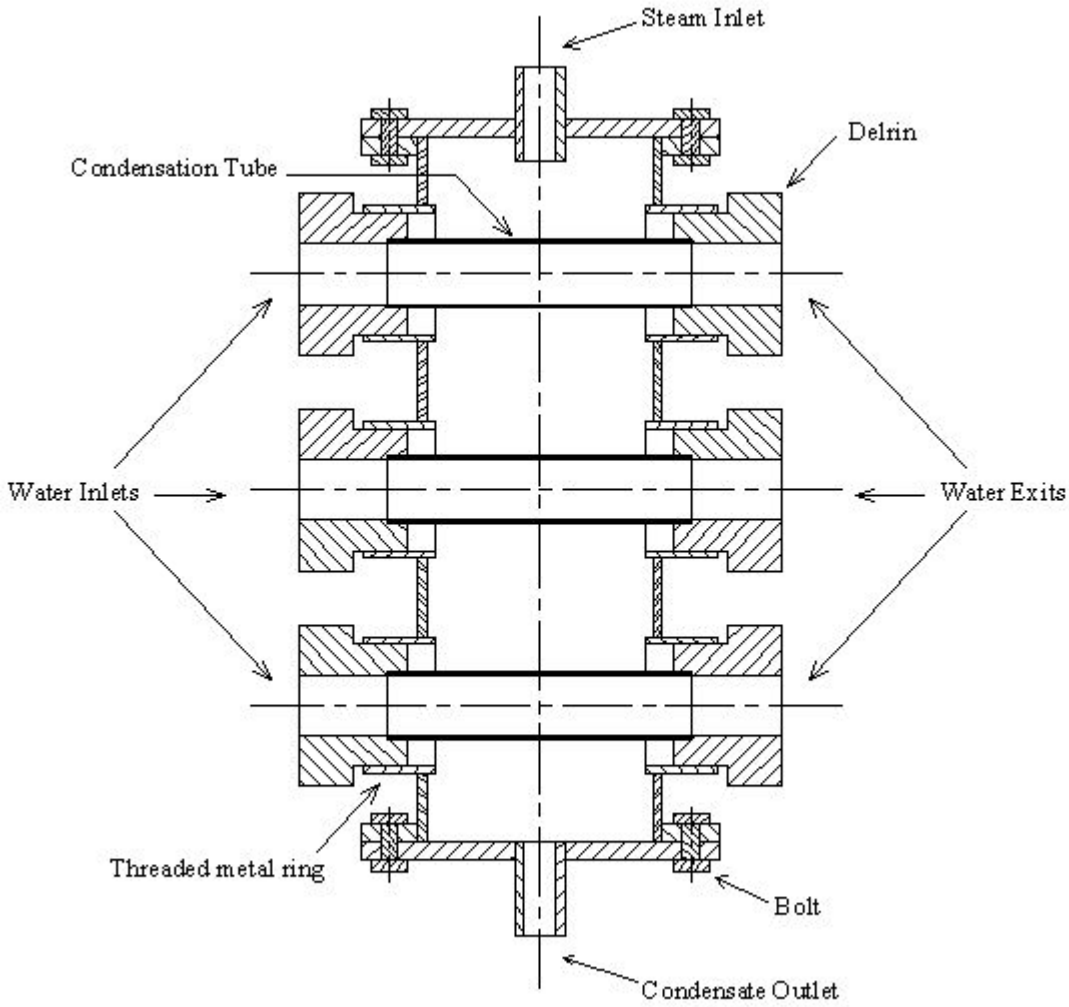

Figure 4.4 Drawing of the Test Section

Two flanges are welded on both ends of the test section. During all the welding processes throughout the manufacture, specially designed electrodes for the stainless

steel are used. Two caps are mounted on the flanges with eight bolts and a rubber seal in order to reach inside the setup whenever it is needed. The center of the top cap is drilled and a connector is placed and welded on this hole so as to provide a connection between the test section and the boiler. The high temperature resistant hose, which comes from the boiler, is fastened to the connector. The center of the bottom cap is also drilled and a pipe is welded here to make the condensate flows out of the setup. The whole test section is covered with an insulation material in order to prevent undesired condensation of steam on the inner surfaces of the setup.

4.4 Temperature Measurement System

The installation of thermocouples has been carried out in the heat transfer laboratory. T type copper-constantan thermocouples are located on ten different positions of the setup in order to get temperature measurements. Three thermocouples are stuck on the middle outer surfaces of the horizontal condensation tubes to measure the wall temperature (T_w) of the tubes. Before the thermocouples are stuck, a hole is bored on the middle surface of the test section to take them out of the setup as it is seen in Figure 4.6. In order to prevent undesired effects of the steam, thermocouples are covered by a protective sheath. Thermocouples are stuck on the condensation tubes by a very strong adhesive, named Sun-Fix which is produced for this kind of special applications. Once it is applied, three hours are needed for a proper merging.

As three of the thermocouples are placed on the entrances of cooling water, three of them are placed on the exits as well, in order to get cold water inlet and outlet temperatures (T_{in} and T_{out}). The last thermocouple is located at the inlet of the

steam to the test section to find out the steam temperature, T_s. The layout of the thermocouples is shown in Figure 4.5.

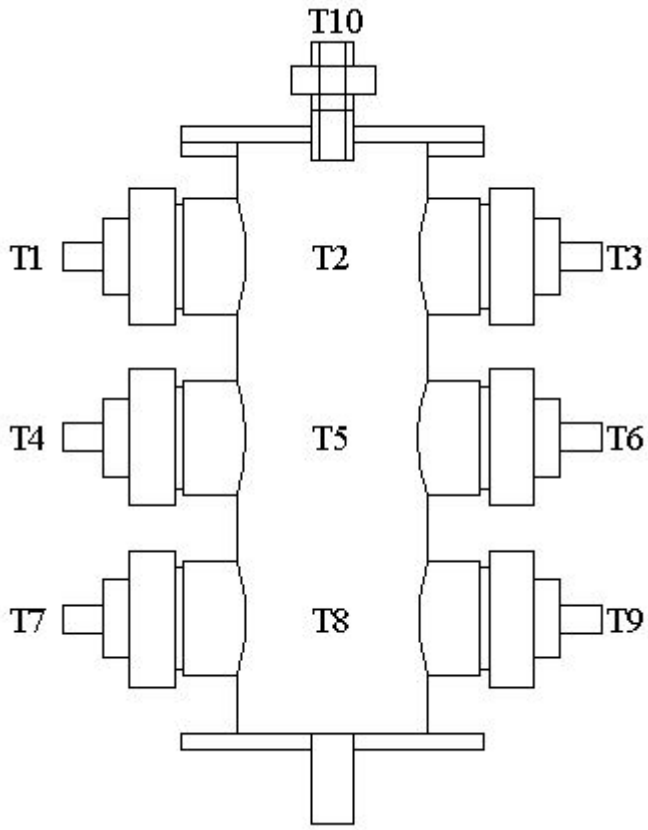

Figure 4.5 Thermocouple Layout

The other ends of the thermocouples are connected to a thermocouple reader which is manufactured by Cole-Parmer Instrument Co. It provides input for 12 thermocouple probes, each connected to a separate channel but all thermocouples must be of the same type. The instrument can show the results in Fahrenheit or Celsius temperature scales and its display resolution is 0.1°.

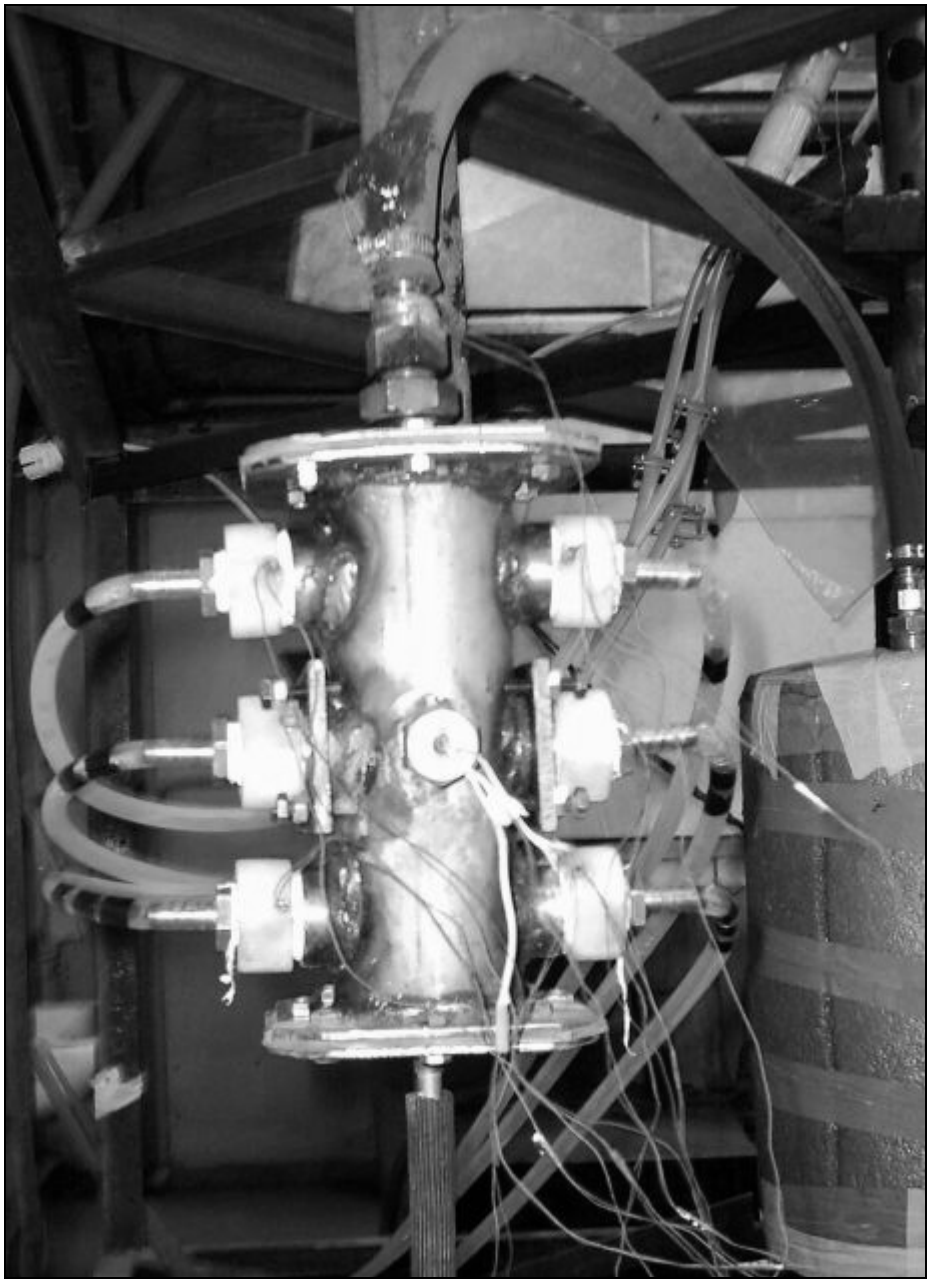

Figure 4.6 General View of the Test Section

4.5 Experimental Procedure

The purposes of the experiments are to find out the amount of heat transfer rate from steam to cold water and the heat transfer coefficient of the condensate layer. As the steam condenses on the horizontal tubes, the energy in the latent heat form is released from the steam to cold water. Since this energy given by the steam is equal to the energy taken by the cold water, heat transfer coefficient can be obtained from the equality below:

$$Q = \dot{m}C_p\left(T_{out} - T_{in}\right) = h_{cond}A\left(T_{sat} - T_w\right) \tag{4.1}$$

Experiments are performed in three different stages:

1. Condensation phenomenon on multiple horizontal tubes has been investigated at different inclination angles of the setup. The reason of inclining the setup is to see how condensation is affected at the lower tubes when condensate does not fall onto the center line of the tubes. Experiments of this stage have been achieved for 0°, 3°, 6°, 10° and 15° of inclination angles. The schematic drawings of condensate behaviour at different angles are given in Appendix A. The inclination angle, which ensures that the condensate spilling from the upper tube does not fall onto the lower tubes, is determined as 15° in the computer environment. The results of the experiments made with this angle show that the heat transfer rates of three condensation tubes are very close to each other. Therefore, the angle assumed at the beginning of the experiments is verified.

The other angles are determined by dividing the angle interval evenly considering the situation of the condensate's fall.

2. Additional flow delimiters are placed into the setup to narrow the flow area of the steam. The idea behind this stage is to improve the condensation phenomenon as the steam is forced to flow in narrower section. Thus, the sweep effect of the steam on the condensate layer has been increased, resulting the film thickness of the condensate decreases. A schematic representation of this stage is depicted in Figure 4.7.

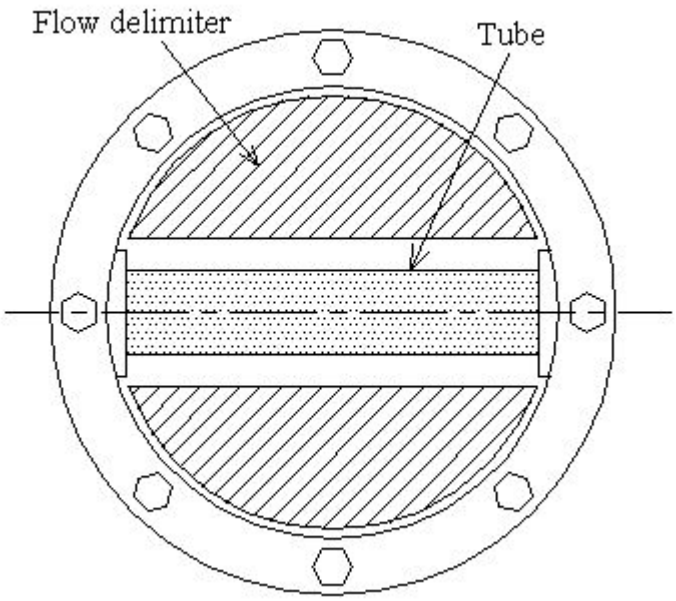

Figure 4.7 Top View of the Test Section with Flow Delimiters

3. The condensation tube in the middle and the flow delimiters are removed from the setup. Hence, the distance between two horizontal tubes is increased resulting splashing and attenuation effects of the condensate are increased.

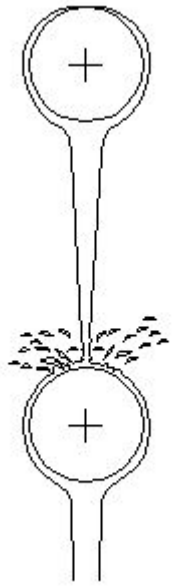

Figure 4.8 Demonstration of the Stage 3

Experiments start with turning on the heater of the boiler. The heater of the cold water tank may be initiated depending on the cooling water temperature desired by the experiment. As soon as cooling water temperature reaches to desired value, the heater is plugged out. Meanwhile, boiler is about to begin sending the steam to the setup. A certain period of time is waited for the test section to be purged and free of air. After the test section is filled up with steam, the valve of the cooling water tank is opened and the water flows down to the horizontal condensation tubes. Cooling water flow rate is determined by measuring the time for filling out a predefined vessel. After the system has stabilized, data recording is commenced.

The varying factor of the experiments is the cooling water temperature value. Surface temperature of the condensation tubes changes by adjusting the cold water temperature. Variac is used to control the steam flow rate in some experiments. The data tables obtained from the experiments are given in Appendix B.

CHAPTER 5

RESULTS AND DISCUSSIONS

The results are discussed in three categories; analytical results, experimental results and the comparison of results. Film thickness, velocity of the condensate, heat flux and heat transfer coefficient are studied by means of the computer program prepared. Furthermore, the effects of tube diameter and temperature difference between steam and the tube wall on the heat transfer in condensation are also discussed. The results of the experiments which were conducted at three different stages that are described in Chapter 4 are graphically presented. Experimental results are compared with the results in the literature as well as with the analytical results of this study.

5.1 Analytical Results

A computer code in Mathcad has been implemented for the analysis of film condensation of steam. It is based on the theoretical model which is developed to calculate film thickness and velocity distribution in the condensate film. Thermophysical properties and geometric dimensions are defined at the beginning of the program. By changing the thermophysical properties, it is possible to examine

condensation phenomenon on a vertical tier of three horizontal tubes for various working fluids. The fundamental geometric parameter is the diameter of the tubes. The effect of the tube diameter on the film thickness, velocity of the condensate, heat flux and heat transfer coefficient will be discussed. The analytical results which are obtained at different tube diameters will be used to study the effect of tube diameter on condensation heat transfer. Another parameter that significantly affects condensation rate is the difference between the saturation temperature of steam and the wall temperature of the tube. The results which are obtained for different ΔT values will be used to study the effect of steam to wall temperature difference on condensation heat transfer.

Numerical results are presented at D=19mm and ΔT=9K in Figures 5.1 to 5.4. Variations of film thickness as a function of angular position (ϕ) at the upper, middle and the bottom tubes, obtained from the computer program, are given in Figure 5.1. The angular position (ϕ) is measured from the top of the tube. Calculations show that the film thickness increases as the condensate flows downward on the tube. The reason of this increase is the additional condensation of steam as the condensate flows downward. The upper tube has a comparatively faster increase in the film thickness as compared to the lower tubes in the column. However, the smallest film thickness is observed on the upper tube. The lower the tube is, the larger the condensate film thickness becomes. The reason of this increase in the condensate thickness is obviously the condensate dripping from the upper tubes.

A fluctuation in the film thickness is observed at the angular positions smaller than 20° at the middle and the bottom tubes. This fluctuation in the film thickness is

due to the numerical instability taking place at the very small angular position values. Calculations stabilize after a few steps later.

The behaviour of the variation of the velocity as a function of the angular position is similar to the behaviour of the film thickness variation as can be seen in Figure 5.2. Whereas the acceleration of the condensate on the upper tube is higher than those on the lower tubes, the velocities on the upper tube are less than those on the lower tubes. Since the thickness of the condensate is much smaller at the small angular positions on the upper tube, condensation rate is higher there which results in a rapid increment in the velocity. However, on the lower tubes velocities reached considerably high values and consequently shear stresses are large and balance the gravitational forces. As a result, velocity changes on the lower tubes become smaller.

Since linear temperature distribution and only conduction type of heat transfer through the condensate are assumed at the beginning of the analysis, heat fluxes can be calculated by Fourier's law of conduction:

$$q = k\frac{\left(T_{sat} - T_w\right)}{\delta} \tag{5.1}$$

Heat fluxes calculated as a function of the angular position by Equation 5.1 are shown in Figure 5.3. If the heat flux curve of the upper tube is observed, it is seen that the heat flux values gradually decrease while the condensate gets thicker as it flows downward on the tube. The lower tubes have less heat flux values because of

the condensate inundation. Since the condensate resists to heat transfer, the lower tubes can hardly conduct the heat as compared to the upper tube.

Heat transfer coefficients for the condensate can be calculated by the convection heat transfer formula:

$$h_{cond} = \frac{q}{\left(T_{sat} - T_w\right)} \tag{5.2}$$

Since the heat transfer coefficient is directly proportional to the heat flux, a similar attitude is expected for the heat transfer coefficient curves. As a consequence, the larger the condensate film thickness gets, the less heat transfer coefficient becomes. Variation of the condensation heat transfer coefficient with respect to the angular position from the top is presented in Figure 5.4.

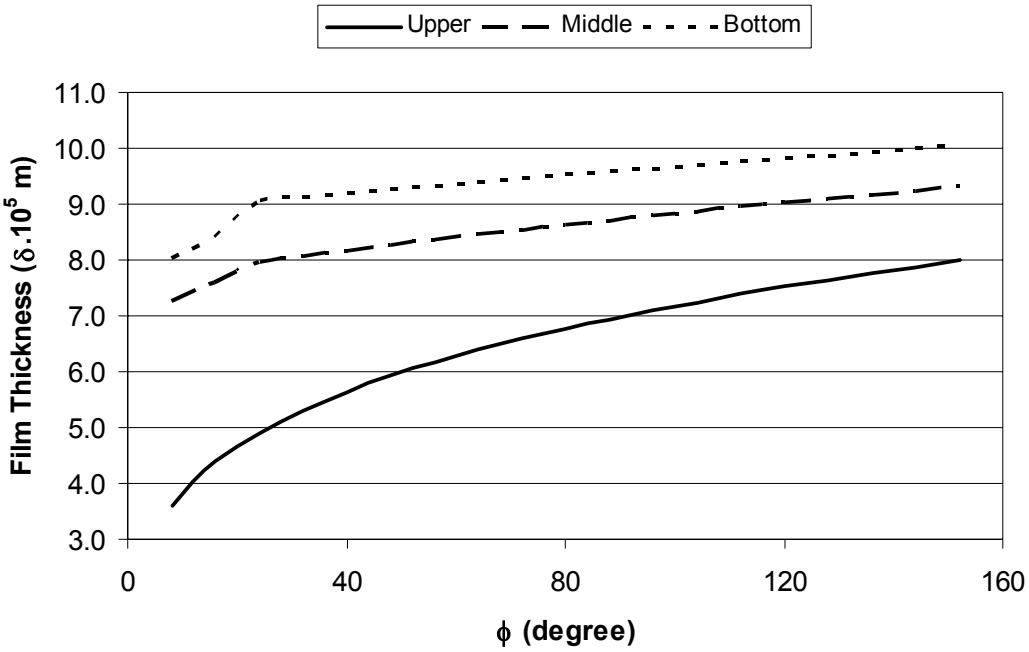

Figure 5.1 Variation of Film Thickness with Angular Position at D=19mm and ΔT=9K

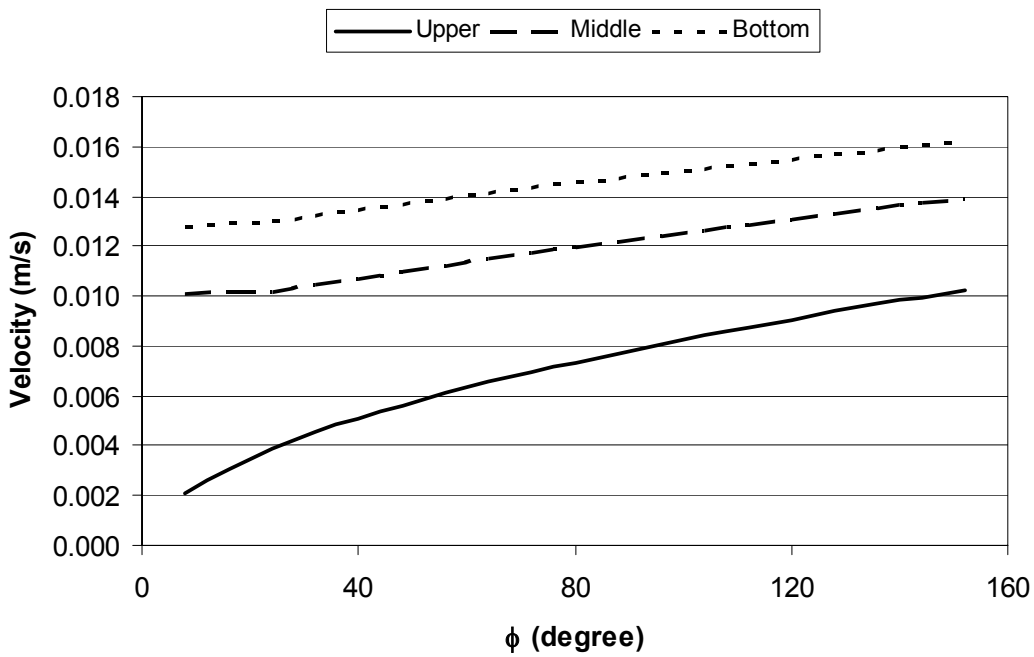

Figure 5.2 Variation of Velocity of the Condensate with Angular Position at D=19mm and ΔT=9K

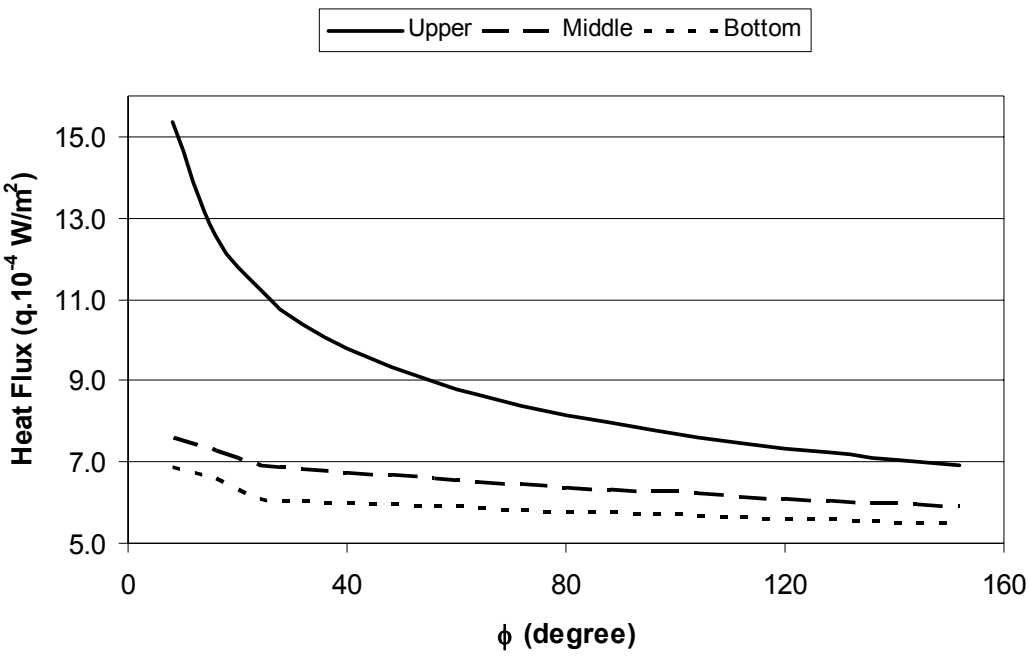

Figure 5.3 Variation of Heat Flux with Angular Position at D=19mm and ΔT=9K

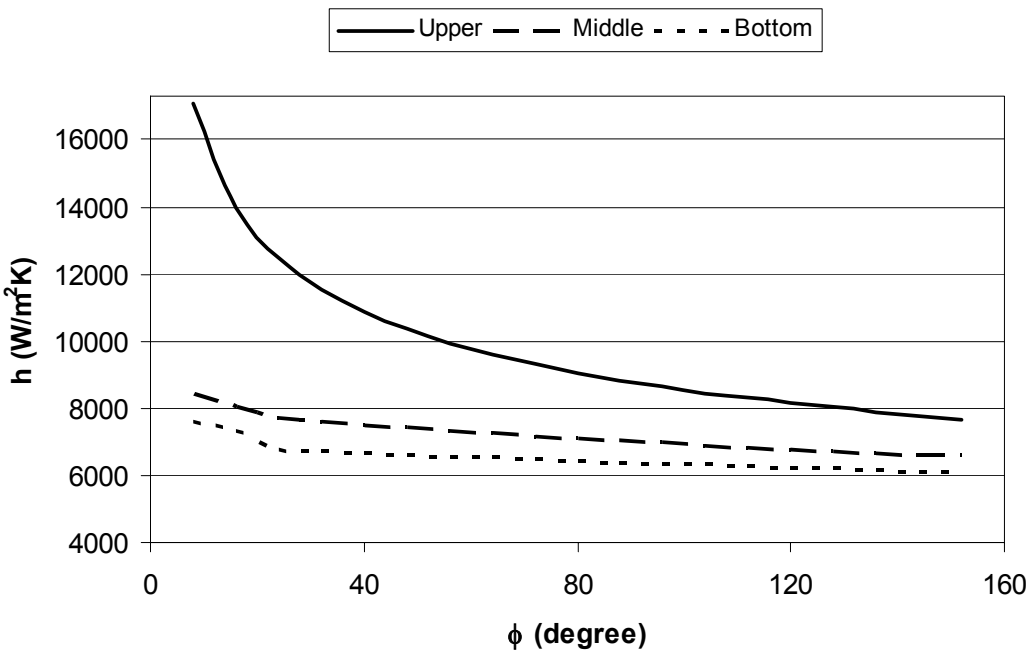

Figure 5.4 Variation of Heat Transfer Coefficient with Angular Position at D=19mm and ΔT=9K

5.1.1 Effect of Tube Diameter on Condensation Heat Transfer

Variations of the film thickness and the velocity of the condensate with angular position for various tube diameters are presented in Figure 5.5 through Figure 5.10 for comparison purpose. It is aimed in these figures to find out how tube diameter affects the condensation heat transfer as the temperature difference between the steam and the tube wall, which is equal to 9K, is kept constant. Diameter of the tubes used in the experiments inside the test section is 19mm. Therefore, the calculations are performed in the theoretical analysis at the tube diameters of 19mm, 24mm, 30mm and 36mm. It is seen in these figures that film thickness and velocities increase as the diameter of the tubes increases for the same angular position. Since the condensate first begins to form on the upper tube, film thickness of the upper tube is less than those of the lower tubes.

The average values of heat flux and heat transfer coefficient are also calculated for a given tube diameter in order to investigate the effect of tube diameter on condensation. Linear curves fitted to the analytical results are shown in Figures 5.11 and 5.12. In Figure 5.11, a decrease in the mean heat flux is observed as the tube diameter is increased. Larger film thickness causes a larger thermal resistance and, as a result, heat flux decreases as the tube diameter increases. A similar pattern is observed in the heat transfer coefficient curves which is shown in Figure 5.12.

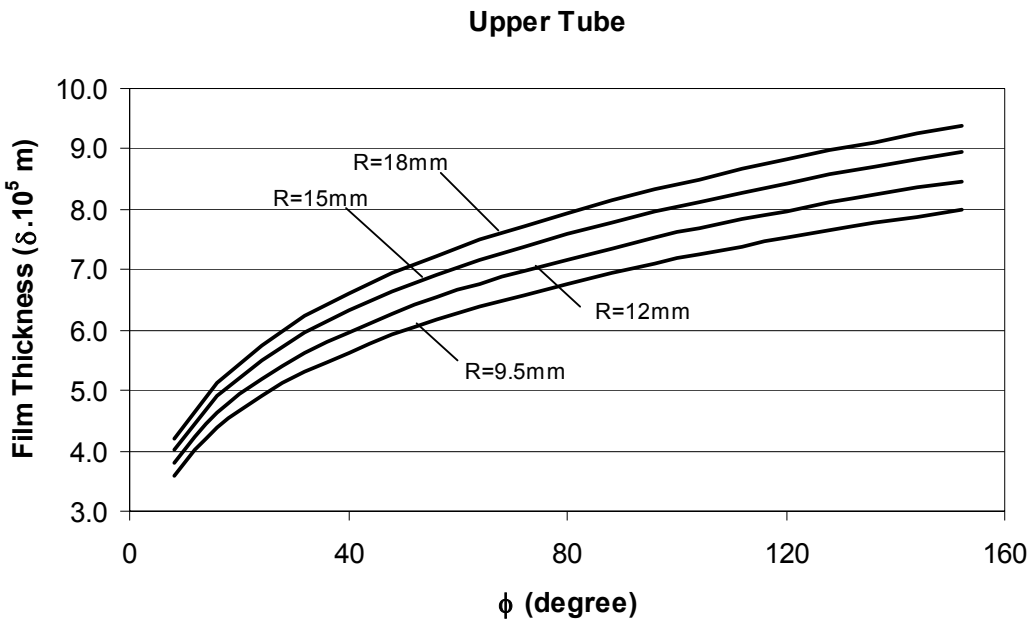

Figure 5.5 Variation of Film Thickness of the Upper Tube with Angular Position for Different Tube Diameters

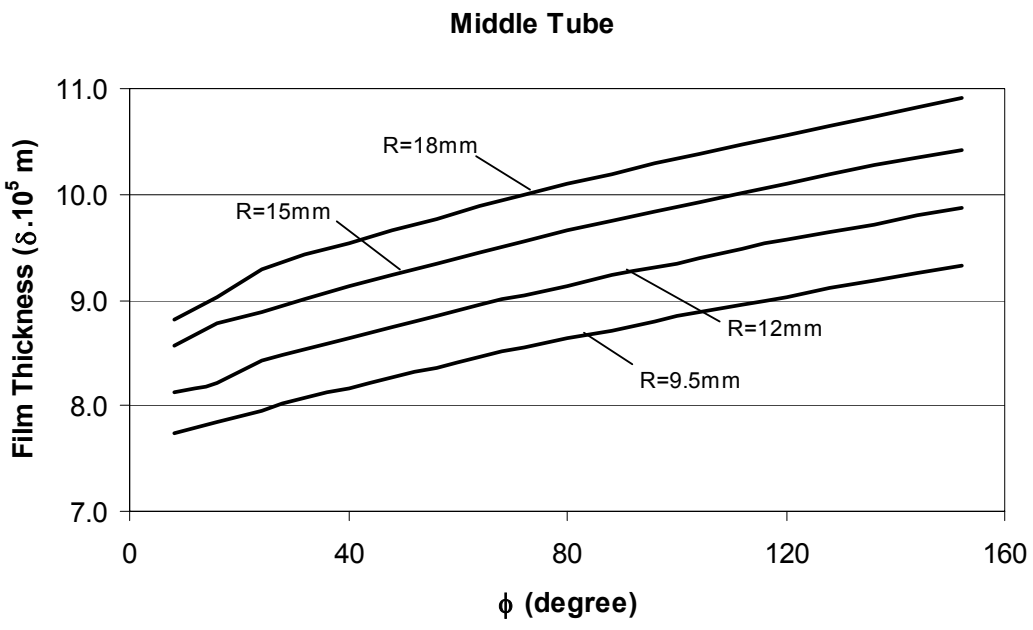

Figure 5.6 Variation of Film Thickness of the Middle Tube with Angular Position for Different Tube Diameters

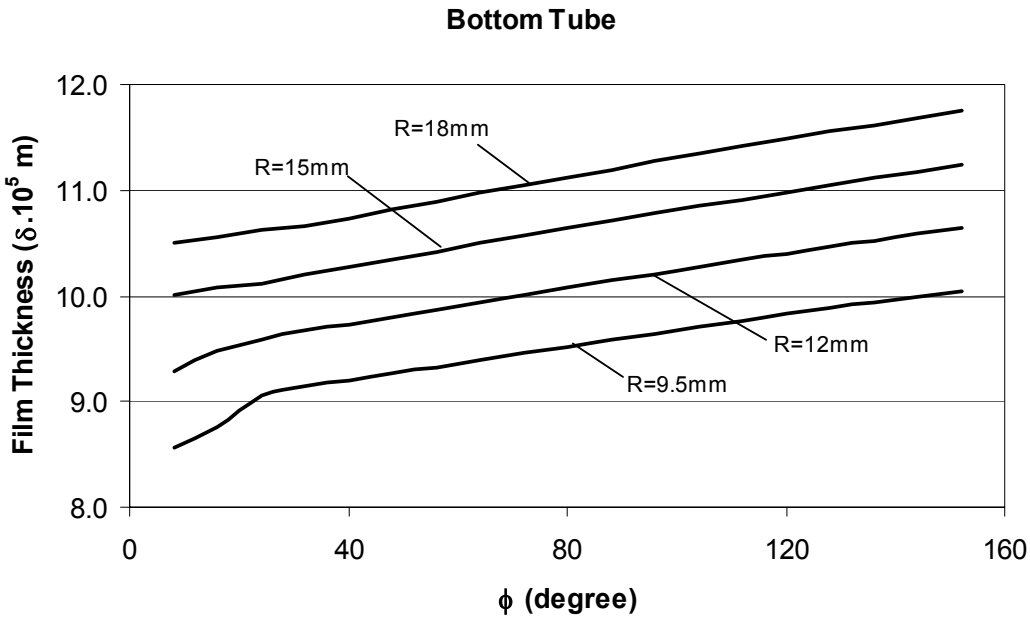

Figure 5.7 Variation of Film Thickness of the Bottom Tube with Angular Position for Different Tube Diameters

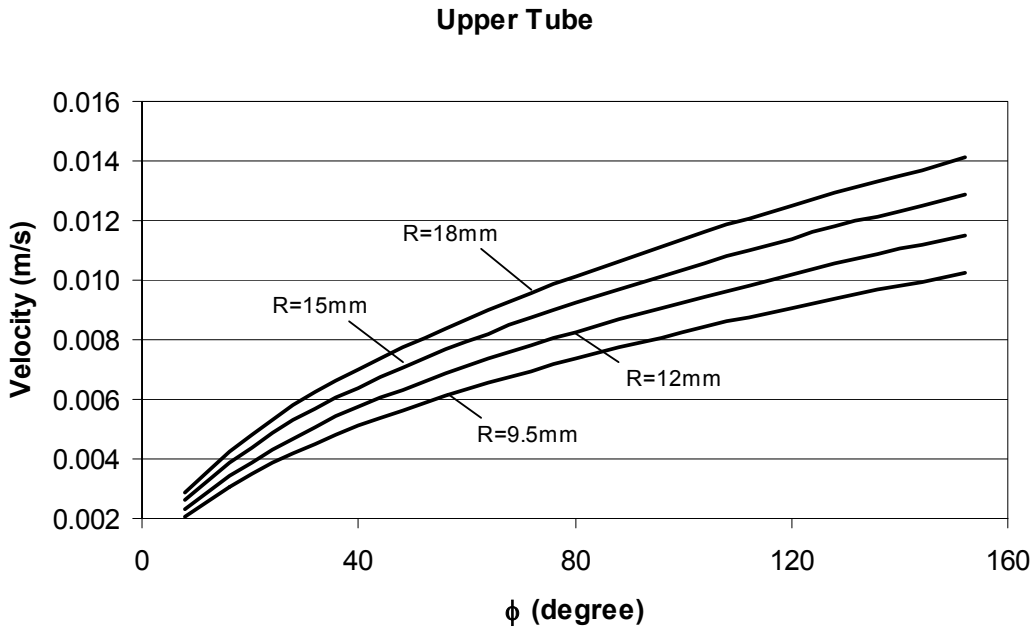

Figure 5.8 Variation of Velocity of the Condensate of the Upper Tube with Angular Position for Different Tube Diameters

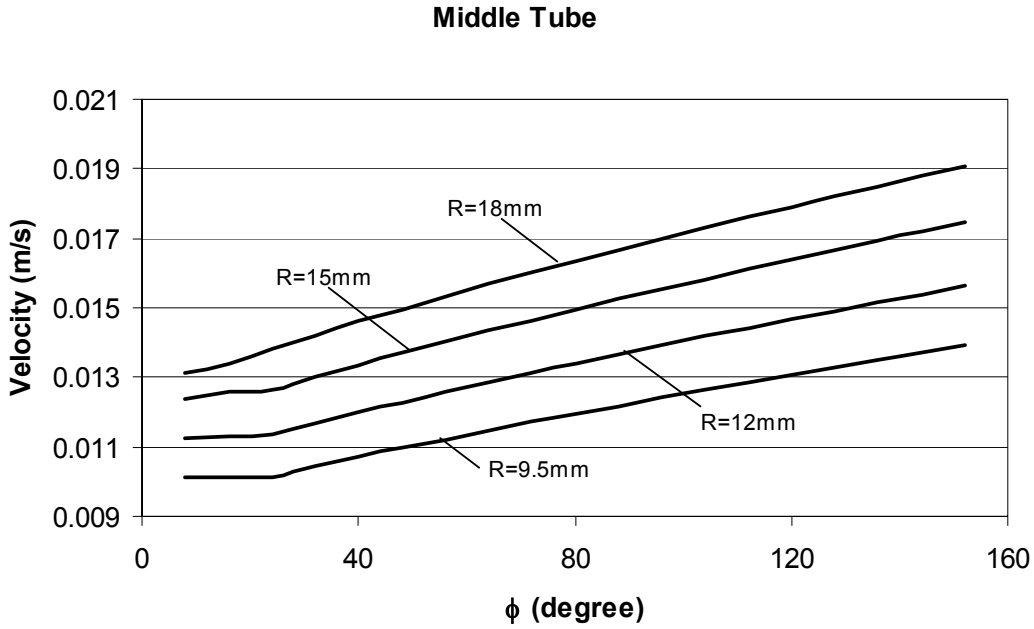

Figure 5.9 Variation of Velocity of the Condensate of the Middle Tube with Angular Position for Different Tube Diameters

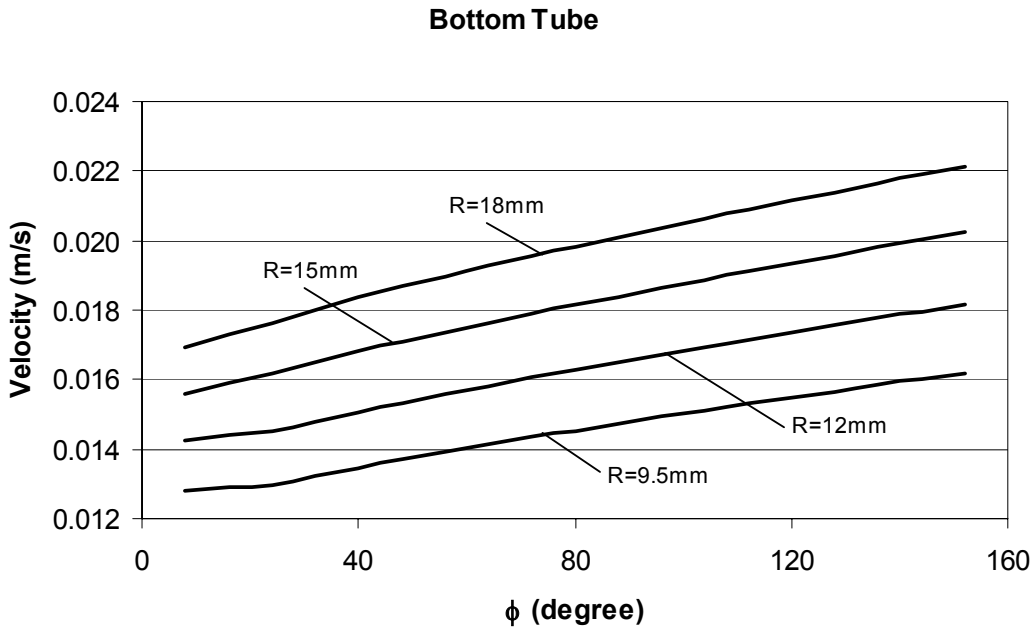

Figure 5.10 Variation of Velocity of the Condensate of the Bottom Tube with Angular Position for Different Tube Diameters

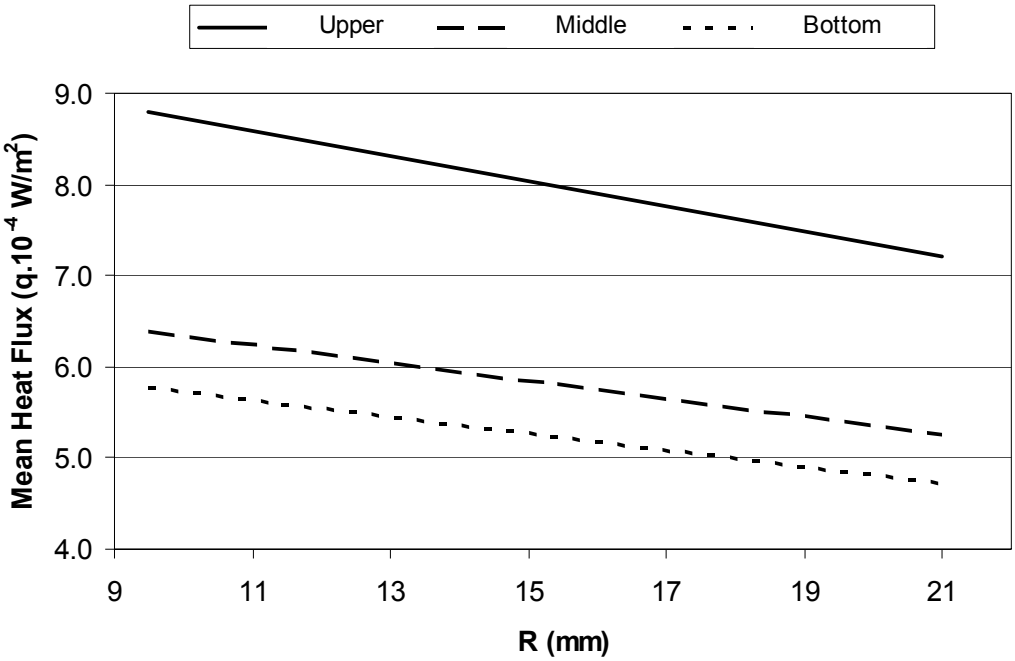

Figure 5.11 Variation of Mean Heat Flux with the Tube Diameter

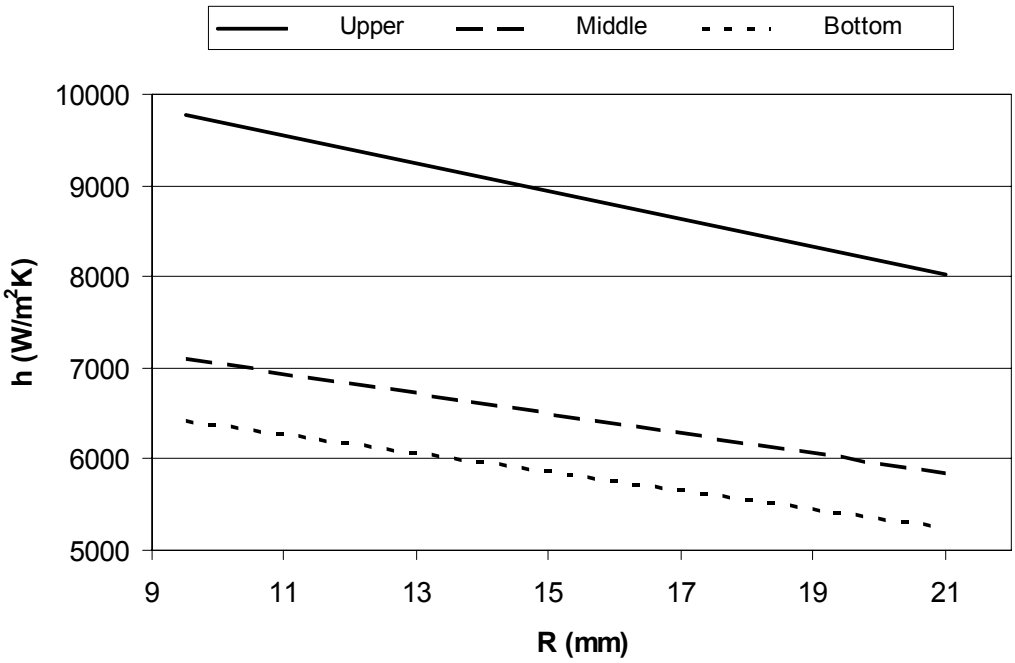

Figure 5.12 Variation of Mean Heat Transfer Coefficient with the Tube Diameter

5.1.2 Effect of Steam to Wall Temperature Difference on Condensation Heat Transfer

The theoretical analysis has been extended to investigate condensation phenomenon for different ΔT values. Since the saturation temperature of steam remains nearly constant, the only way to change ΔT is to change wall temperature of the tube. Cooling water inlet temperature should be adjusted so that the wall temperature reaches to the value desired.

Variations of the film thickness and the velocity of the condensate with angular position for different steam to wall temperature differences are presented in Figures 5.13 to 5.18. It is seen from the figures that a small temperature difference has a considerable effect on the thickness and the velocity of the condensate.

It is deduced from Figure 5.19 and Figure 5.20 that while the mean heat flux increases, the mean heat transfer coefficient decreases with increasing ΔT. At higher heat flux, the rate of condensation is higher and thus the condensate layer becomes thicker, which in turn reduces the value of heat transfer coefficient.

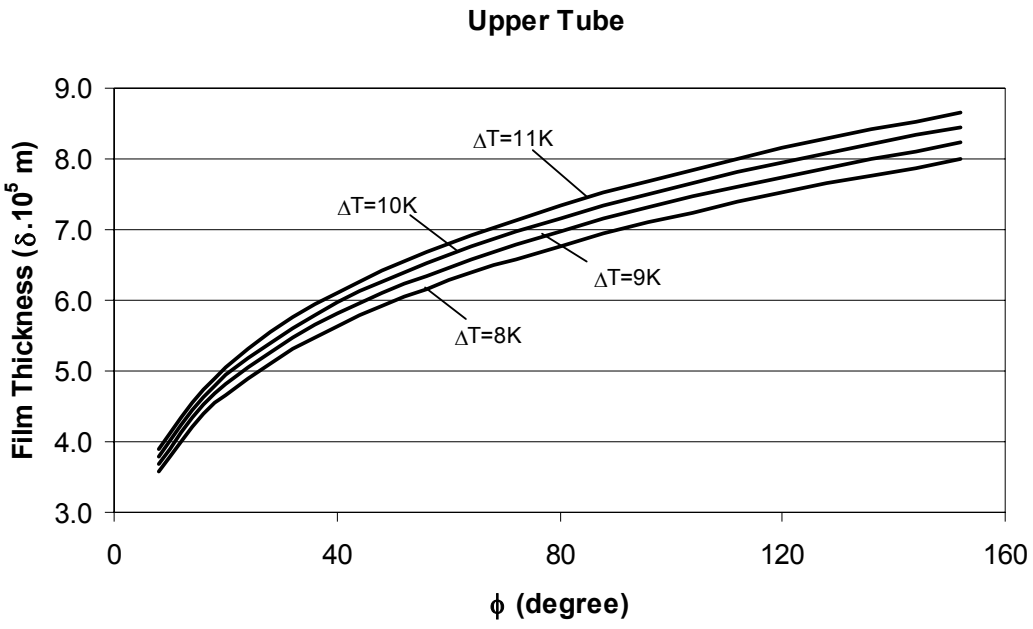

Figure 5.13 Variation of Film Thickness of the Upper Tube with Angular Position for Various Steam to Wall Temperature Differences

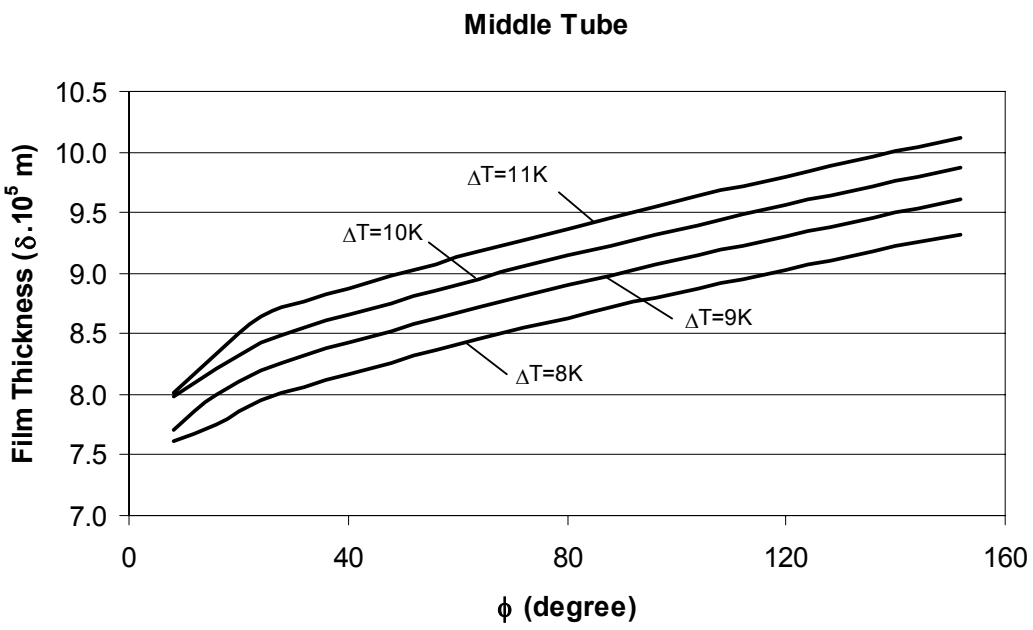

Figure 5.14 Variation of Film Thickness of the Middle Tube with Angular Position for Various Steam to Wall Temperature Differences

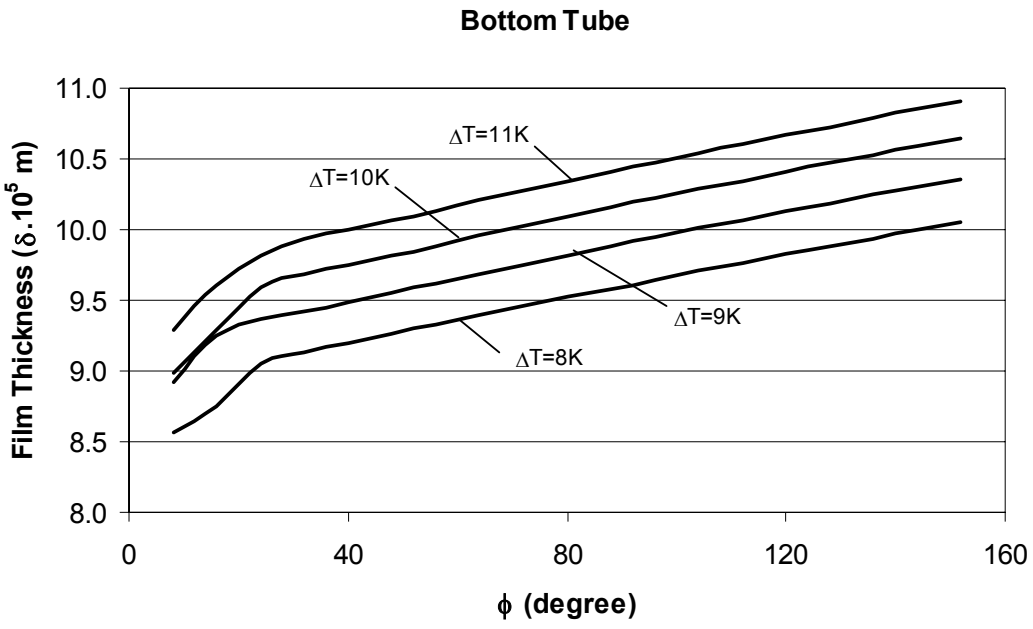

Figure 5.15 Variation of Film Thickness of the Bottom Tube with Angular Position for Various Steam to Wall Temperature Differences

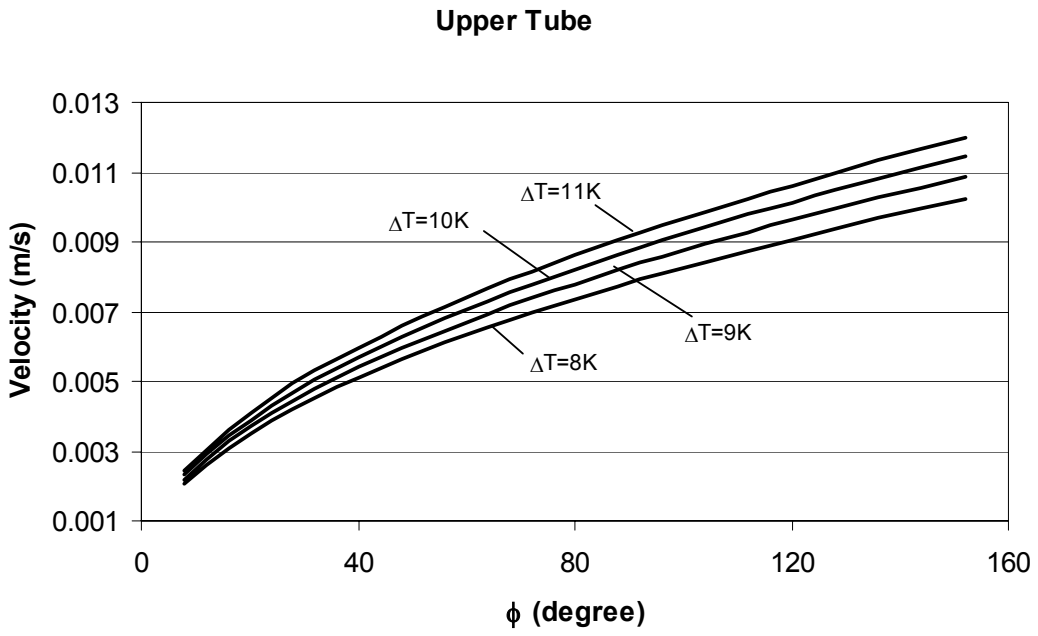

Figure 5.16 Variation of Velocity of the Condensate with Angular Position for Various Steam to Wall Temperature Differences

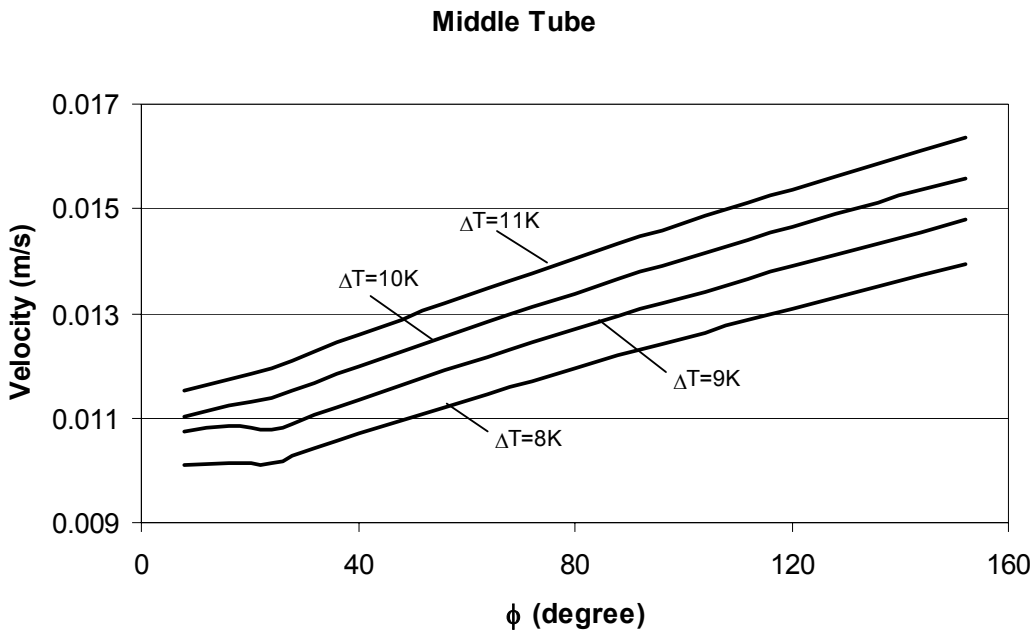

Figure 5.17 Variation of Velocity of the Condensate with Angular Position for Various Steam to Wall Temperature Differences

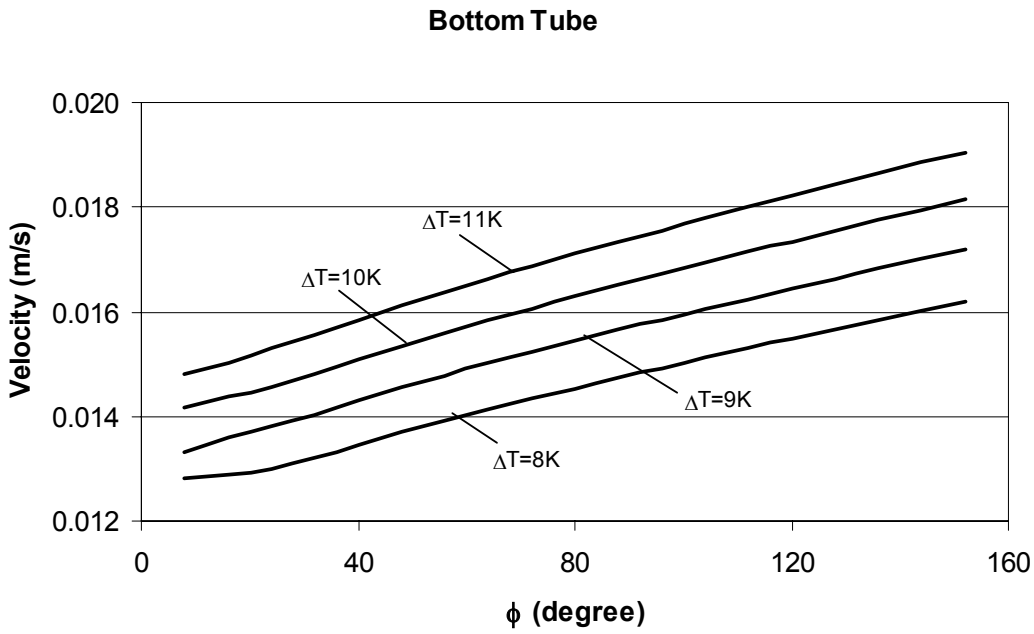

Figure 5.18 Variation of Velocity of the Condensate with Angular Position for Various Steam to Wall Temperature Differences

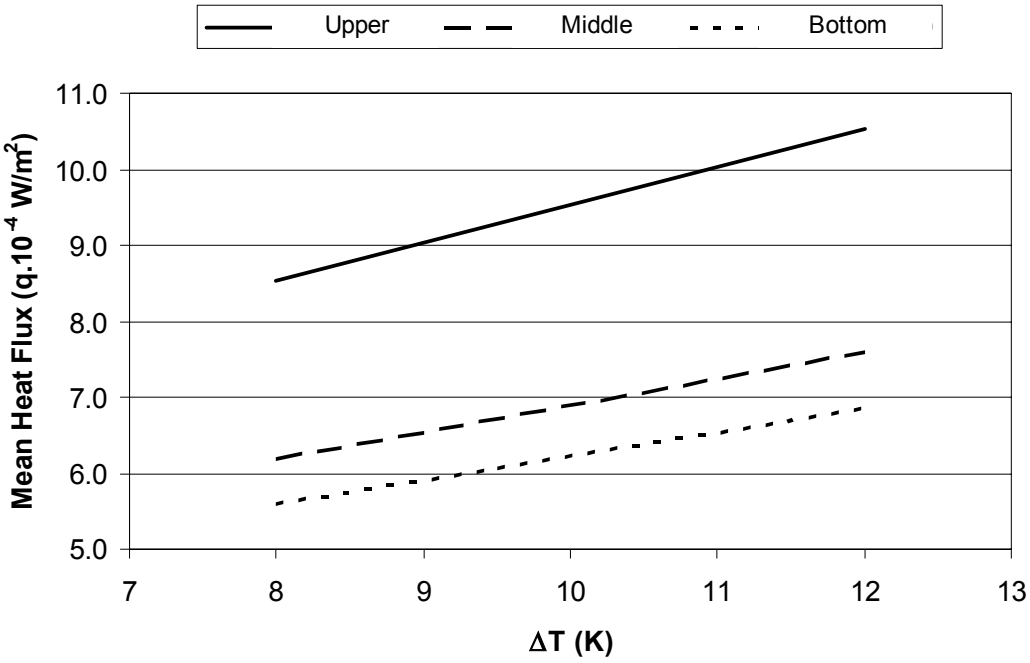

Figure 5.19 Variation of Mean Heat Flux With Respect To the Steam to Wall Temperature Difference

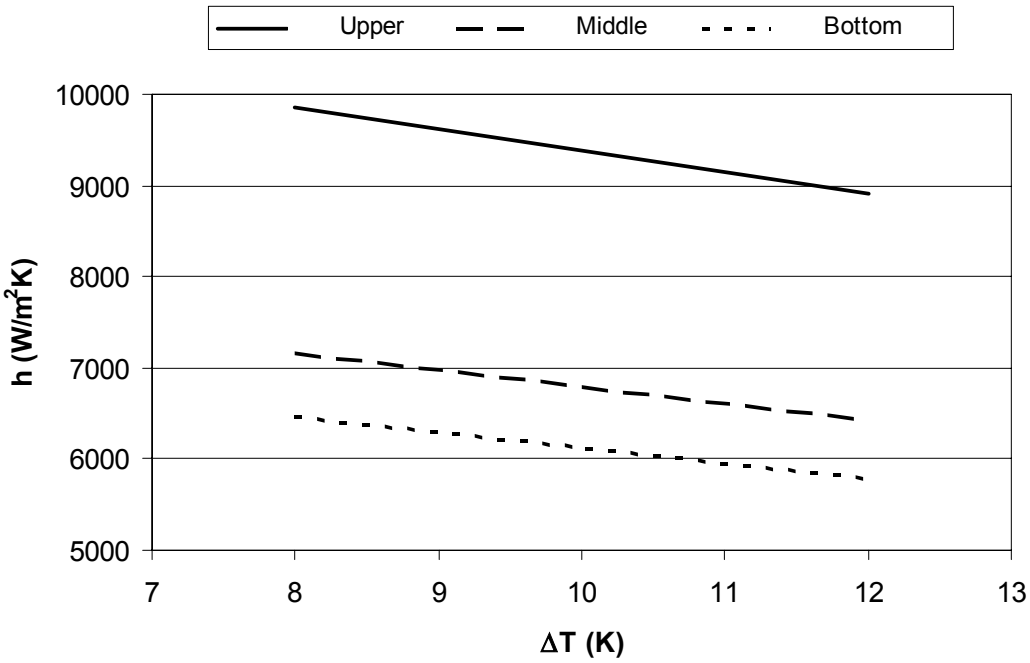

Figure 5.20 Variation of Mean Heat Transfer Coefficient With Respect To the Steam to Wall Temperature Difference

5.2 Experimental Results

The results of the experiments are obtained for three different stages which are described in Chapter 4. Heat transfer rate is obtained from the measured mass flow rate, the inlet and outlet temperatures of the cooling water. Condensation heat transfer coefficient is calculated by the convection heat transfer formula:

$$Q = \dot{m} C_p \left(T_{out} - T_{in} \right) \tag{5.3}$$

$$h_{cond} = \frac{Q}{2\pi R L \left(T_{sat} - T_w \right)} \tag{5.4}$$

5.2.1 Results of the Experiments Made at Different Angular Orientation of Tube Columns

In the first stage, experiments are performed by inclining the setup to predetermined angles in order to investigate the effect of staggering of tubes on the heat transfer rates and the heat transfer coefficients. The results of the experiments for 0°, 3°, 6°, 10° and 15° of inclination angles are given in Appendix B.

The experiments were performed at five different temperatures of the cooling water in order to examine the behaviour of the heat transfer rate and the heat transfer coefficient for different steam to wall temperature differences. The power of the electric heater is 2 kW at this stage. Straight lines are fitted to the data points which are shown in Figure 5.21 through Figure 5.30. The experiments showed that the highest heat transfer rate is obtained at the lowest inlet temperature of the cooling

water. Furthermore, the rate of heat transfer and the heat transfer coefficient gradually decrease as the condensate flows downward over the condenser tubes, which was also observed in the analytical results.

It can be deduced from Figure 5.21 that the rate of heat transfer increases as the steam to wall temperature difference increases. In contrast to increase in the heat transfer rate, a decrease is observed in the heat transfer coefficient for the high values of temperature difference. At higher heat transfer rates, the rate of condensation is higher, meaning that the condensate layer becomes thicker, which in turn reduced the value of heat transfer coefficient.

The rate of heat transfer for the first tube does not significantly change in the experiments which were conducted at different angles, as expected. However, it is seen that the heat transfer rate is slightly increased for the second and third tubes by increasing the inclination of the rows. When the inclination angle is set to 15°, both heat transfer rate and the heat transfer coefficient results are nearly the same for all tubes since none of the condensate falls on the lower tubes.

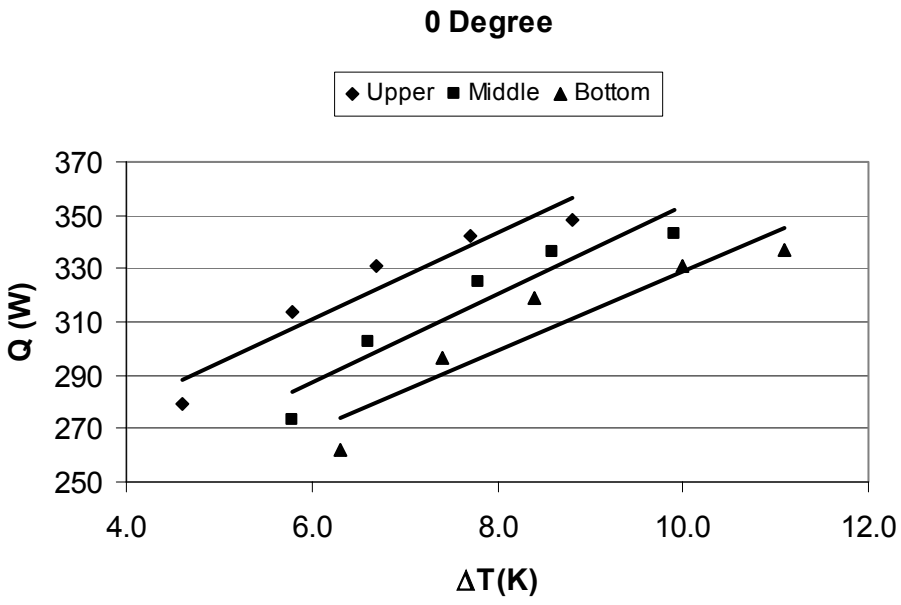

Figure 5.21 Heat Transfer Rates for 0° of Inclination

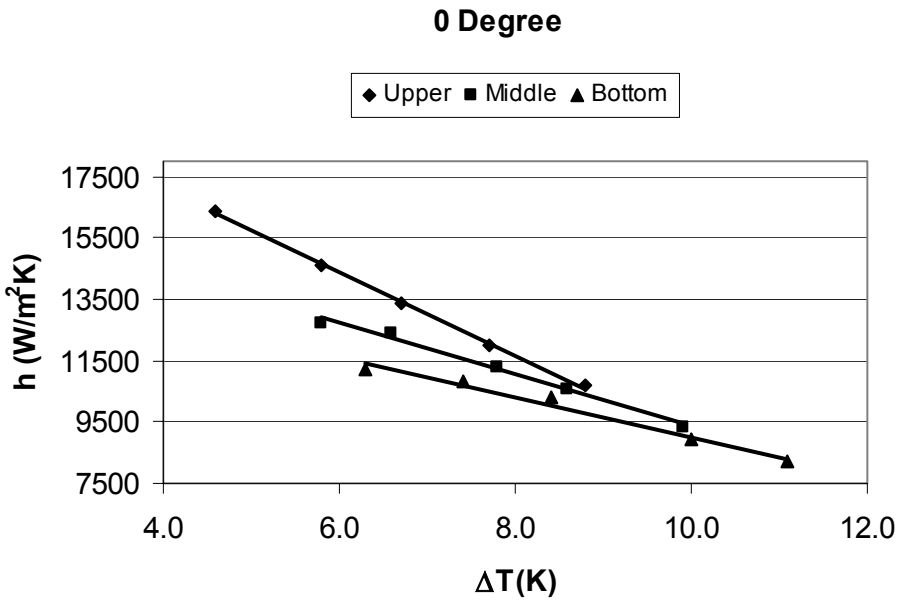

Figure 5.22 Heat Transfer Coefficients for 0° of Inclination

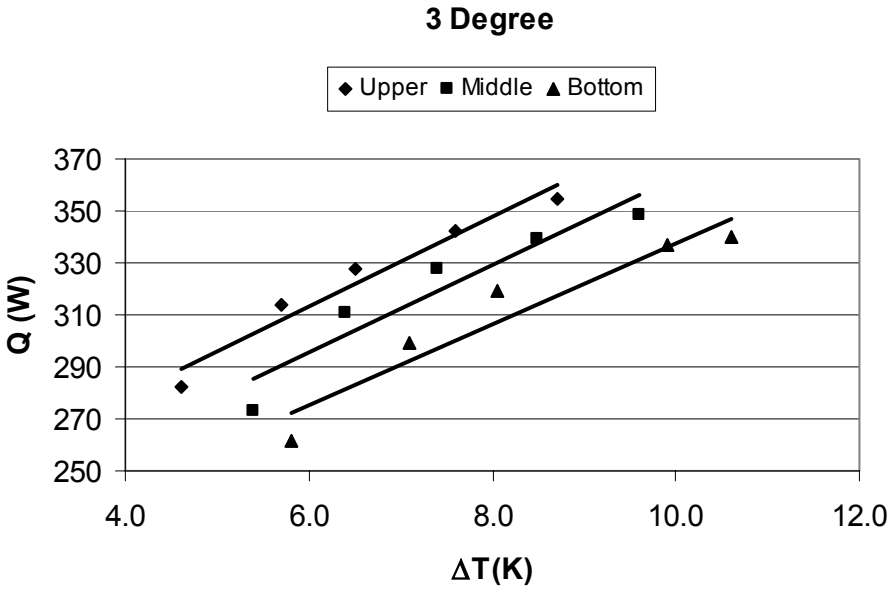

Figure 5.23 Heat Transfer Rates for 3° of Inclination

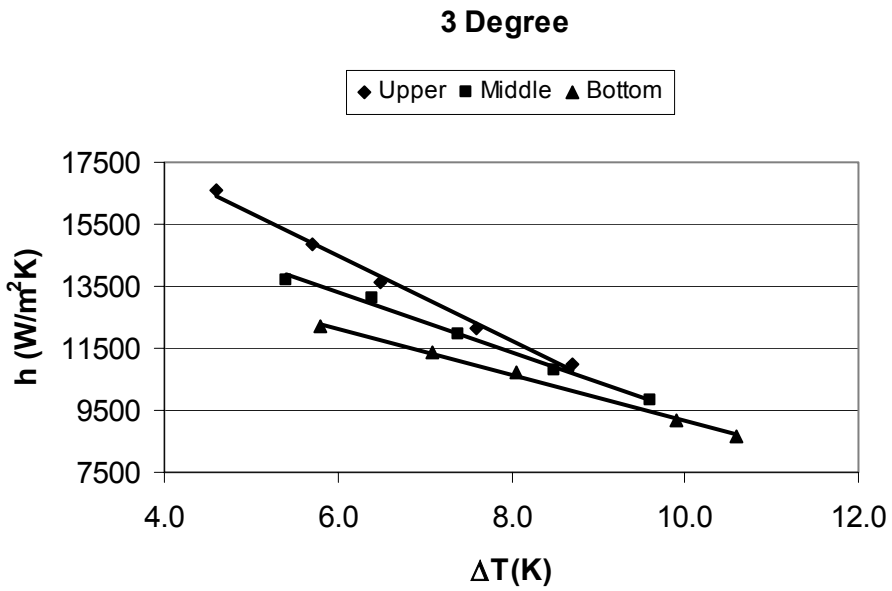

Figure 5.24 Heat Transfer Coefficients for 3° of Inclination

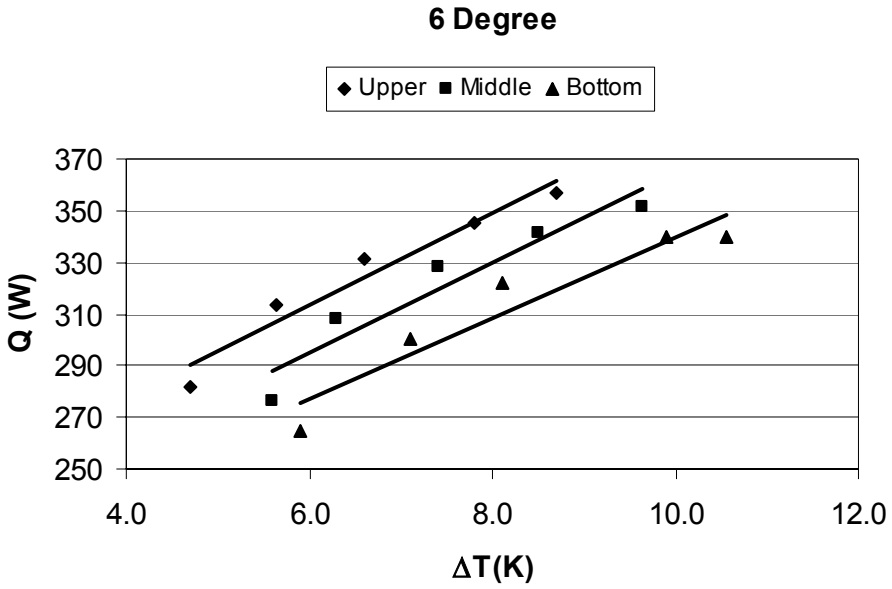

Figure 5.25 Heat Transfer Rates for 6° of Inclination

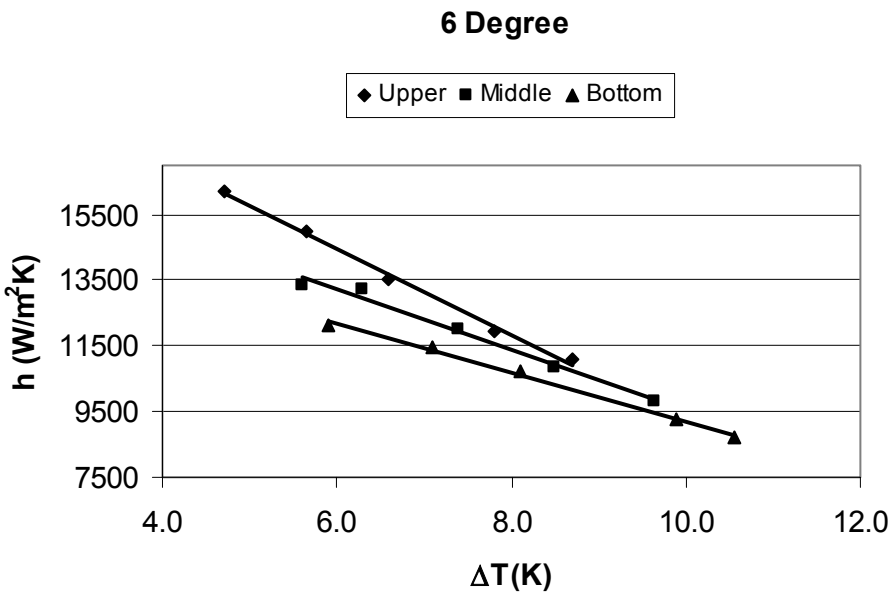

Figure 5.26 Heat Transfer Coefficients for 6° of Inclination

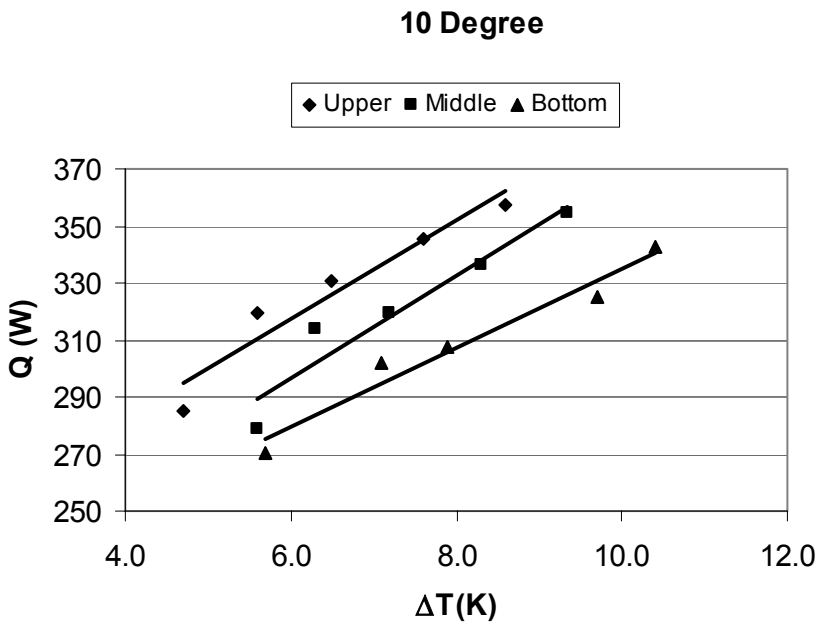

Figure 5.27 Heat Transfer Rates for 10° of Inclination

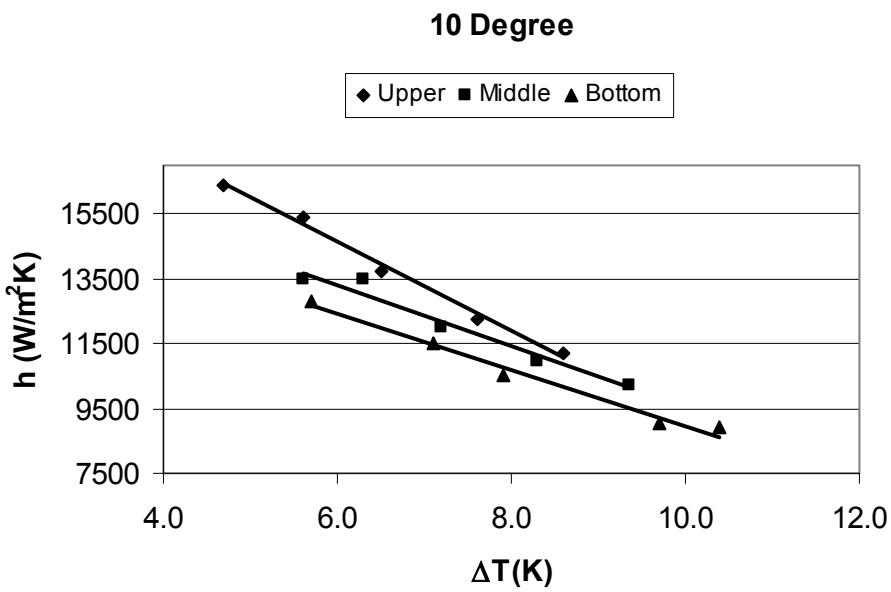

Figure 5.28 Heat Transfer Coefficients for 10° of Inclination

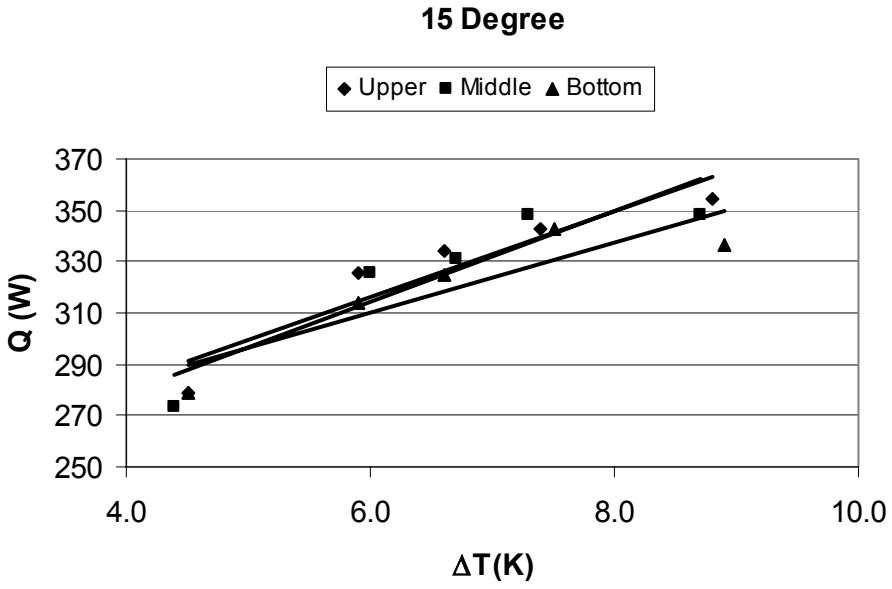

Figure 5.29 Heat Transfer Rates for 15° of Inclination

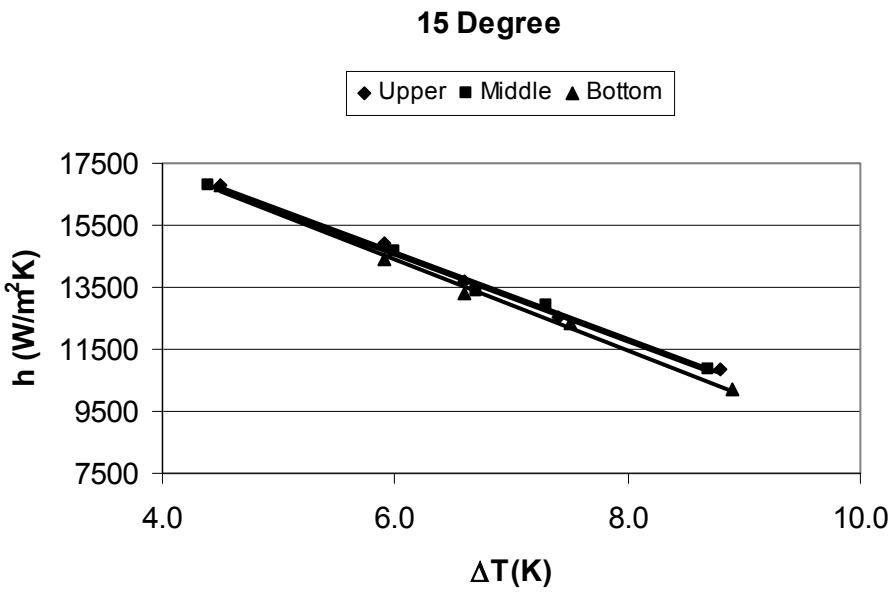

Figure 5.30 Heat Transfer Coefficients for 15° of Inclination

5.2.2 Effect of Steam Velocity over the Tubes

Two half cylindrical flow delimiters are placed inside the test section in order to narrow the flow area of the steam as depicted in Figure 4.7. The aim of narrowing the flow area is to accelerate the steam and to investigate the behaviour of the condensate under the sweeping effect of the steam. Steam is supplied at 1 kW and 2 kW of power respectively by using a variable ac transformer in order to adjust the mass flow rate of the steam to the desired values.

The experiments which were conducted with flow delimiters at 2 kW of power show that the rate of heat transfer is significantly increased due to the sweep effect of the steam as can be seen in Figure 5.33. It can be inferred from Figure 5.31 and Figure 5.32 that reducing the power which is supplied to steam, causes a decrease in the heat transfer rate and the heat transfer coefficient, as expected.

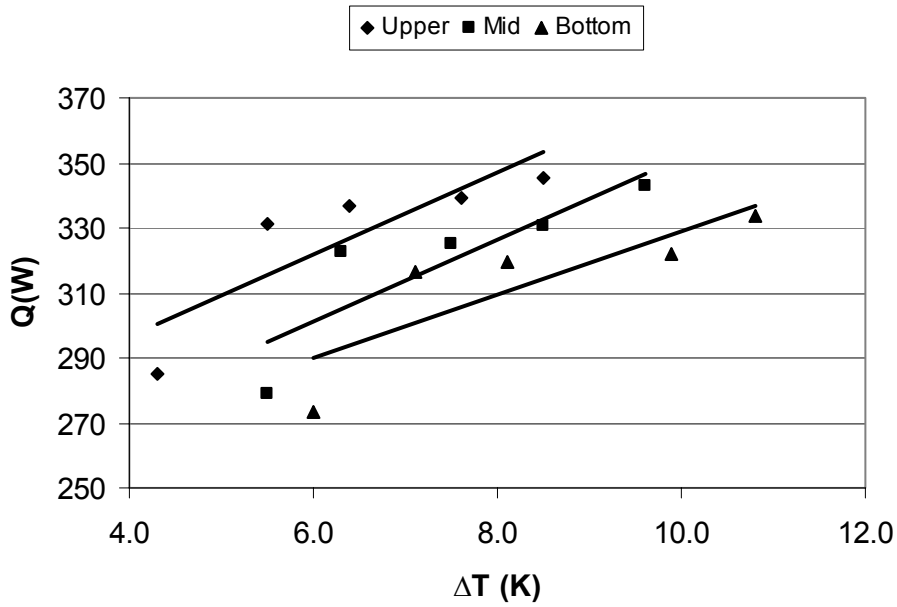

Figure 5.31 Heat Transfer Rates for Half Power of the Steam

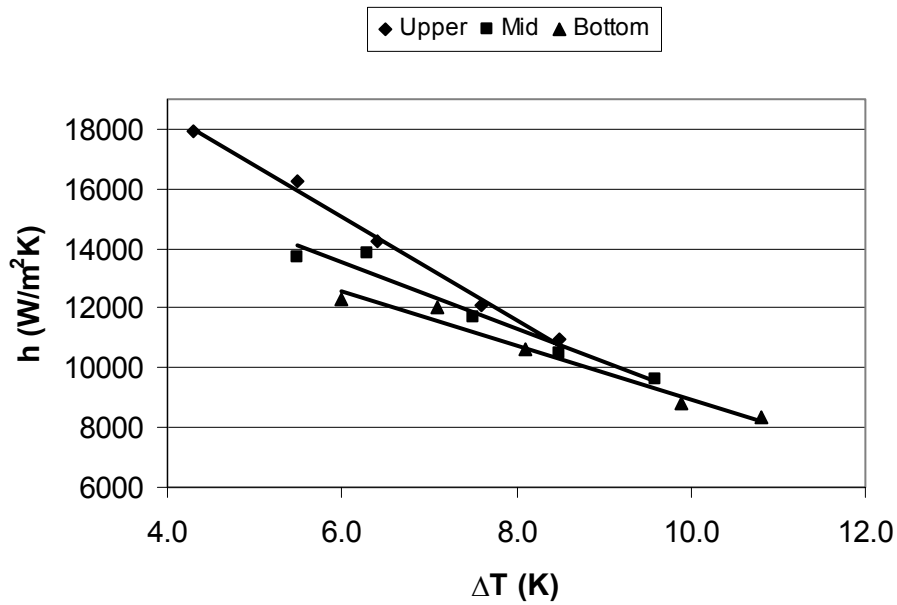

Figure 5.32 Heat Transfer Coefficients for Half Power of the Steam

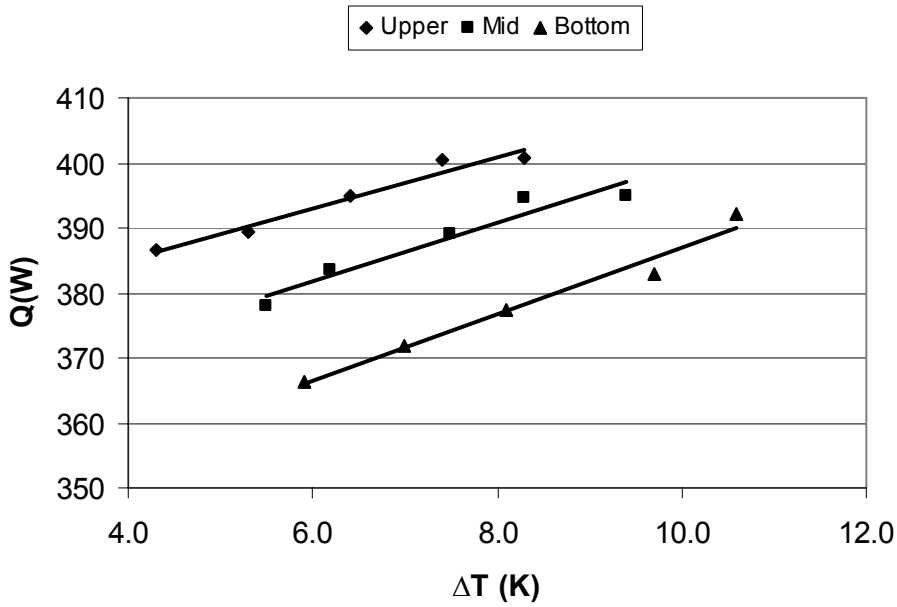

Figure 5.33 Heat Transfer Rates for Full Power of the Steam

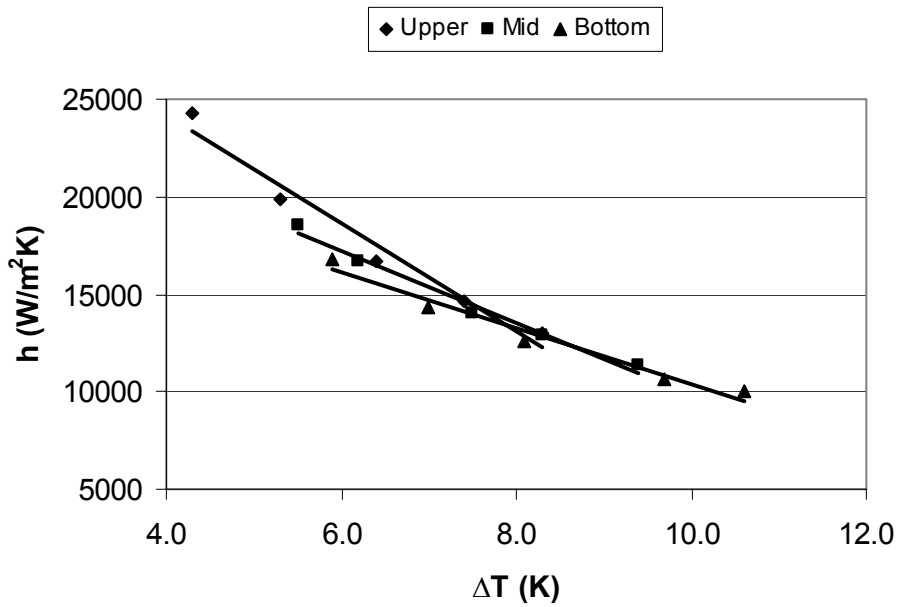

Figure 5.34 Heat Transfer Coefficients for Full Power of the Steam

5.2.3 Effect of Distance Between Condensation Tubes

The condensation tube in the middle is removed from the test section at this stage. Thus, the distance between the upper tube and the bottom tube is increased. The increment in the distance between the tubes means that the condensate will accelerate more and hit the lower tube with a higher velocity. Therefore, the condensate splashes more compared to the situation where the distance between the tubes is shorter. Steam is supplied at 2 kW of power during the experiments of this stage.

It is deduced from Figure 5.35 and Figure 5.36 that the rate of heat transfer and the heat transfer coefficient of the lowest tube are slightly increased due to the increased distance between the two tubes.

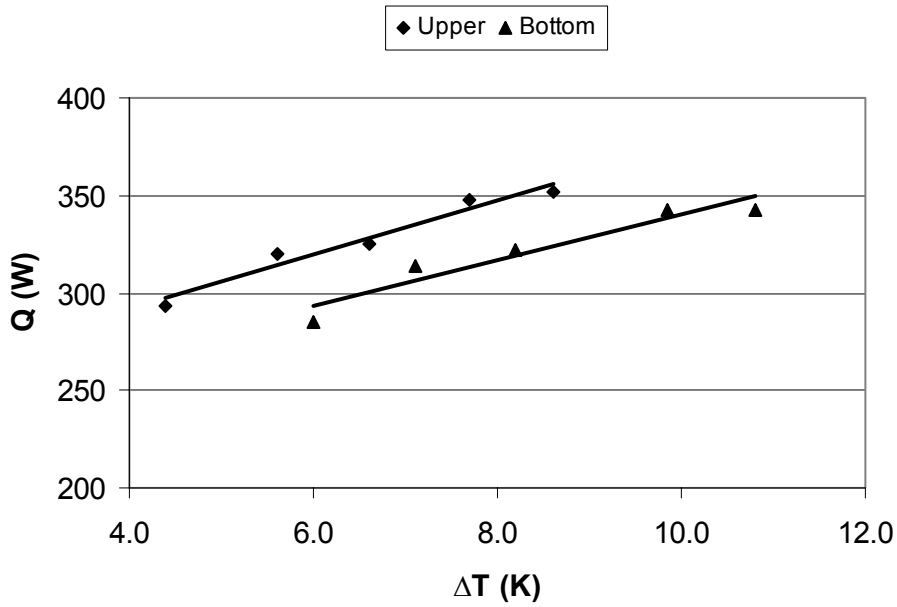

Figure 5.35 Heat Transfer Rates of the Experiments Without Middle Tube

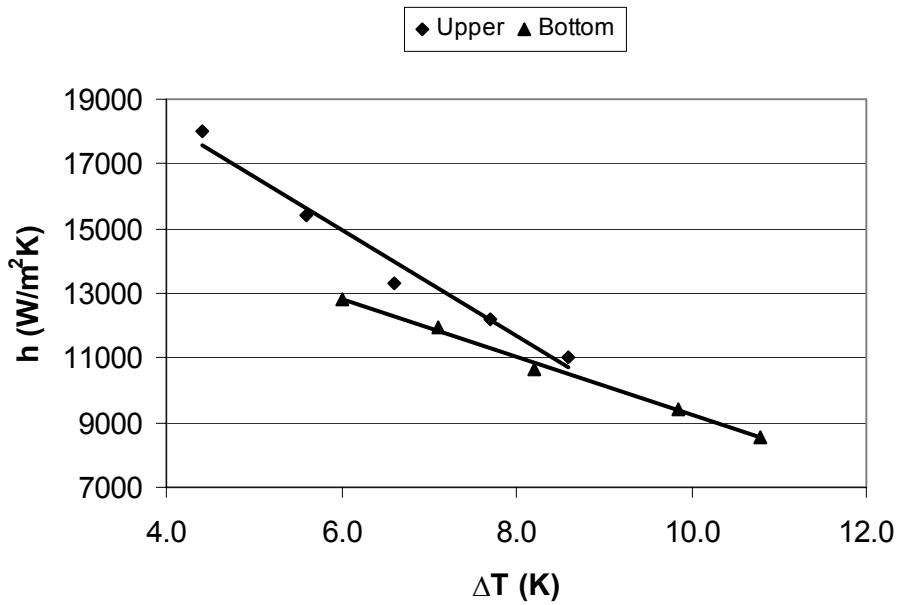

Figure 5.36 Heat Transfer Coefficients of the Experiments Without Middle Tube

5.3 Comparison of Results

In this section, experimental results are compared to those obtained by some researchers in the literature as well as to the analytical analysis and are presented graphically.

5.3.1 Comparison of Experimental Results with Literature

Abdullah et al. [6] presented an experimental study for condensation of steam and R113 on a bank of horizontal copper tubes. The test section, and the sections immediately before and after it, were constructed from anodized cast aluminum alloy modules. All other parts of the test loop were made from stainless steel. The test section was rectangular in cross-section with internal dimensions of 272 x 143 mm and contained a staggered tube bank consisting of 10 rows, each of four or five copper tubes with outside diameter 18.7 mm and inside diameter 12.7 mm. The tubes were located in an equilateral triangular arrangement, with horizontal pitch 26.2 mm and vertical pitch 22.7 mm. The comparison of heat transfer coefficients between the present study and the study of Abdullah et al. is presented in Figure 5.37. Data points of the present study are obtained for 30.5°C of cooling water inlet temperature of the experiments which were conducted at the vertical position of the test section. Since Abdullah et al. stated that the odd and even rows should be treated as separate columns for a staggered tube bank; first, third and fifth rows of their setup correspond to upper, middle and bottom tubes of the present study, respectively.

It is seen from Figure 5.37 that the heat transfer coefficients found by Abdullah et al. are higher than those found by the present study. The reason can be 1.5 m/s of steam velocity of their investigation whereas almost quiescent steam is used in the present study.

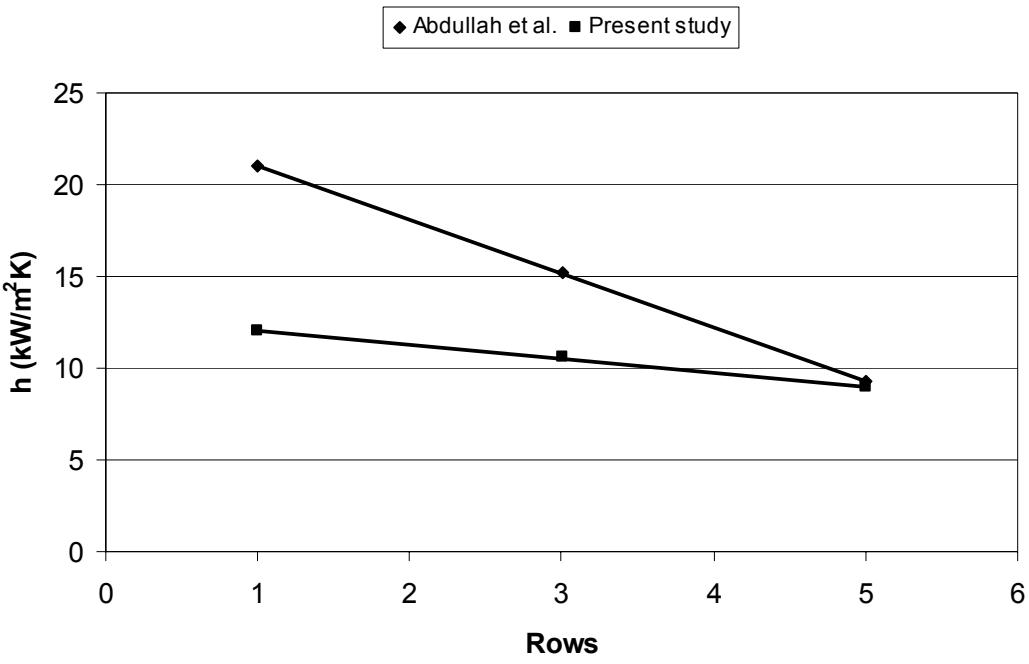

Figure 5.37 Comparison of Heat Transfer Coefficients Between the Present Study and Abdullah et al.

Kumar et al. [14] performed an experimental investigation to find the heat transfer coefficient during condensation of steam over a plain tube, a circular integral-fin tube and a spine integral-fin tube. Their experiments, which were conducted on a plain copper tube, are of interest and the comparison between the upper tube of the present study and the study of Kumar et al. is given in Figure 5.38. The copper condensation tube has an outside diameter of 22.21 mm and an inside

diameter of 18.42 mm. Kumar et al. stated that their experimental values of heat transfer coefficients are higher than those predicted by Nusselt's model in a range of 5 to 15 percent. It is seen from Figure 5.38 that the experimental results of Kumar et al. are also higher than those found by the present study.

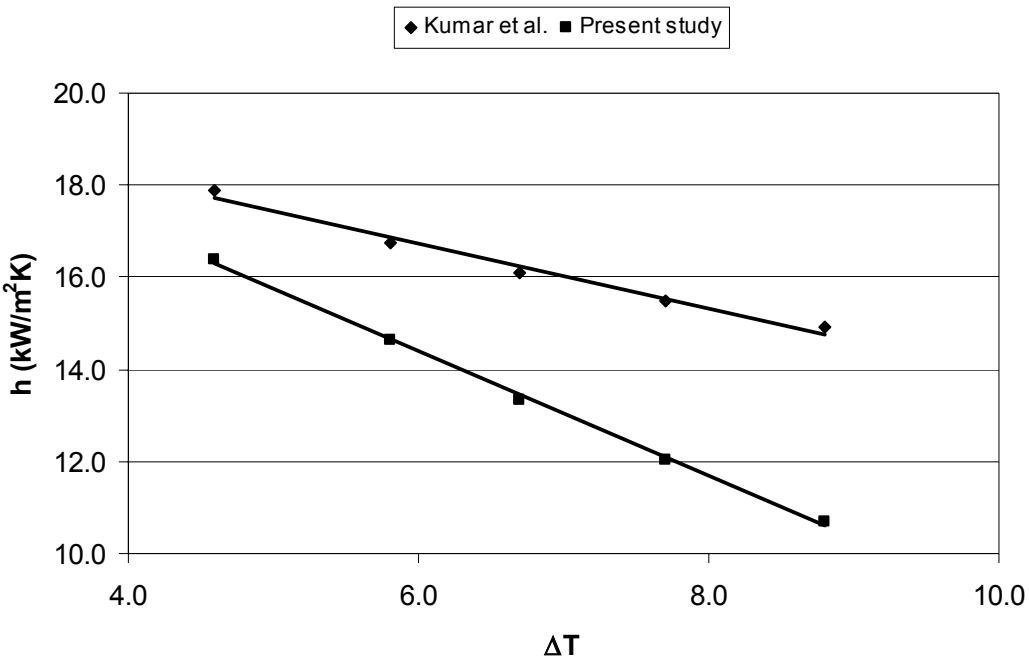

Figure 5.38 Comparison of Heat Transfer Coefficients Between the Present Study and Kumar et al.

The heat transfer coefficient for a horizontal tube can be calculated from the Nusselt's original formula for the radial systems [30]. In order to compare Nusselt's analysis with the present study, heat transfer coefficient values of the upper tube are compared with the following formula:

$$\bar{h} = 0.729\left[\frac{g\rho_f\left(\rho_f - \rho_g\right)k_f^3 h_{fg}}{\mu_f\left(T_{sat} - T_w\right)D}\right]^{1/4} \tag{5.5}$$

A comparison between the present study and the Nusselt's original formula is presented in Figure 5.39. It is deduced from the figure that experimental results of heat transfer coefficients are higher than those predicted by Nusselt. Most researchers have found that the Nusselt's original formula is conservative as it is found in the present study.

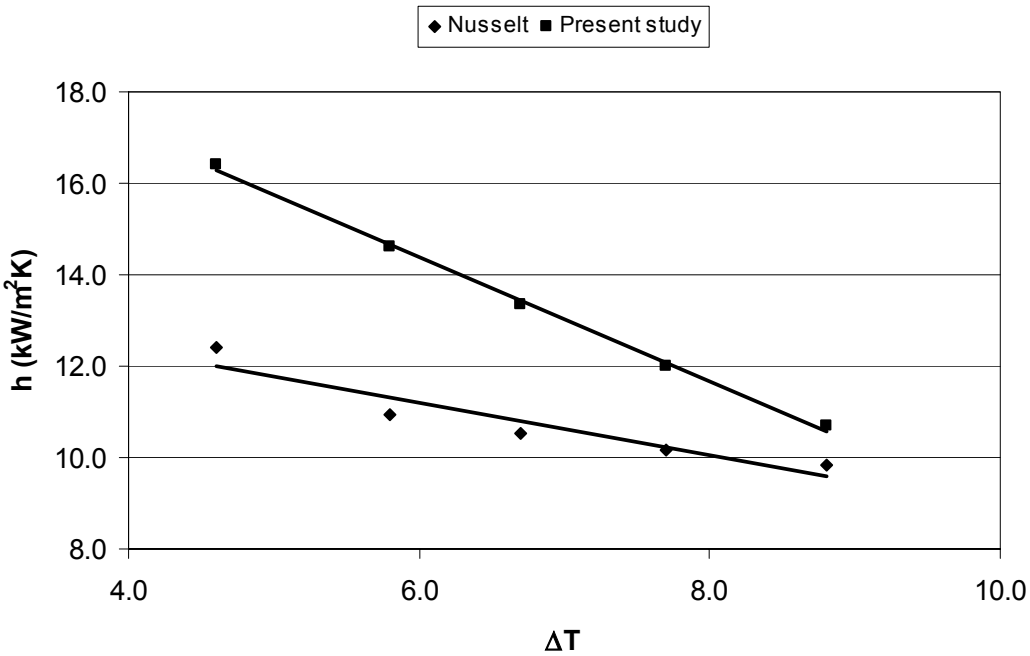

Figure 5.39 Comparison of Heat Transfer Coefficients Between the Present Study and the Nusselt Analysis

5.3.2 Comparison of Experimental Results with Analytical Results

The heat transfer coefficients of each condensation tubes which were obtained from the experiments conducted at the vertical position and the analytical investigation are presented in Figures 5.40 to 5.42. Even though the heat transfer coefficients obtained by the analytical method agree with the Nusselt's analysis, they are less than those of the experimental results.

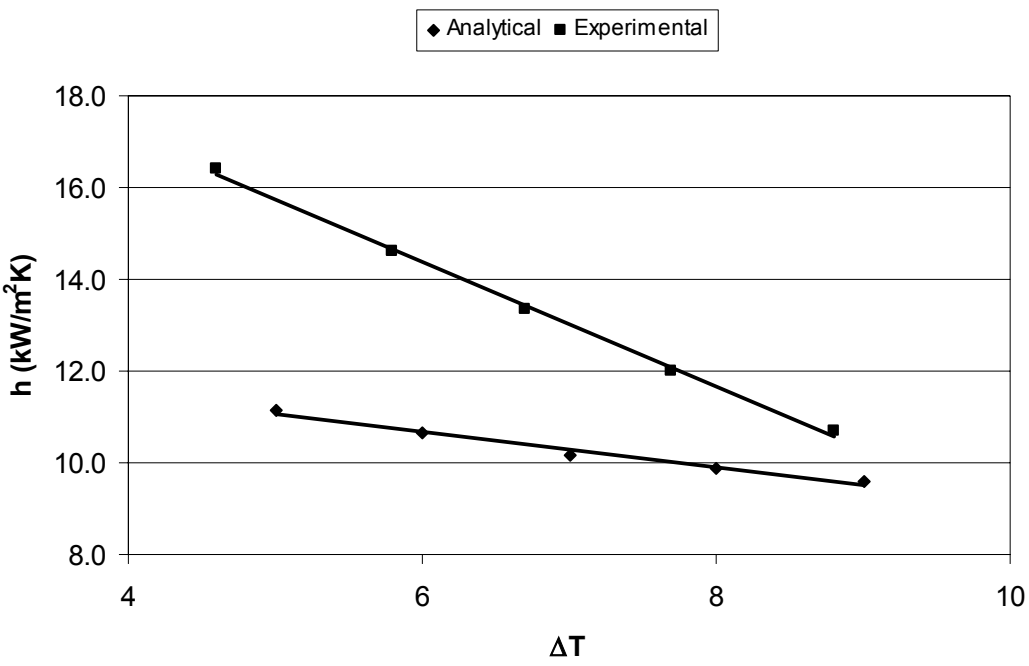

Figure 5.40 Comparison of Heat Transfer Coefficients Between Analytical and Experimental Analyses for the Upper Tube

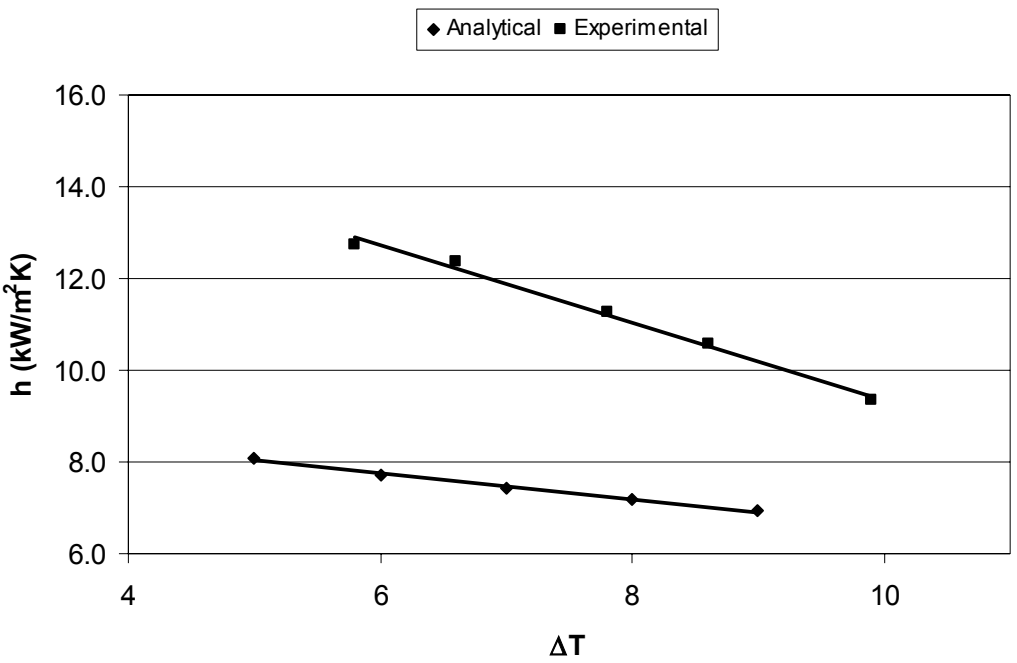

Figure 5.41 Comparison of Heat Transfer Coefficients Between Analytical and Experimental Analyses for the Middle Tube

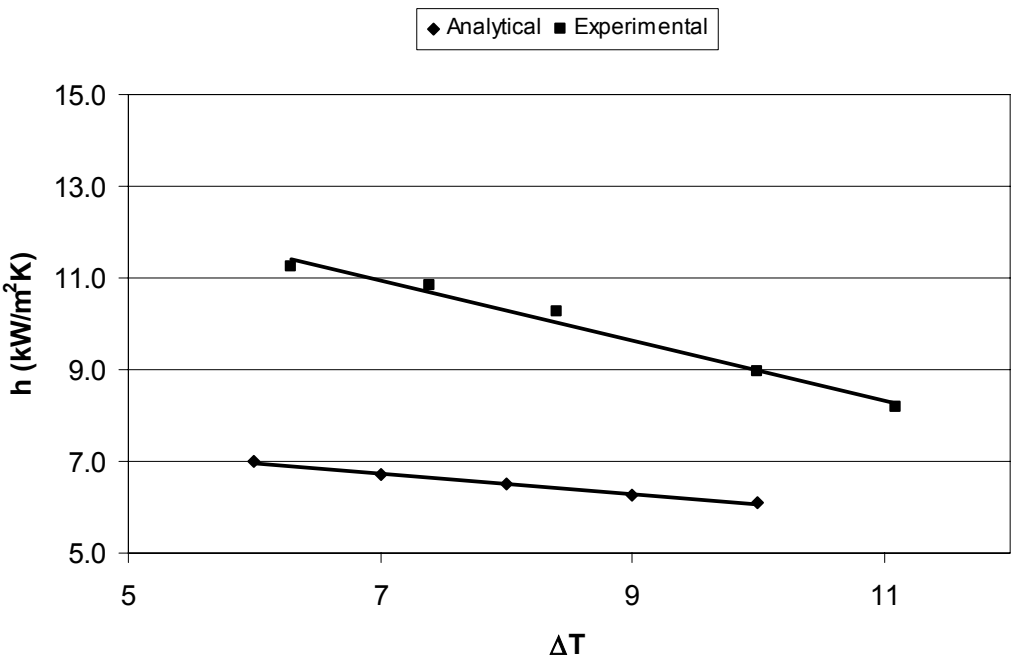

Figure 5.42 Comparison of Heat Transfer Coefficients Between Analytical and Experimental Analyses for the Bottom Tube

CHAPTER 6

CONCLUSIONS

Analytical and experimental data are presented for condensation of steam on a vertical tier of three condensation tubes. The conclusions drawn from the present study are as follows:

Heat transfer coefficient decreases due to condensate inundation as the condensate flows downward on the tube column.

The results of analytical investigation show that heat transfer coefficient decreases by increasing tube diameter or temperature difference between steam and tube wall.

It is concluded from the experiments of the first stage that the heat transfer rate is slightly increased at the middle and the bottom tubes by inclining the test section, and no significant change in the heat transfer coefficient of the upper tube is observed.

It is concluded from the experiments of the second stage that the rate of heat transfer is significantly increased due to the sweep effect of steam on the condensate.

However, it is seen from the third stage experiments that the distance between the condensation tubes does not have a considerable effect on condensation.

Comparison of the experimental results with the literature show that although the heat transfer coefficients found by the present study are less than those found by some researchers, they are greater than those predicted by Nusselt's analysis.

6.1 Recommendations for Future Work

In further studies, the geometry of the condenser tubes can be changed, e.g., spherical condenser tubes may be constructed, or additional condensation tubes can be put into the setup to increase the condensation surface.

The working fluids may also be changed in advanced studies. Different fluids may be used instead of both steam and the cooling water.

REFERENCES

1. Nusselt, W., Die Oberflachen-Kondensation des Wasserdampfes, Zeitschrift des Vereines deutscher Ingenieure, **60**, 541-546, 569-575, 1916.

2. Dukler, A. E., Fluid mechanics and heat transfer in vertical falling-film systems, Chemical Engineering Progress Symposium Series No.30, **56**, 1-10, 1960.

3. Chen, M. M., An analytical study of laminar film condensation: Part 2- Single and multiple horizontal tubes, Journal of Heat Transfer, **83C**, 55-60, 1961.

4. Sarma, P. K., Vijayalakshmi, B., Mayinger, F., Kakac, S., Turbulent film condensation on a horizontal tube with external flow of pure vapors, International Journal of Heat and Mass Transfer, **41**, 537-545, 1998.

5. Karabulut, H. and Ataer, Ö. E., Numerical analysis of laminar film-wise condensation, International Journal of Refrigeration, **19**, 117-123, 1996.

6. Abdullah, R., Cooper, J. R., Briggs, A., Rose, J. W., Condensation of steam and R113 on a bank of horizontal tubes in the presence of a noncondensing gas, Experimental Thermal and Fluid Science, **10**, 298-306, 1995.

7. Sparrow, E. M. and Gregg, J. L., A boundary-layer treatment of laminar-film condensation, Journal of Heat Transfer, **81C**, 13-18, 1959.

8. Sparrow, E. M. and Gregg, J. L., Laminar condensation heat transfer on a horizontal cylinder, Journal of Heat Transfer, **81C**, 291-295, 1959.

9. Denny, V. E. and Mills, A. F., Laminar film condensation of a flowing vapor on a horizontal cylinder at normal gravity, Journal of Heat Transfer, 495-501, 1969.

10. Fujii, T. and Uehara, H., Laminar filmwise condensation on a vertical surface, International Journal of Heat and Mass Transfer, **15**, 217-233, 1972.

11. Rao, V. D. and Sarma, P. K., Condensation heat transfer on laminar, falling film, Journal of Heat Transfer, **106**, 518-523, 1984.

12. Hsu, C. H. and Yang, S. A., Pressure gradient and variable wall temperature effects during filmwise condensation from downward flowing vapors onto a horizontal tube, International Journal of Heat and Mass Transfer, **42**, 2419-2426, 1999.

13. Mosaad, M., Combined free and forced convection laminar film condensation on an inclined circular tube with isothermal surface, International Journal of Heat and Mass Transfer, **42**, 4017-4025, 1999.

14. Kumar, R., Varma, H. K., Mohanty, B., Agrawal, K. N., Augmentation of outside tube heat transfer coefficient during condensation of steam over horizontal copper tubes, International Communications in Heat and Mass Transfer, **25**, 81-91, 1998.

15. Memory, S. B., Adams, V. H., Marto, P. J., Free and forced convection laminar film condensation on horizontal elliptical tubes, International Journal of Heat and Mass Transfer, **40**, 3395-3406, 1997.

16. Browne, M. W. and Bansal, P. K., An overview of condensation heat transfer on horizontal tube bundles, Applied Thermal Engineering, **19**, 565-594, 1999.

17. Lee, J., Turbulent film condensation, American Institute of Chemical Engineering Journal, **10**, 540-544, 1964.

18. Koh, J. C. Y., Film condensation in a forced-convection boundary-layer flow, International Journal of Heat and Mass Transfer, **5**, 941-954, 1962.

19. Lee, W. C. and Rose, J. W., Forced convection film condensation on a horizontal tube with and without non-condensing gases, International Journal of Heat and Mass Transfer, **27**, 519-528, 1984.

20. Rose, J. W., Effect of pressure gradient in forced convection film condensation on a horizontal tube, International Journal of Heat and Mass Transfer, **27**, 39-47, 1984.

21. Kutateladze, S. S. and Gogonin, I. I., Investigation of heat transfer in film condensation of flowing vapor on horizontal tube banks, International Journal of Heat and Mass Transfer, **28**, 1831-1836, 1985.

22. Kutateladze, S. S., Gogonin, I. I., Sosunov, V. I., The influence of condensate flow rate on heat transfer in film condensation of stationary vapor on horizontal tube banks, International Journal of Heat and Mass Transfer, **28**, 1011-1018, 1985.

23. Churchill, S. W., Laminar film condensation, International Journal of Heat and Mass Transfer, **29**, 1219-1226, 1986.

24. Chen, C. K. and Hu, H. P., Turbulent film condensation on a half oval body, International Journal of Heat and Mass Transfer, **46**, 4271-4277, 2003.

25. Rose, J. W., Approximate equations for forced-convection condensation in the presence of a non-condensing gas on a flat plate and horizontal tube, International Journal of Heat and Mass Transfer, **23**, 539-546, 1980.

26. Kutateladze, S. S. and Gogonin, I. I., Heat transfer in condensation of flowing vapour on a single horizontal cylinder, International Journal of Heat and Mass Transfer, **28**, 1019-1030, 1985.

27. Fujii, T., Uehara, H., Hirata, K., Oda, K., Heat transfer and flow resistance in condensation of low pressure steam flowing through tube banks, International Journal of Heat and Mass Transfer, **15**, 247-260, 1972.

28. Holman, J. P., Heat transfer, McGraw-Hill, U.S.A., 1990.

29. Incropera, F. P. and DeWitt, D. P., Fundamentals of heat and mass transfer, 3. edition, Wiley, U.S.A., 1990.

30. Kakaç, S. and Liu, H., Heat exchangers: selection, rating, and thermal design, CRC Press, Boca Raton, Fla, 1998.

31. www.51-50racing.com/dictionary.htm

32. Arpacı, V., Lecture Notes, University of Michigan, 8.9-8.14.

33. Kline, S. J. and McClintock, F. A., Describing Uncertainties in Single Sample Experiments, Mechanical Engineering, Jan. 1953.

34. Yamalı, C., Dropwise Condensation Under High Gravity and At Large Subcooling, Ph.D. Dissertation, University of Michigan, 1983.

APPENDIX A

CONDENSATE BEHAVIOUR AT DIFFERENT ANGLES

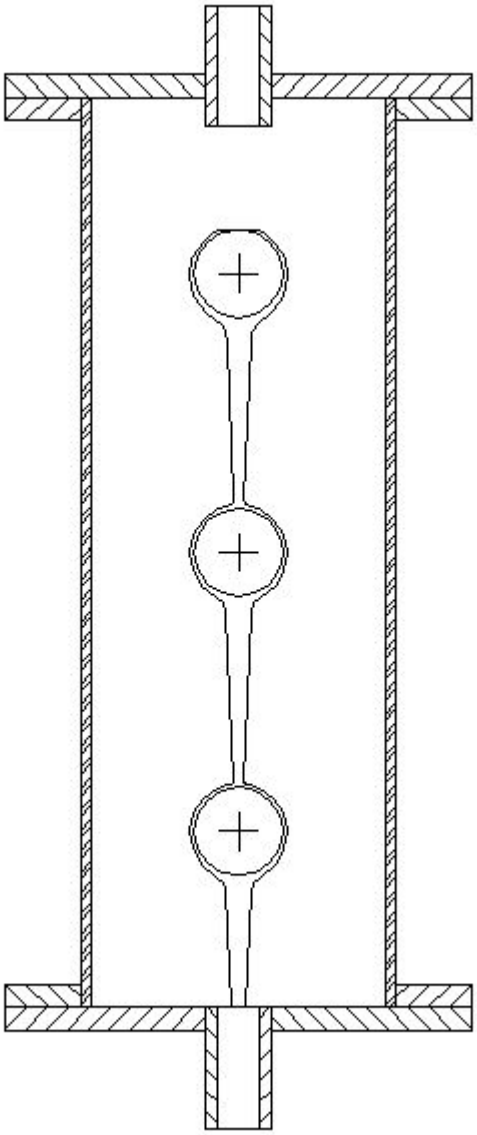

Figure A.1 Condensate Behaviour in the Setup at 0 Degree of Inclination

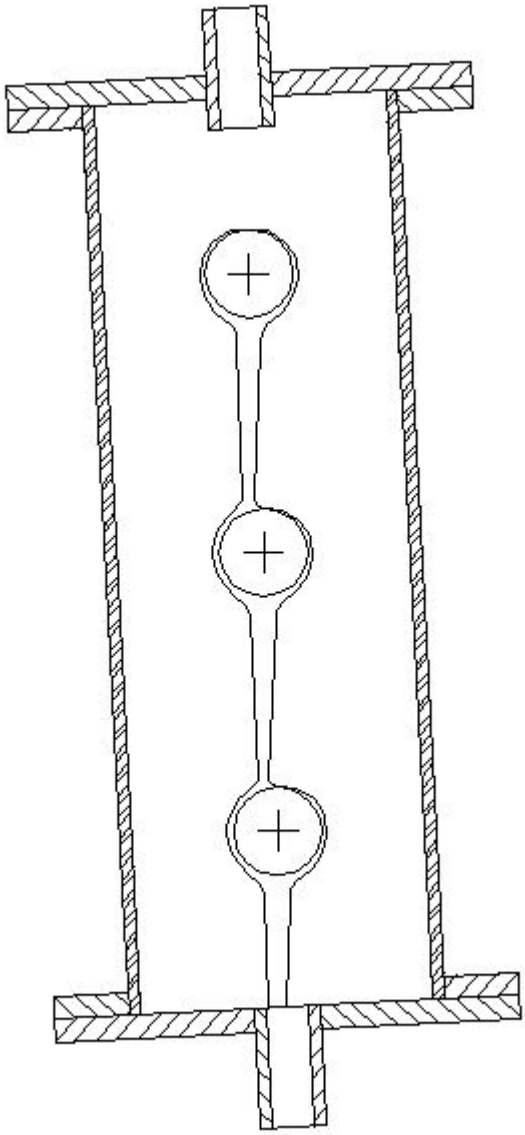

Figure A.2 Condensate Behaviour in the Setup at 3 Degree of Inclination

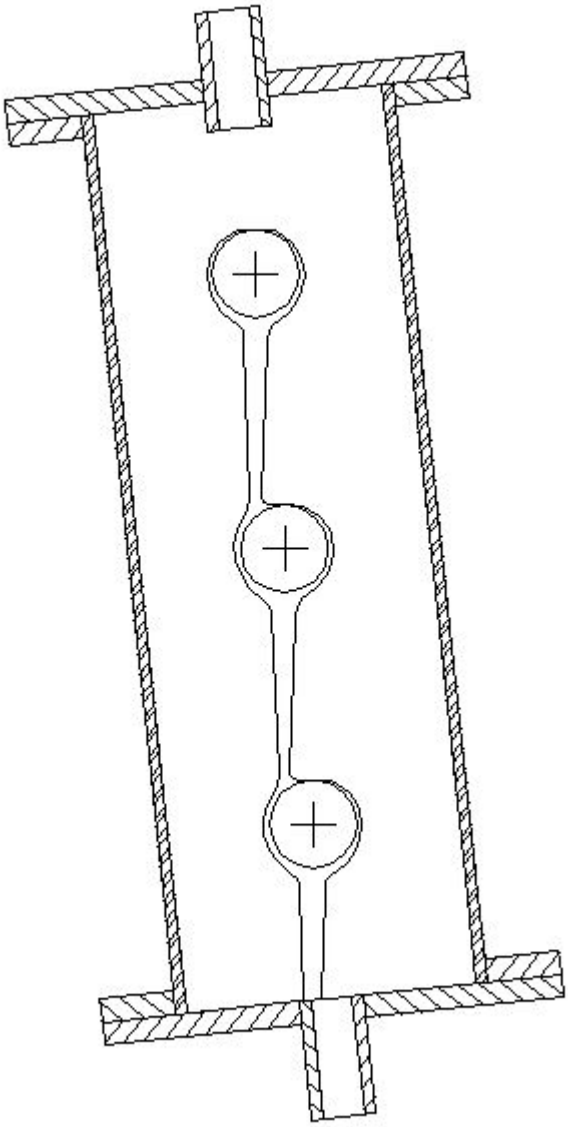

Figure A.3 Condensate Behaviour in the Setup at 6 Degree of Inclination

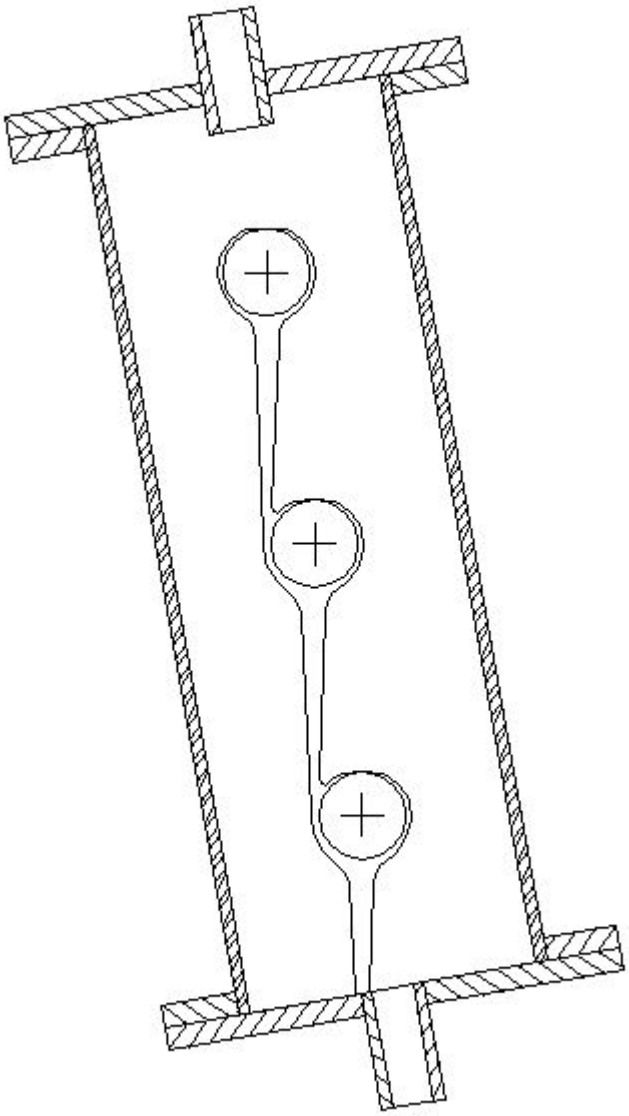

Figure A.4 Condensate Behaviour in the Setup at 10 Degree of Inclination

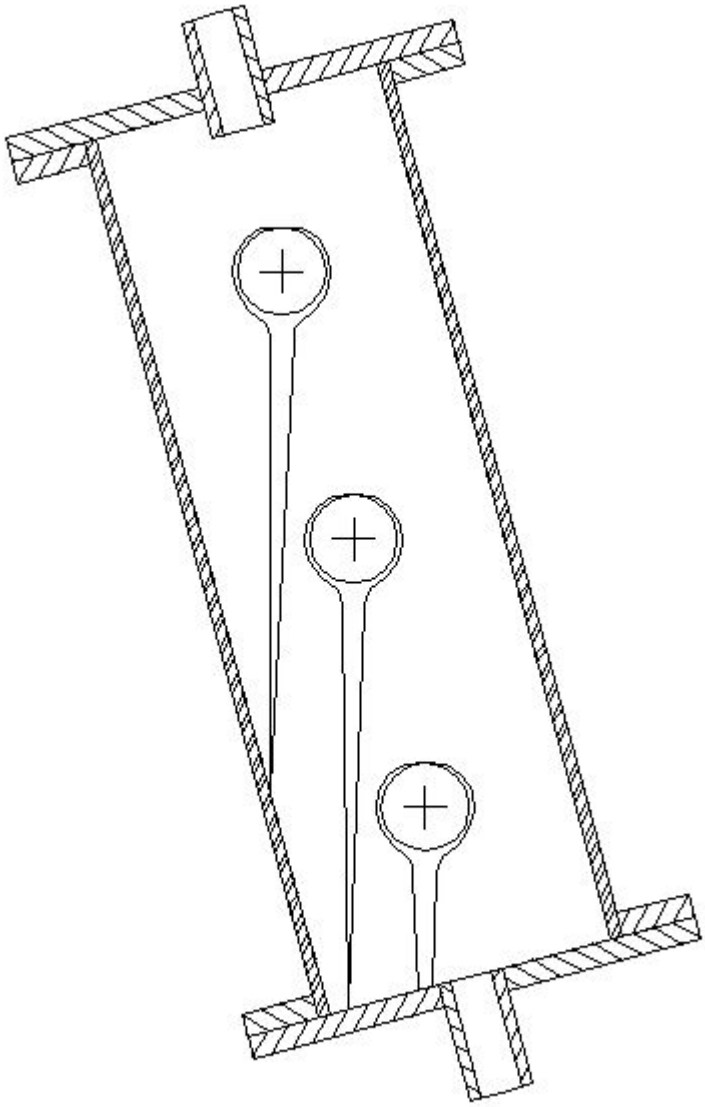

Figure A.5 Condensate Behaviour in the Setup at 15 Degree of Inclination

APPENDIX B

RESULTS OF THE EXPERIMENTS

Table B.1 Experimental Data and Results for 0° of Inclination

Data	1	2	3	4	5
T1	17.1	30.5	44.0	53.5	61.0
T2	89.1	90.1	91.4	92.3	93.5
T3	23.1	36.4	49.7	58.9	65.8
T4	17.0	30.5	44.0	53.5	61.0
T5	88.0	89.2	90.3	91.5	92.3
T6	22.9	36.3	49.6	58.7	65.7
T7	17.0	30.5	44.0	53.5	61.0
T8	86.8	87.8	89.7	90.7	91.8
T9	22.8	36.2	49.5	58.6	65.5
T10	97.9	97.8	98.1	98.1	98.1
Q1 (W)	348	342	331	314	279
Q2 (W)	343	337	325	302	273
Q3 (W)	337	331	319	296	262
h1 (W/m^2K)	10702	12018	13350	14620	16398
h2 (W/m^2K)	9354	10578	11266	12372	12734
h3 (W/m^2K)	8201	8940	10274	10822	11225

Table B.2 Experimental Data and Results for 3° of Inclination

Data	1	2	3	4	5
T1	17.0	31.5	41.5	51.0	62.0
T2	89.0	90.2	91.4	92.2	93.3
T3	23.1	37.4	47.2	56.4	66.9
T4	17.0	31.5	41.5	51.0	62.0
T5	88.1	89.3	90.5	91.5	92.5
T6	23.0	37.4	47.2	56.4	66.7
T7	17.0	31.5	41.4	51.0	62.0
T8	87.1	87.9	89.9	90.8	92.1
T9	22.9	37.3	46.9	56.2	66.5
T10	97.7	97.8	97.9	97.9	97.9
Q1 (W)	354	342	328	314	282
Q2 (W)	348	339	328	311	273
Q3 (W)	340	337	319	299	262
h1 (W/m^2K)	11005	12176	13640	14877	16569
h2 (W/m^2K)	9810	10795	11981	13127	13677
h3 (W/m^2K)	8662	9189	10721	11390	12192

Table B.3 Experimental Data and Results for 6° of Inclination

Data	1	2	3	4	5
T1	19.0	33.0	40.5	51.2	61.0
T2	89.1	90.1	91.5	92.3	93.4
T3	25.2	39.0	46.2	56.6	65.9
T4	19.0	33.0	40.5	51.2	61.0
T5	88.2	89.4	90.7	91.6	92.5
T6	25.1	38.9	46.2	56.5	65.8
T7	19.0	33.0	40.5	51.2	61.0
T8	87.3	88.0	90.0	90.8	92.2
T9	24.9	38.9	46.1	56.4	65.6
T10	97.8	97.9	98.1	97.9	98.1
Q1 (W)	357	345	331	314	282
Q2 (W)	351	341	328	308	276
Q3 (W)	340	339	322	300	265
h1 (W/m^2K)	11095	11964	13552	15008	16216
h2 (W/m^2K)	9840	10850	11981	13211	13329
h3 (W/m^2K)	8703	9268	10752	11435	12119

Table B.4 Experimental Data and Results for 10° of Inclination

Data	1	2	3	4	5
T1	18.1	31.5	37.0	51.0	60.3
T2	89.0	90.2	91.3	92.2	93.1
T3	24.3	37.5	42.7	56.5	65.2
T4	18.1	31.5	37.0	51.0	60.3
T5	88.3	89.5	90.6	91.5	92.2
T6	24.2	37.3	42.5	56.4	65.1
T7	18.1	31.5	37.0	51.0	60.3
T8	87.2	88.1	89.9	90.7	92.1
T9	24.0	37.1	42.3	56.2	65.0
T10	97.6	97.8	97.8	97.8	97.8
Q1 (W)	357	345	331	320	285
Q2 (W)	354	337	319	314	279
Q3 (W)	343	325	308	302	270
h1 (W/m^2K)	11224	12279	13761	15423	16383
h2 (W/m^2K)	10240	10960	11987	13460	13470
h3 (W/m^2K)	8904	9055	10528	11501	12820

Table B.5 Experimental Data and Results for 15° of Inclination

Data	1	2	3	4	5
T1	17.0	30.0	42.1	52.7	62.9
T2	89.0	90.2	91.2	91.9	93.3
T3	23.1	35.9	47.9	58.3	67.7
T4	17.0	30.0	42.1	52.7	62.9
T5	89.1	90.3	91.1	91.8	93.4
T6	23.0	36.0	47.8	58.3	67.6
T7	17.1	30.0	42.1	52.7	62.9
T8	88.9	90.1	91.2	91.9	93.3
T9	22.9	35.9	47.7	58.1	67.7
T10	97.8	97.6	97.8	97.8	97.8
Q1 (W)	354	342	334	325	279
Q2 (W)	348	348	331	325	273
Q3 (W)	337	342	325	314	279
h1 (W/m^2K)	10880	12505	13671	14905	16762
h2 (W/m^2K)	10825	12891	13350	14656	16786
h3 (W/m^2K)	10229	12338	13314	14372	16762

APPENDIX C

UNCERTAINTY ANALYSIS

There are two methods to calculate uncertainties; the worst-case combination and constant odds combination. According to the constant odds method, if a result R is to be calculated by a function $R = R(x_1, x_2, ..., x_n)$ from a single set of values of the input data x_i, then the uncertainty in R is given by:

$$w_R = \left[\left(\frac{\partial R}{\partial x_1} w_1 \right)^2 + \left(\frac{\partial R}{\partial x_2} w_2 \right)^2 + \cdots + \left(\frac{\partial R}{\partial x_n} w_n \right)^2 \right]^{1/2} \tag{C.1}$$

where w_n denotes the uncertainty in the nth independent variable.

As Kline and McClintock [33] claimed, Equation C.1 gives the uncertainty in R with good accuracy for most functions of engineering importance, and therefore will be employed to calculate the uncertainties in this study [34]. The rate of heat transfer and the heat transfer coefficient of the experiments are calculated with Equations 5.3 and 5.4. The uncertainties in the calculations of these equations will be determined for the results of the experiments which were conducted at vertical

position. The values of the variables used in the equations and the uncertainties related to these variables are presented in Table C.1.

Table C.1 Uncertainties of the Independent Variables Used in Equation 5.3 and 5.4

Variable	**Upper Tube**	**Middle Tube**	**Bottom Tube**
$\dot{m}(g/s)$	13.89 ± 0.1	13.89 ± 0.1	13.89 ± 0.1
$C_p\ (J/kgK)$	4181 ± 1	4181 ± 1	4181 ± 1
$T_{in}\left(°C\right)$	17.1 ± 0.1	17.0 ± 0.1	17.0 ± 0.1
$T_{out}\left(°C\right)$	23.1 ± 0.1	22.9 ± 0.1	22.8 ± 0.1
$r\left(mm\right)$	9.5 ± 0.01	9.5 ± 0.01	9.5 ± 0.01
$L\left(mm\right)$	62 ± 1	62 ± 1	62 ± 1
$T_{sat}\left(°C\right)$	97.9 ± 0.1	97.9 ± 0.1	97.9 ± 0.1
$T_w\left(°C\right)$	89.1 ± 0.1	88.0 ± 0.1	86.8 ± 0.1

A sample calculation of uncertainty in Equation 5.3 for the upper tube is presented in the following.

$$Q = \dot{m}C_p\left(T_{out} - T_{in}\right) = 348.45\ W$$

$$\frac{\partial Q}{\partial \dot{m}} = C_p\left(T_{out} - T_{in}\right)$$

$$\frac{\partial Q}{\partial C_p} = \dot{m}\left(T_{out} - T_{in}\right)$$

$$\frac{\partial Q}{\partial T_{in}} = -\dot{m}C_p$$

$$\frac{\partial Q}{\partial T_{out}} = \dot{m}C_p$$

$$w_{\dot{m}} = \pm 0.1$$

$$w_{Cp} = \pm 1$$

$$w_{T_{in}} = \pm 0.1$$

$$w_{T_{out}} = \pm 0.1$$

Substituting these values into Equation C.1

$$w_Q = \left[\left(\frac{\partial Q}{\partial \dot{m}} w_{\dot{m}} \right)^2 + \left(\frac{\partial Q}{\partial C_p} w_{C_p} \right)^2 + \left(\frac{\partial Q}{\partial T_{in}} w_{T_{in}} \right)^2 + \left(\frac{\partial Q}{\partial T_{out}} w_{T_{out}} \right)^2 \right]^{1/2}$$

$$w_Q = 8.59$$

$$\text{Uncertainty } (\%) = \frac{w_Q}{Q} = 2.47\%$$

If the same procedure is applied to Equations 5.3 and 5.4 for all condensation tubes, the following table is obtained for the uncertainties in the experimental results.

Table C.2 Uncertainties in the Experimental Results

	Uncertainty in Q (%)	Uncertainty in h (%)
Upper Tube	2.47	2.28
Middle Tube	2.50	2.16
Bottom Tube	2.54	2.06

APPENDIX D

MATHCAD PROGRAM SOURCE

$r \equiv 15 \cdot 10^{-3} \cdot m$ $\quad g \equiv 9.81 \cdot \frac{m}{s^2}$ $\quad h \equiv 30 \cdot mm$ $\quad axis2 := 0.5$

$\rho_f \equiv 963 \cdot \frac{kg}{m^3}$ $\quad C_{pw} \equiv 4180 \cdot \frac{J}{kg \cdot K}$ $\quad h_g \equiv 2676 \cdot 10^3 \cdot \frac{J}{kg}$

$\rho_g \equiv 0.596 \cdot \frac{kg}{m^3}$ $\quad C_{pc} \equiv 4210 \cdot \frac{J}{kg \cdot K}$ $\quad h_{fg} \equiv 2278 \cdot 10^3 \cdot \frac{J}{kg}$

$k_f \equiv 613 \cdot 10^{-3} \cdot \frac{W}{m \cdot K}$ $\quad \nu \equiv 0.318 \cdot 10^{-6} \cdot \frac{m^2}{s}$ $\quad \mu \equiv 3.062 \cdot 10^{-4} \cdot Pa \cdot s$

$$
\text{result} := \left|
\begin{array}{l}
neq \leftarrow 18 \\
\Delta x \leftarrow \dfrac{\pi \cdot r}{40} \\
xloc \leftarrow \Delta x \\
\text{for } i \in 0..neq \\
\quad \left|
\begin{array}{l}
\delta_i \leftarrow \left[\dfrac{\nu \cdot \left(3 \cdot k_f \cdot \Delta T \cdot xloc\right)}{g \cdot \rho_f \cdot h_{fg} \cdot \sin\left(\dfrac{xloc}{r}\right)} \right]^{\frac{1}{4}} \\
U\omega_i \leftarrow \dfrac{g \cdot \rho_f \cdot \left(\delta_i\right)^2}{2 \cdot \mu} \\
xloc \leftarrow xloc + \Delta x
\end{array}
\right. \\
\delta inc \leftarrow \dfrac{\delta_{18}}{1000} \\
Uinc \leftarrow \dfrac{U\omega_{18}}{1000} \\
\text{for } iter \in 1..20 \\
\quad \left| C_0 \leftarrow \dfrac{5}{8} \cdot \dfrac{\delta_0 \cdot U\omega_0 - 0}{\Delta x} - \dfrac{k_f \cdot \Delta T}{\rho_f \cdot h_{fg} \cdot \delta_0} \right.
\end{array}
\right.
$$

$$C_1 \leftarrow \frac{17}{35}\cdot\rho_f\cdot\left[\frac{\delta_0\cdot\left(U\omega_0\right)^2 - 0}{\Delta x}\right] - \delta_0\cdot\rho_f\cdot g\cdot\sin\left(\frac{\Delta x}{r}\right) + \frac{3}{2}\cdot\mu\cdot\frac{U\omega_0}{\delta_0}$$

$$\psi_{(0,0)} \leftarrow \frac{\left[\frac{5}{8}\cdot\frac{\left(\delta_0 + \delta inc\right)\cdot U\omega_0 - 0}{\Delta x} - \frac{k_f\cdot\Delta T}{\rho_f\cdot h_{fg}\cdot\left(\delta_0 + \delta inc\right)}\right] - \left(\frac{5}{8}\cdot\frac{\delta_0\cdot U\omega_0 - 0}{\Delta x} - \frac{k_f\cdot\Delta T}{\rho_f\cdot h_{fg}\cdot\delta_0}\right)}{\delta inc}$$

$$\psi_{(0,1)} \leftarrow \frac{\left[\frac{5}{8}\cdot\frac{\delta_0\cdot\left(U\omega_0 + Uinc\right) - 0}{\Delta x}\right] - \left(\frac{5}{8}\cdot\frac{\delta_0\cdot U\omega_0 - 0}{\Delta x}\right)}{Uinc}$$

$$\psi_{(1,0)} \leftarrow \frac{\left[\frac{17}{35}\cdot\rho_f\cdot\left[\frac{\left(\delta_0 + \delta inc\right)\cdot\left(U\omega_0\right)^2 - 0}{\Delta x}\right] - \left(\delta_0 + \delta inc\right)\cdot\rho_f\cdot g\cdot\sin\left(\frac{\Delta x}{r}\right) + \frac{3}{2}\cdot\mu\cdot\frac{U\omega_0}{\left(\delta_0 + \delta inc\right)}\right] \ldots + \blacksquare - \left[\frac{17}{35}\cdot\rho_f\cdot\left[\frac{\delta_0\cdot\left(U\omega_0\right)^2 - 0}{\Delta x}\right] - \delta_0\cdot\rho_f\cdot g\cdot\sin\left(\frac{\Delta x}{r}\right) + \frac{3}{2}\cdot\mu\cdot\frac{U\omega_0}{\delta_0}\right]}{\delta inc}$$

$$\psi_{(1,1)} \leftarrow \frac{\left[\frac{17}{35}\cdot\rho_f\cdot\left[\frac{\delta_0\cdot\left(U\omega_0 + Uinc\right)^2 - 0}{\Delta x}\right] - \delta_0\cdot\rho_f\cdot g\cdot\sin\left(\frac{\Delta x}{r}\right) + \frac{3}{2}\cdot\mu\cdot\frac{\left(U\omega_0 + Uinc\right)}{\delta_0}\right] \ldots + \blacksquare - \left[\frac{17}{35}\cdot\rho_f\cdot\left[\frac{\delta_0\cdot\left(U\omega_0\right)^2 - 0}{\Delta x}\right] - \delta_0\cdot\rho_f\cdot g\cdot\sin\left(\frac{\Delta x}{r}\right) + \frac{3}{2}\cdot\mu\cdot\frac{U\omega_0}{\delta_0}\right]}{Uinc}$$

$$\mathrm{del} \leftarrow -\left(\psi^{-1}\cdot C\right)$$

$$\delta_0 \leftarrow \delta_0 + \mathrm{del}_0$$

$$U\omega_0 \leftarrow U\omega_0 + \mathrm{del}_1$$

for $ie \in 1..neq$

for $iter \in 1..20$

$$C_0 \leftarrow \frac{5}{8}\cdot\frac{\delta_{ie}\cdot U\omega_{ie} - \delta_{ie-1}\cdot U\omega_{ie-1}}{\Delta x} - \frac{k_f\cdot\Delta T}{\rho_f\cdot h_{fg}\cdot\delta_{ie}}$$

$$C_1 \leftarrow \frac{17}{35}\cdot\rho_f\cdot\frac{\left[\left(\delta_{ie}\right)\cdot\left(U\omega_{ie}\right)^2 - \delta_{ie-1}\cdot\left(U\omega_{ie-1}\right)^2\right]}{\Delta x} - \delta_{ie}\cdot\rho_f\cdot g\cdot\sin\left(\frac{\Delta x}{r}\right) + \frac{3}{2}\cdot\mu\cdot\frac{U\omega_{ie}}{\delta_{ie}}$$

$$\psi_{(0,0)} \leftarrow \frac{\left[\frac{5}{8}\cdot\frac{\left(\delta_{ie}+\delta inc\right)\cdot U\omega_{ie} - \delta_{ie-1}\cdot U\omega_{ie-1}}{\Delta x} - \frac{k_f\cdot\Delta T}{\rho_f\cdot h_{fg}\cdot\left(\delta_{ie}+\delta inc\right)}\right] \ldots + \blacksquare - \left(\frac{5}{8}\cdot\frac{\delta_{ie}\cdot U\omega_{ie} - \delta_{ie-1}\cdot U\omega_{ie-1}}{\Delta x} - \frac{k_f\cdot\Delta T}{\rho_f\cdot h_{fg}\cdot\delta_{ie}}\right)}{\delta inc}$$

$$\psi_{(0,1)} \leftarrow \frac{\left[\frac{5}{8}\cdot\frac{\delta_{ie}\cdot\left(U\omega_{ie}+Uinc\right) - \delta_{ie-1}\cdot U\omega_{ie-1}}{\Delta x}\right] - \left(\frac{5}{8}\cdot\frac{\delta_{ie}\cdot U\omega_{ie} - \delta_{ie-1}\cdot U\omega_{ie-1}}{\Delta x}\right)}{Uinc}$$

$$\psi_{(1,0)} \leftarrow \frac{\left[\frac{17}{35}\cdot\rho_f\cdot\frac{\left[\left(\delta_{ie}+\delta inc\right)\cdot\left(U\omega_{ie}\right)^2-\delta_{ie-1}\cdot\left(U\omega_{ie-1}\right)^2\right]}{\Delta x}-\left(\delta_{ie}+\delta inc\right)\cdot\rho_f\cdot g\cdot\sin\left(\frac{\Delta x}{r}\right)+\frac{3}{2}\cdot\mu\cdot\frac{U\omega_{ie}}{\left(\delta_{ie}+\delta inc\right)}\right]\ldots + \blacksquare - \left[\frac{17}{35}\cdot\rho_f\cdot\frac{\left[\delta_{ie}\cdot\left(U\omega_{ie}\right)^2-\delta_{ie-1}\cdot\left(U\omega_{ie-1}\right)^2\right]}{\Delta x}-\delta_{ie}\cdot\rho_f\cdot g\cdot\sin\left(\frac{\Delta x}{r}\right)+\frac{3}{2}\cdot\mu\cdot\frac{U\omega_{ie}}{\delta_{ie}}\right]}{\delta inc}$$

$$\psi_{(1,1)} \leftarrow \frac{\left[\frac{17}{35}\cdot\rho_f\cdot\frac{\left[\delta_{ie}\cdot\left(U\omega_{ie}+Uinc\right)^2-\delta_{ie-1}\cdot\left(U\omega_{ie-1}\right)^2\right]}{\Delta x}-\delta_{ie}\cdot\rho_f\cdot g\cdot\sin\left(\frac{\Delta x}{r}\right)+\frac{3}{2}\cdot\mu\cdot\frac{\left(U\omega_{ie}+Uinc\right)}{\delta_{ie}}\right]\ldots + \blacksquare - \left[\frac{17}{35}\cdot\rho_f\cdot\frac{\left[\delta_{ie}\cdot\left(U\omega_{ie}\right)^2-\delta_{ie-1}\cdot\left(U\omega_{ie-1}\right)^2\right]}{\Delta x}-\delta_{ie}\cdot\rho_f\cdot g\cdot\sin\left(\frac{\Delta x}{r}\right)+\frac{3}{2}\cdot\mu\cdot\frac{U\omega_{ie}}{\delta_{ie}}\right]}{Uinc}$$

$$del \leftarrow -\left(\psi^{-1}\cdot C\right)$$

$$\delta_{ie} \leftarrow \delta_{ie} + del_0$$

$$U\omega_{ie} \leftarrow U\omega_{ie} + del_1$$

$$result1 \leftarrow augment\left(\delta, U\omega\right)$$

$$Um \leftarrow result1_{18,1}$$

$$v1 \leftarrow Um$$

$$\delta 1 \leftarrow result1_{18,0}$$

$$v2 \leftarrow \sqrt{v1^2 + 2\cdot g\cdot h}$$

$$\delta 2 \leftarrow \frac{\delta 1 \cdot v1}{v2}$$

for $i \in 0..neq$

$$\delta_i \leftarrow \left[\frac{\nu \cdot \left(3 \cdot k_f \cdot \Delta T \cdot xloc\right)}{g \cdot \rho_f \cdot h_{fg} \cdot \sin\left(\frac{xloc}{r}\right)}\right]^{\frac{1}{4}}$$

$$U\omega_i \leftarrow \frac{g \cdot \rho_f \cdot \left(\delta_i\right)^2}{2 \cdot \mu}$$

$$xloc \leftarrow xloc + \Delta x$$

$$U\omega_0 \leftarrow v2$$

$$\Delta_0 \leftarrow \delta 2 \cdot axis2$$

$$\delta inc \leftarrow \frac{\delta_{18}}{1000}$$

$$Uinc \leftarrow \frac{U\omega_{18}}{1000}$$

$$h \leftarrow r \cdot \left(1 - \cos\left(\frac{\Delta x}{r}\right)\right)$$

$$U\omega_0 \leftarrow \sqrt{(v2)^2 + 2\cdot g\cdot h}$$

$$\Delta_0 \leftarrow \frac{v2\cdot\Delta_0}{U\omega_0}$$

for $iter \in 1 .. 10$

$$C_0 \leftarrow \frac{5}{8}\cdot\frac{\delta_0\cdot U\omega_0 - 0}{\Delta x} - \frac{k_f\cdot\Delta T}{\rho_f\cdot h_{fg}\cdot(\delta_0 + \Delta_0)} + \frac{\Delta_0\cdot U\omega_0 - \delta 2\cdot axis2\cdot v2}{\Delta x}$$

$$C_1 \leftarrow \frac{17}{35}\cdot\rho_f\cdot\left[\frac{\delta_0\cdot(U\omega_0)^2 - 0}{\Delta x}\right] - \delta_0\cdot\rho_f\cdot g\cdot\sin\left(\frac{\Delta x}{r}\right) + \left(\frac{3}{2}\cdot\mu\cdot\frac{U\omega_0}{\delta_0}\right) + \rho_f\cdot\left[\frac{\Delta_0\cdot(U\omega_0)^2 - \delta 2\cdot axis2\cdot v2^2}{\Delta x}\right]$$

$$\psi_{(0,0)} \leftarrow \frac{\left[\frac{5}{8}\cdot\frac{(\delta_0 + \delta inc)\cdot U\omega_0 - 0}{\Delta x} - \frac{k_f\cdot\Delta T}{\rho_f\cdot h_{fg}\cdot(\delta_0 + \delta inc + \Delta_0)} + \frac{\Delta_0\cdot U\omega_0 - 0}{\Delta x}\right] \ldots + \blacksquare - \left[\frac{5}{8}\cdot\frac{\delta_0\cdot U\omega_0 - 0}{\Delta x} - \frac{k_f\cdot\Delta T}{\rho_f\cdot h_{fg}\cdot(\delta_0 + \Delta_0)} + \frac{\Delta_0\cdot U\omega_0 - 0}{\Delta x}\right]}{\delta inc}$$

$$\psi_{(0,1)} \leftarrow \frac{\left[\frac{5}{8}\cdot\frac{\delta_0\cdot(U\omega_0 + Uinc) - 0}{\Delta x}\right] - \left(\frac{5}{8}\cdot\frac{\delta_0\cdot U\omega_0 - 0}{\Delta x}\right)}{Uinc}$$

$\blacksquare$

$\blacksquare$

$$\psi_{(1,0)} \leftarrow \frac{\left[\frac{17}{35}\cdot\rho_f\cdot\left[\frac{(\delta_0+\delta inc)\cdot(U\omega_0)^2-0}{\Delta x}\right]-(\delta_0+\delta inc)\cdot\rho_f\cdot g\cdot\sin\left(\frac{\Delta x}{r}\right)+\frac{3}{2}\cdot\mu\cdot\frac{U\omega_0}{(\delta_0+\delta inc)}\right]\ldots + \blacksquare - \left[\frac{17}{35}\cdot\rho_f\cdot\left[\frac{\delta_0\cdot(U\omega_0)^2-0}{\Delta x}\right]-\delta_0\cdot\rho_f\cdot g\cdot\sin\left(\frac{\Delta x}{r}\right)+\frac{3}{2}\cdot\mu\cdot\frac{U\omega_0}{\delta_0}\right]}{\delta inc}$$

$$\psi_{(1,1)} \leftarrow \frac{\left[\frac{17}{35}\cdot\rho_f\cdot\left[\frac{\delta_0\cdot(U\omega_0+Uinc)^2-0}{\Delta x}\right]-\delta_0\cdot\rho_f\cdot g\cdot\sin\left(\frac{\Delta x}{r}\right)+\frac{3}{2}\cdot\mu\cdot\frac{(U\omega_0+Uinc)}{\delta_0}\right]\ldots + \blacksquare - \left[\frac{17}{35}\cdot\rho_f\cdot\left[\frac{\delta_0\cdot(U\omega_0)^2-0}{\Delta x}\right]-\delta_0\cdot\rho_f\cdot g\cdot\sin\left(\frac{\Delta x}{r}\right)+\frac{3}{2}\cdot\mu\cdot\frac{U\omega_0}{\delta_0}\right]}{Uinc}$$

$$del \leftarrow -\left(\psi^{-1}\cdot C\right)$$

$$\delta_0 \leftarrow \delta_0 + del_0$$

$$U\omega_0 \leftarrow U\omega_0 + del_1$$

for $ie \in 1..neq$

$$\Delta_{ie} \leftarrow \frac{U\omega_{ie-1}\cdot\Delta_{ie-1}}{U\omega_{ie}}$$

$$h \leftarrow r\cdot\left(1-\cos\left(\frac{\Delta x}{r}\right)\right)$$

$$U\omega_{ie} \leftarrow \sqrt{\left(U\omega_{ie-1}\right)^2 + 2\cdot g\cdot h}$$

for $iter \in 1..10$

$$C_0 \leftarrow \frac{5}{8}\cdot\frac{\delta_{ie}\cdot U\omega_{ie} - \delta_{ie-1}\cdot U\omega_{ie-1}}{\Delta x} - \frac{k_f\cdot\Delta T}{\rho_f\cdot h_{fg}\cdot\left(\delta_{ie}+\Delta_{ie}\right)} + \frac{\Delta_{ie}\cdot U\omega_{ie} - \Delta_{ie-1}\cdot U\omega_{ie-1}}{\Delta x}$$

$$C_1 \leftarrow \left[\frac{17}{35}\cdot\rho_f\cdot\frac{\left[\left(\delta_{ie}\right)\cdot\left(U\omega_{ie}\right)^2 - \delta_{ie-1}\cdot\left(U\omega_{ie-1}\right)^2\right]}{\Delta x} - \delta_{ie}\cdot\rho_f\cdot g\cdot\sin\left(\frac{\Delta x}{r}\right) + \left(\frac{3}{2}\cdot\mu\cdot\frac{U\omega_{ie}}{\delta_{ie}}\right)\right]\ldots$$
$$+\rho_f\cdot\frac{\Delta_{ie}\cdot\left(U\omega_{ie}\right)^2 - \Delta_{ie-1}\cdot\left(U\omega_{ie-1}\right)^2}{\Delta x}$$

$$\psi(0,0) \leftarrow \frac{\left[\frac{5}{8}\cdot\frac{\left(\delta_{ie}+\delta inc\right)\cdot U\omega_{ie} - \delta_{ie-1}\cdot U\omega_{ie-1}}{\Delta x} - \frac{k_f\cdot\Delta T}{\rho_f\cdot h_{fg}\cdot\left(\delta_{ie}+\delta inc+\Delta_{ie}\right)}\right]\ldots + \blacksquare - \left[\frac{5}{8}\cdot\frac{\delta_{ie}\cdot U\omega_{ie} - \delta_{ie-1}\cdot U\omega_{ie-1}}{\Delta x} - \frac{k_f\cdot\Delta T}{\rho_f\cdot h_{fg}\cdot\left(\delta_{ie}+\Delta_{ie}\right)}\right]}{\delta inc}$$

$$\psi(0,1) \leftarrow \frac{\left[\frac{5}{8}\cdot\frac{\delta_{ie}\cdot\left(U\omega_{ie}+Uinc\right) - \delta_{ie-1}\cdot U\omega_{ie-1}}{\Delta x}\right] - \left(\frac{5}{8}\cdot\frac{\delta_{ie}\cdot U\omega_{ie} - \delta_{ie-1}\cdot U\omega_{ie-1}}{\Delta x}\right)}{Uinc}$$

$\blacksquare$

$\blacksquare$

$$\psi_{(1,0)} \leftarrow \frac{\left[\frac{17}{35}\cdot\rho_f\cdot\frac{\left[\left(\delta_{ie}+\delta inc\right)\cdot\left(U\omega_{ie}\right)^2-\delta_{ie-1}\cdot\left(U\omega_{ie-1}\right)^2\right]}{\Delta x}-\left(\delta_{ie}+\delta inc\right)\cdot\rho_f\cdot g\cdot\sin\left(\frac{\Delta x}{r}\right)+\frac{3}{2}\cdot\mu\cdot\frac{U\omega_{ie}}{\left(\delta_{ie}+\delta inc\right)}\right]\ldots + \blacksquare-\left[\frac{17}{35}\cdot\rho_f\cdot\frac{\left[\delta_{ie}\cdot\left(U\omega_{ie}\right)^2-\delta_{ie-1}\cdot\left(U\omega_{ie-1}\right)^2\right]}{\Delta x}-\delta_{ie}\cdot\rho_f\cdot g\cdot\sin\left(\frac{\Delta x}{r}\right)+\frac{3}{2}\cdot\mu\cdot\frac{U\omega_{ie}}{\delta_{ie}}\right]}{\delta inc}$$

$$\psi_{(1,1)} \leftarrow \frac{\left[\frac{17}{35}\cdot\rho_f\cdot\frac{\left[\delta_{ie}\cdot\left(U\omega_{ie}+Uinc\right)^2-\delta_{ie-1}\cdot\left(U\omega_{ie-1}\right)^2\right]}{\Delta x}-\delta_{ie}\cdot\rho_f\cdot g\cdot\sin\left(\frac{\Delta x}{r}\right)+\frac{3}{2}\cdot\mu\cdot\frac{\left(U\omega_{ie}+Uinc\right)}{\delta_{ie}}\right]\ldots + \blacksquare-\left[\frac{17}{35}\cdot\rho_f\cdot\frac{\left[\delta_{ie}\cdot\left(U\omega_{ie}\right)^2-\delta_{ie-1}\cdot\left(U\omega_{ie-1}\right)^2\right]}{\Delta x}-\delta_{ie}\cdot\rho_f\cdot g\cdot\sin\left(\frac{\Delta x}{r}\right)+\frac{3}{2}\cdot\mu\cdot\frac{U\omega_{ie}}{\delta_{ie}}\right]}{Uinc}$$

$$del \leftarrow -\left(\psi^{-1}\cdot C\right)$$

$$\delta_{ie} \leftarrow \delta_{ie} + del_0$$

$$U\omega_{ie} \leftarrow U\omega_{ie} + del_1$$

for $iter \in 1..10$

$$C_0 \leftarrow \frac{5}{8}\cdot\frac{\delta_{ie}\cdot U\omega_{ie}-\delta_{ie-1}\cdot U\omega_{ie-1}}{\Delta x}-\frac{k_f\cdot\Delta T}{\rho_f\cdot h_{fg}\cdot\delta_{ie}}$$

$\blacksquare$

$\blacksquare$

$$C_1 \leftarrow \frac{17}{35}\cdot\rho_f\cdot\frac{\left[\left(\delta_{ie}\right)\cdot\left(U\omega_{ie}\right)^2-\delta_{ie-1}\cdot\left(U\omega_{ie-1}\right)^2\right]}{\Delta x}-\delta_{ie}\cdot\rho_f\cdot g\cdot\sin\left(\frac{\Delta x}{r}\right)+\left(\frac{3}{2}\cdot\mu\cdot\frac{U\omega_{ie}}{\delta_{ie}}\right)$$

$$\psi_{(0,0)} \leftarrow \frac{\left[\frac{5}{8}\cdot\frac{\left(\delta_{ie}+\delta inc\right)\cdot U\omega_{ie}-\delta_{ie-1}\cdot U\omega_{ie-1}}{\Delta x}-\frac{k_f\cdot\Delta T}{\rho_f\cdot h_{fg}\cdot\left(\delta_{ie}+\delta inc\right)}\right]\ldots + \blacksquare - \left(\frac{5}{8}\cdot\frac{\delta_{ie}\cdot U\omega_{ie}-\delta_{ie-1}\cdot U\omega_{ie-1}}{\Delta x}-\frac{k_f\cdot\Delta T}{\rho_f\cdot h_{fg}\cdot\delta_{ie}}\right)}{\delta inc}$$

$$\psi_{(0,1)} \leftarrow \frac{\left[\frac{5}{8}\cdot\frac{\delta_{ie}\cdot\left(U\omega_{ie}+Uinc\right)-\delta_{ie-1}\cdot U\omega_{ie-1}}{\Delta x}\right]-\left(\frac{5}{8}\cdot\frac{\delta_{ie}\cdot U\omega_{ie}-\delta_{ie-1}\cdot U\omega_{ie-1}}{\Delta x}\right)}{Uinc}$$

$$\psi_{(1,0)} \leftarrow \frac{\left[\frac{17}{35}\cdot\rho_f\cdot\frac{\left[\left(\delta_{ie}+\delta inc\right)\cdot\left(U\omega_{ie}\right)^2-\delta_{ie-1}\cdot\left(U\omega_{ie-1}\right)^2\right]}{\Delta x}-\left(\delta_{ie}+\delta inc\right)\cdot\rho_f\cdot g\cdot\sin\left(\frac{\Delta x}{r}\right)+\frac{3}{2}\cdot\mu\cdot\frac{U\omega_{ie}}{\left(\delta_{ie}+\delta inc\right)}\right]\ldots + \blacksquare - \left[\frac{17}{35}\cdot\rho_f\cdot\frac{\left[\delta_{ie}\cdot\left(U\omega_{ie}\right)^2-\delta_{ie-1}\cdot\left(U\omega_{ie-1}\right)^2\right]}{\Delta x}-\delta_{ie}\cdot\rho_f\cdot g\cdot\sin\left(\frac{\Delta x}{r}\right)+\frac{3}{2}\cdot\mu\cdot\frac{U\omega_{ie}}{\delta_{ie}}\right]}{\delta inc}$$

$\blacksquare$

$\blacksquare$

$\blacksquare$

$\blacksquare$

$$\psi_{(1,1)} \leftarrow \frac{\left[\frac{17}{35}\cdot\rho_f\cdot\frac{\left[\delta_{ie}\cdot\left(U\omega_{ie}+Uinc\right)^2-\delta_{ie-1}\cdot\left(U\omega_{ie-1}\right)^2\right]}{\Delta x}-\delta_{ie}\cdot\rho_f\cdot g\cdot\sin\left(\frac{\Delta x}{r}\right)+\frac{3}{2}\cdot\mu\cdot\frac{\left(U\omega_{ie}+Uinc\right)}{\delta_{ie}}\right]\ldots + \blacksquare - \left[\frac{17}{35}\cdot\rho_f\cdot\frac{\left[\delta_{ie}\cdot\left(U\omega_{ie}\right)^2-\delta_{ie-1}\cdot\left(U\omega_{ie-1}\right)^2\right]}{\Delta x}-\delta_{ie}\cdot\rho_f\cdot g\cdot\sin\left(\frac{\Delta x}{r}\right)+\frac{3}{2}\cdot\mu\cdot\frac{U\omega_{ie}}{\delta_{ie}}\right]}{Uinc}$$

$$del \leftarrow -\left(\psi^{-1}\cdot C\right)$$

$$\delta_{ie} \leftarrow \delta_{ie} + del_0$$

$$U\omega_{ie} \leftarrow U\omega_{ie} + del_1$$

$$\delta \leftarrow \delta + \Delta$$

$$result2 \leftarrow augment(\delta, U\omega)$$

$$result2 \leftarrow augment(result1, result2)$$

$$Um \leftarrow result2_{18,3}$$

$$v1 \leftarrow Um$$

$$\delta 1 \leftarrow result2_{18,2}$$

$$h \leftarrow 20\cdot 10^{-3}$$

$$xloc \leftarrow \Delta x$$

$$v2 \leftarrow \sqrt{v1^2 + 2\cdot g\cdot h}$$

$\blacksquare$

$$\delta 2 \leftarrow \frac{\delta 1 \cdot v1}{v2}$$

for $i \in 0..neq$

$$\delta_i \leftarrow \left[\frac{\nu \cdot \left(3 \cdot k_f \cdot \Delta T \cdot xloc\right)}{g \cdot \rho_f \cdot h_{fg} \cdot \sin\left(\frac{xloc}{r}\right)}\right]^{\frac{1}{4}}$$

$$U\omega_i \leftarrow \frac{g \cdot \rho_f \cdot \left(\delta_i\right)^2}{2 \cdot \mu}$$

$$xloc \leftarrow xloc + \Delta x$$

$$U\omega_0 \leftarrow v2$$

$$\Delta_0 \leftarrow \delta 2 \cdot axis2$$

$$\delta inc \leftarrow \frac{\delta_{18}}{1000}$$

$$Uinc \leftarrow \frac{U\omega_{18}}{1000}$$

$$h \leftarrow r \cdot \left(1 - \cos\left(\frac{\Delta x}{r}\right)\right)$$

$$U\omega_0 \leftarrow \sqrt{(v2)^2 + 2\cdot g\cdot h}$$

$$\Delta_0 \leftarrow \frac{v2\cdot\Delta_0}{U\omega_0}$$

for $iter \in 1 .. 10$

$$C_0 \leftarrow \frac{5}{8}\cdot\frac{\delta_0\cdot U\omega_0 - 0}{\Delta x} - \frac{k_f\cdot\Delta T}{\rho_f\cdot h_{fg}\cdot(\delta_0 + \Delta_0)} + \frac{\Delta_0\cdot U\omega_0 - \delta 2\cdot axis2\cdot v2}{\Delta x}$$

$$C_1 \leftarrow \frac{17}{35}\cdot\rho_f\cdot\left[\frac{\delta_0\cdot(U\omega_0)^2 - 0}{\Delta x}\right] - \delta_0\cdot\rho_f\cdot g\cdot\sin\left(\frac{\Delta x}{r}\right) + \left(\frac{3}{2}\cdot\mu\cdot\frac{U\omega_0}{\delta_0}\right) + \rho_f\cdot\left[\frac{\Delta_0\cdot(U\omega_0)^2 - \delta 2\cdot axis2\cdot v2^2}{\Delta x}\right]$$

$$\psi_{(0,0)} \leftarrow \frac{\left[\frac{5}{8}\cdot\frac{(\delta_0 + \delta inc)\cdot U\omega_0 - 0}{\Delta x} - \frac{k_f\cdot\Delta T}{\rho_f\cdot h_{fg}\cdot(\delta_0 + \delta inc + \Delta_0)} + \frac{\Delta_0\cdot U\omega_0 - 0}{\Delta x}\right] \ldots + \blacksquare - \left[\frac{5}{8}\cdot\frac{\delta_0\cdot U\omega_0 - 0}{\Delta x} - \frac{k_f\cdot\Delta T}{\rho_f\cdot h_{fg}\cdot(\delta_0 + \Delta_0)} + \frac{\Delta_0\cdot U\omega_0 - 0}{\Delta x}\right]}{\delta inc}$$

$$\psi_{(0,1)} \leftarrow \frac{\left[\frac{5}{8}\cdot\frac{\delta_0\cdot(U\omega_0 + Uinc) - 0}{\Delta x}\right] - \left(\frac{5}{8}\cdot\frac{\delta_0\cdot U\omega_0 - 0}{\Delta x}\right)}{Uinc}$$

$\blacksquare$

$\blacksquare$

$$\psi_{(1,0)} \leftarrow \frac{\left[\frac{17}{35}\cdot\rho_f\cdot\left[\frac{(\delta_0+\delta inc)\cdot(U\omega_0)^2-0}{\Delta x}\right]-(\delta_0+\delta inc)\cdot\rho_f\cdot g\cdot\sin\left(\frac{\Delta x}{r}\right)+\frac{3}{2}\cdot\mu\cdot\frac{U\omega_0}{(\delta_0+\delta inc)}\right]\ldots + \blacksquare - \left[\frac{17}{35}\cdot\rho_f\cdot\left[\frac{\delta_0\cdot(U\omega_0)^2-0}{\Delta x}\right]-\delta_0\cdot\rho_f\cdot g\cdot\sin\left(\frac{\Delta x}{r}\right)+\frac{3}{2}\cdot\mu\cdot\frac{U\omega_0}{\delta_0}\right]}{\delta inc}$$

$$\psi_{(1,1)} \leftarrow \frac{\left[\frac{17}{35}\cdot\rho_f\cdot\left[\frac{\delta_0\cdot(U\omega_0+Uinc)^2-0}{\Delta x}\right]-\delta_0\cdot\rho_f\cdot g\cdot\sin\left(\frac{\Delta x}{r}\right)+\frac{3}{2}\cdot\mu\cdot\frac{(U\omega_0+Uinc)}{\delta_0}\right]\ldots + \blacksquare - \left[\frac{17}{35}\cdot\rho_f\cdot\left[\frac{\delta_0\cdot(U\omega_0)^2-0}{\Delta x}\right]-\delta_0\cdot\rho_f\cdot g\cdot\sin\left(\frac{\Delta x}{r}\right)+\frac{3}{2}\cdot\mu\cdot\frac{U\omega_0}{\delta_0}\right]}{Uinc}$$

$$del \leftarrow -\left(\psi^{-1}\cdot C\right)$$

$$\delta_0 \leftarrow \delta_0 + del_0$$

$$U\omega_0 \leftarrow U\omega_0 + del_1$$

for $ie \in 1..neq$

$$\Delta_{ie} \leftarrow \frac{U\omega_{ie-1}\cdot\Delta_{ie-1}}{U\omega_{ie}}$$

$$h \leftarrow r\cdot\left(1-\cos\left(\frac{\Delta x}{r}\right)\right)$$

$$U\omega_{ie} \leftarrow \sqrt{\left(U\omega_{ie-1}\right)^2 + 2\cdot g\cdot h}$$

for $iter \in 1 .. 10$

$$C_0 \leftarrow \frac{5}{8}\cdot\frac{\delta_{ie}\cdot U\omega_{ie} - \delta_{ie-1}\cdot U\omega_{ie-1}}{\Delta x} - \frac{k_f\cdot \Delta T}{\rho_f\cdot h_{fg}\cdot\left(\delta_{ie} + \Delta_{ie}\right)} + \frac{\Delta_{ie}\cdot U\omega_{ie} - \Delta_{ie-1}\cdot U\omega_{ie-1}}{\Delta x}$$

$$C_1 \leftarrow \left[\frac{17}{35}\cdot\rho_f\cdot\frac{\left[\left(\delta_{ie}\right)\cdot\left(U\omega_{ie}\right)^2 - \delta_{ie-1}\cdot\left(U\omega_{ie-1}\right)^2\right]}{\Delta x} - \delta_{ie}\cdot\rho_f\cdot g\cdot\sin\left(\frac{\Delta x}{r}\right) + \left(\frac{3}{2}\cdot\mu\cdot\frac{U\omega_{ie}}{\delta_{ie}}\right)\right] \ldots$$
$$+\rho_f\cdot\frac{\Delta_{ie}\cdot\left(U\omega_{ie}\right)^2 - \Delta_{ie-1}\cdot\left(U\omega_{ie-1}\right)^2}{\Delta x}$$

$$\psi_{(0,0)} \leftarrow \frac{\left[\frac{5}{8}\cdot\frac{\left(\delta_{ie} + \delta inc\right)\cdot U\omega_{ie} - \delta_{ie-1}\cdot U\omega_{ie-1}}{\Delta x} - \frac{k_f\cdot\Delta T}{\rho_f\cdot h_{fg}\cdot\left(\delta_{ie} + \delta inc + \Delta_{ie}\right)}\right] \ldots + \blacksquare - \left[\frac{5}{8}\cdot\frac{\delta_{ie}\cdot U\omega_{ie} - \delta_{ie-1}\cdot U\omega_{ie-1}}{\Delta x} - \frac{k_f\cdot\Delta T}{\rho_f\cdot h_{fg}\cdot\left(\delta_{ie} + \Delta_{ie}\right)}\right]}{\delta inc}$$

$$\psi_{(0,1)} \leftarrow \frac{\left[\frac{5}{8}\cdot\frac{\delta_{ie}\cdot\left(U\omega_{ie} + Uinc\right) - \delta_{ie-1}\cdot U\omega_{ie-1}}{\Delta x}\right] - \left(\frac{5}{8}\cdot\frac{\delta_{ie}\cdot U\omega_{ie} - \delta_{ie-1}\cdot U\omega_{ie-1}}{\Delta x}\right)}{Uinc}$$

$\blacksquare$

$\blacksquare$

$$\psi_{(1,0)} \leftarrow \frac{\left[\frac{17}{35}\cdot\rho_f\cdot\frac{\left[\left(\delta_{ie}+\delta inc\right)\cdot\left(U\omega_{ie}\right)^2-\delta_{ie-1}\cdot\left(U\omega_{ie-1}\right)^2\right]}{\Delta x}-\left(\delta_{ie}+\delta inc\right)\cdot\rho_f\cdot g\cdot\sin\left(\frac{\Delta x}{r}\right)+\frac{3}{2}\cdot\mu\cdot\frac{U\omega_{ie}}{\left(\delta_{ie}+\delta inc\right)}\right]\ldots + \blacksquare - \left[\frac{17}{35}\cdot\rho_f\cdot\frac{\left[\delta_{ie}\cdot\left(U\omega_{ie}\right)^2-\delta_{ie-1}\cdot\left(U\omega_{ie-1}\right)^2\right]}{\Delta x}-\delta_{ie}\cdot\rho_f\cdot g\cdot\sin\left(\frac{\Delta x}{r}\right)+\frac{3}{2}\cdot\mu\cdot\frac{U\omega_{ie}}{\delta_{ie}}\right]}{\delta inc}$$

$$\psi_{(1,1)} \leftarrow \frac{\left[\frac{17}{35}\cdot\rho_f\cdot\frac{\left[\delta_{ie}\cdot\left(U\omega_{ie}+Uinc\right)^2-\delta_{ie-1}\cdot\left(U\omega_{ie-1}\right)^2\right]}{\Delta x}-\delta_{ie}\cdot\rho_f\cdot g\cdot\sin\left(\frac{\Delta x}{r}\right)+\frac{3}{2}\cdot\mu\cdot\frac{\left(U\omega_{ie}+Uinc\right)}{\delta_{ie}}\right]\ldots + \blacksquare - \left[\frac{17}{35}\cdot\rho_f\cdot\frac{\left[\delta_{ie}\cdot\left(U\omega_{ie}\right)^2-\delta_{ie-1}\cdot\left(U\omega_{ie-1}\right)^2\right]}{\Delta x}-\delta_{ie}\cdot\rho_f\cdot g\cdot\sin\left(\frac{\Delta x}{r}\right)+\frac{3}{2}\cdot\mu\cdot\frac{U\omega_{ie}}{\delta_{ie}}\right]}{Uinc}$$

$$del \leftarrow -\left(\psi^{-1}\cdot C\right)$$

$$\delta_{ie} \leftarrow \delta_{ie} + del_0$$

$$U\omega_{ie} \leftarrow U\omega_{ie} + del_1$$

for $iter \in 1..10$

$$C_0 \leftarrow \frac{5}{8}\cdot\frac{\delta_{ie}\cdot U\omega_{ie}-\delta_{ie-1}\cdot U\omega_{ie-1}}{\Delta x}-\frac{k_f\cdot\Delta T}{\rho_f\cdot h_{fg}\cdot\delta_{ie}}$$

$$C_1 \leftarrow \frac{17}{35}\cdot\rho_f\cdot\frac{\left[\left(\delta_{ie}\right)\cdot\left(U\omega_{ie}\right)^2-\delta_{ie-1}\cdot\left(U\omega_{ie-1}\right)^2\right]}{\Delta x}-\delta_{ie}\cdot\rho_f\cdot g\cdot\sin\left(\frac{\Delta x}{r}\right)+\left(\frac{3}{2}\cdot\mu\cdot\frac{U\omega_{ie}}{\delta_{ie}}\right)$$

$$\psi_{(0,0)} \leftarrow \frac{\left[\frac{5}{8}\cdot\frac{\left(\delta_{ie}+\delta inc\right)\cdot U\omega_{ie}-\delta_{ie-1}\cdot U\omega_{ie-1}}{\Delta x}-\frac{k_f\cdot\Delta T}{\rho_f\cdot h_{fg}\cdot\left(\delta_{ie}+\delta inc\right)}\right]\ldots + \blacksquare - \left(\frac{5}{8}\cdot\frac{\delta_{ie}\cdot U\omega_{ie}-\delta_{ie-1}\cdot U\omega_{ie-1}}{\Delta x}-\frac{k_f\cdot\Delta T}{\rho_f\cdot h_{fg}\cdot\delta_{ie}}\right)}{\delta inc}$$

$$\psi_{(0,1)} \leftarrow \frac{\left[\frac{5}{8}\cdot\frac{\delta_{ie}\cdot\left(U\omega_{ie}+Uinc\right)-\delta_{ie-1}\cdot U\omega_{ie-1}}{\Delta x}\right]-\left(\frac{5}{8}\cdot\frac{\delta_{ie}\cdot U\omega_{ie}-\delta_{ie-1}\cdot U\omega_{ie-1}}{\Delta x}\right)}{Uinc}$$

$$\psi_{(1,0)} \leftarrow \frac{\left[\frac{17}{35}\cdot\rho_f\cdot\frac{\left[\left(\delta_{ie}+\delta inc\right)\cdot\left(U\omega_{ie}\right)^2-\delta_{ie-1}\cdot\left(U\omega_{ie-1}\right)^2\right]}{\Delta x}-\left(\delta_{ie}+\delta inc\right)\cdot\rho_f\cdot g\cdot\sin\left(\frac{\Delta x}{r}\right)+\frac{3}{2}\cdot\mu\cdot\frac{U\omega_{ie}}{\left(\delta_{ie}+\delta inc\right)}\right]\ldots + \blacksquare - \left[\frac{17}{35}\cdot\rho_f\cdot\frac{\left[\delta_{ie}\cdot\left(U\omega_{ie}\right)^2-\delta_{ie-1}\cdot\left(U\omega_{ie-1}\right)^2\right]}{\Delta x}-\delta_{ie}\cdot\rho_f\cdot g\cdot\sin\left(\frac{\Delta x}{r}\right)+\frac{3}{2}\cdot\mu\cdot\frac{U\omega_{ie}}{\delta_{ie}}\right]}{\delta inc}$$

$$\psi_{(1,1)} \leftarrow \frac{\left[\frac{17}{35}\cdot\rho_f\cdot\frac{\left[\delta_{ie}\cdot\left(U\omega_{ie}+Uinc\right)^2-\delta_{ie-1}\cdot\left(U\omega_{ie-1}\right)^2\right]}{\Delta x}-\delta_{ie}\cdot\rho_f\cdot g\cdot\sin\left(\frac{\Delta x}{r}\right)+\frac{3}{2}\cdot\mu\cdot\frac{\left(U\omega_{ie}+Uinc\right)}{\delta_{ie}}\right]\ldots + \blacksquare - \left[\frac{17}{35}\cdot\rho_f\cdot\frac{\left[\delta_{ie}\cdot\left(U\omega_{ie}\right)^2-\delta_{ie-1}\cdot\left(U\omega_{ie-1}\right)^2\right]}{\Delta x}-\delta_{ie}\cdot\rho_f\cdot g\cdot\sin\left(\frac{\Delta x}{r}\right)+\frac{3}{2}\cdot\mu\cdot\frac{U\omega_{ie}}{\delta_{ie}}\right]}{Uinc}$$

$$del \leftarrow -\left(\psi^{-1}\cdot C\right)$$

$$\delta_{ie} \leftarrow \delta_{ie} + del_0$$

$$U\omega_{ie} \leftarrow U\omega_{ie} + del_1$$

$$\delta \leftarrow \delta + \Delta$$

$$result3 \leftarrow augment\left(\delta, U\omega\right)$$

$$result3 \leftarrow augment(result2, result3)$$